Xiaodong Ma

Stimuli-Responsive Prodrug Nanomaterials for Combination Therapy of Cancer

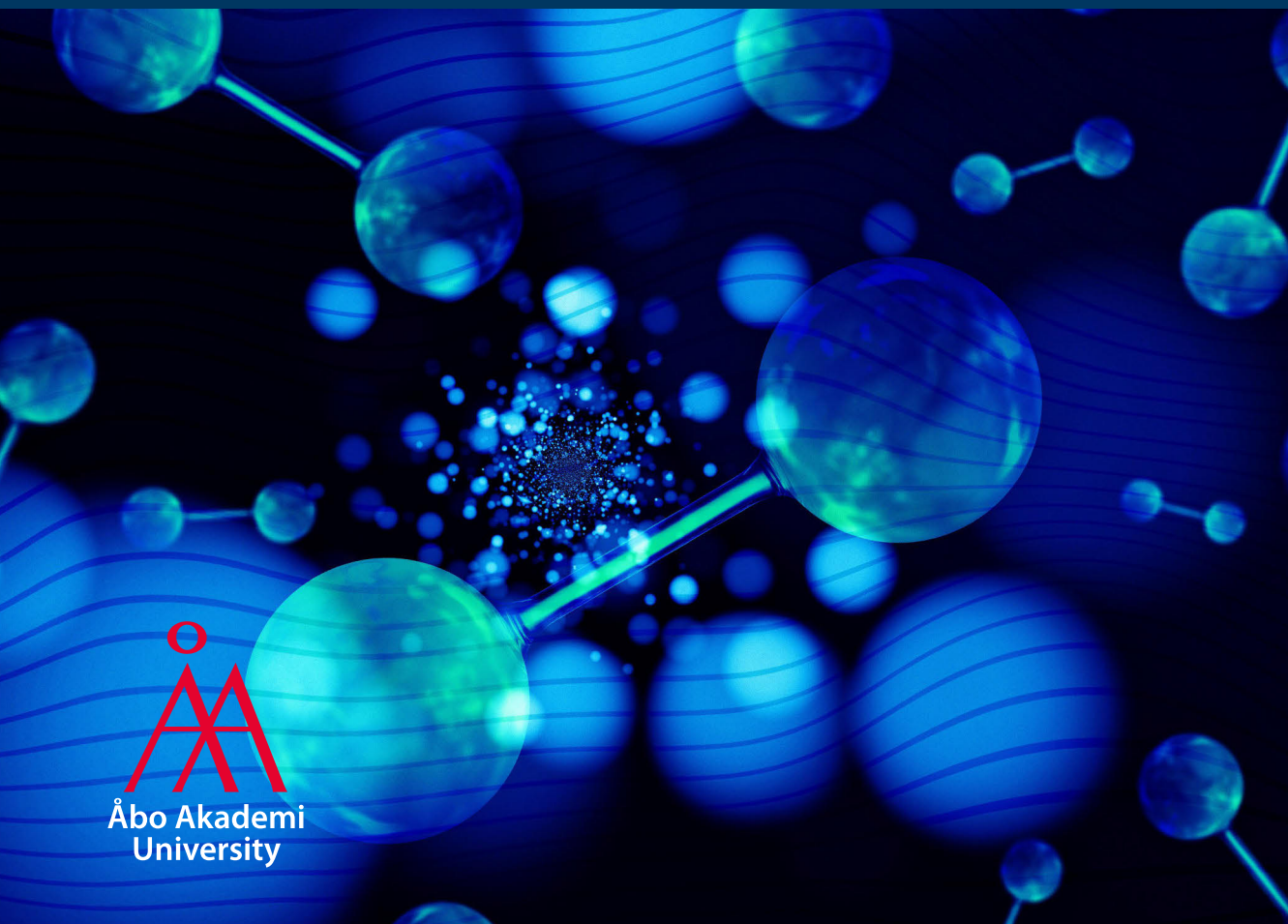

Åbo Akademi University

Xiaodong Ma

Born 1992, Jiangsu, China

Previous studies and degrees

Master of Marine Science, Jiangsu Ocean University, 2019

Bachelor of Pharmaceutical Engineering, Jiangsu Ocean University, 2014

Cover Image by Gerd Altmann from Pixabay

Stimuli-Responsive Prodrug Nanomaterials for Combination Therapy of Cancer

Xiaodong Ma

Pharmaceutical Sciences Laboratory
Faculty of Science and Engineering
Åbo Akademi University
Åbo, Finland, 2023

Supervisors:

Professor Hongbo Zhang (main supervisor)
Pharmaceutical Sciences Laboratory
Åbo Akademi University
Finland

Turku Bioscience Centre
University of Turku and Åbo Akademi University
Finland

Professor Jessica Rosenholm (co-supervisor)
Pharmaceutical Sciences Laboratory
Åbo Akademi University
Finland

Reviewers:

Associate Professor Mingshi Yang
Department of Pharmacy
University of Copenhagen
Denmark

Professor Jarkko Rautio
Faculty of Health Sciences, School of Pharmacy
University of Eastern Finland
Finland

Opponent:

Associate Professor Mingshi Yang
Department of Pharmacy
University of Copenhagen
Denmark

ISBN 978-952-12-4333-2 (printed)
ISBN 978-952-12-4334-9 (electronic)
Painosalama, Turku, Finland 2023

To my family

Abstract

Cancer is a challenging disease to cure. Current treatment methods mainly include chemotherapy and phototherapy. Chemotherapy drugs, due to their high toxicity and systemic distribution, still cause great suffering for cancer patients. Moreover, the clinical efficacy of single-drug treatment is limited due to the complex pathogenesis of malignant tumors and multi-drug resistance often exhibited by tumor cells. To address these challenges, combination therapy with multiple drugs or multiple treatment modalities is widely used to treat various malignancies. In parallel, the rapid development of nanotechnology has promoted the application of nanomedicines in combination chemotherapy. Still, although nanodrugs can increase the drug concentration in the tumor area, the residual nanodrugs in the liver and kidneys still pose a huge threat to human health. Prodrugs are pharmacologically inactive drugs or compounds that are metabolized into pharmacologically active drugs after ingestion by the human body. Prodrug treatment strategies have become an exploratory direction to address the side effects of chemical therapy. Nanomedicine-based prodrugs can be prepared to improve targeting efficiency by using cancer cell targeting ligands and respond to the slightly acidic and reducing microenvironment of the tumor by using different chemical bonds, which can improve the antitumor effect and reduce the toxic side effects on healthy tissues.

In this thesis, we designed prodrug-based nanomaterials and studied the antitumor effects of the prodrugs using different drug delivery systems. First, reduction-sensitive paclitaxel (PTX) prodrugs were synthesized as connecting units to achieve synergistic treatment of cancer chemotherapy and photodynamic therapy using reactive oxygen species to treat cancer cells. The self-assembled nanoparticles of PTX prodrugs were formed by connecting PTX with different chemotherapeutic drugs or photosensitizers. This strategy effectively overcame drug resistance and exhibited enhanced antitumor effects *in vivo* with low toxicity. Second, using a combination of bionic and prodrug technologies, a cancer cell-targeted drug delivery system based on mesoporous silica nanoparticles (MSNs) encapsulated by cancer cell membranes was designed. This system demonstrated synergistically enhanced anticancer effects in cellular experiments. In summary, this thesis has provided new ideas for improving the shortcomings of traditional combined chemotherapy and photodynamic therapy, realizing the synchronous delivery and controlled release of different antitumor drugs, enhancing the synergy of drugs, and improving the efficacy of inhibiting tumor proliferation and metastasis.

Keywords

prodrug nanoparticles, drug delivery, mesoporous silica nanoparticles, stimuli-responsive drug release, combination therapy, tumor targeting, endoplasmic reticulum targeting, microfluidics

Sammanfattning

Cancer är en utmanande sjukdom att bota. Nuvarande behandlingsmetoder inkluderar främst kemoterapi och fototerapi. Kemoterapiläkemedel orsakar fortfarande stort lidande för cancerpatienter på grund av sin höga toxicitet och systemiska distribution. Dessutom är den kliniska effekten av behandling med ett enda läkemedel begränsad på grund av den komplexa patogenesen av maligna tumörer samt multiläkemedelsresistens som ofta uppvisas av tumörceller. För att hantera dessa utmaningar används i stor utsträckning kombinationsterapi med flera läkemedel eller flera behandlingsmetoder för att behandla olika maligniteter. Parallellt har den snabba utvecklingen av nanoteknik främjat tillämpningen av nanoläkemedel i kombinationskemoterapi. Även om nanoläkemedel kan öka läkemedelskoncentrationen i tumörområdet, utgör läkemedlsrester i levern och njurarna fortfarande ett hot mot människors hälsa. Prodroger är farmakologiskt inaktiva läkemedel eller föreningar som metaboliseras till farmakologiskt aktiva läkemedel efter intag av människokroppen. Strategier för behandling med prodroger har blivit en explorativ inriktning för att hantera biverkningarna av kemoterapi. Nanomedicin-baserade prodroger kan framställas för att förbättra målsökningseffektiviteten genom att använda cancercellsmålsökande ligander och endast friätta den aktiva substansen som en respons på tumörens lätt sura och reducerande mikromiljö genom att använda olika kemiska bindningar, vilket i sin tur kan förbättra antitumöreffekten och minska de toxiska biverkningarna på friska vävnader.

I detta examensarbete designade vi prodrog-baserade nanomaterial och studerade antitumöreffekterna av prodrogerna med hjälp av olika läkemedelsadministrationssystem. Först syntetiserades reduktionskänsliga paklitaxel (PTX) prodroger för att uppnå synergistisk behandling av cancerkemoterapi och fotodynamisk terapi för att behandla cancerceller. De självaggregerande nanopartiklarna av PTX-prodroger bildades genom att koppla PTX med olika kemoterapeutiska läkemedel eller fotosensibilisatorer. Denna strategi övervann effektivt läkemedelsresistens och uppvisade förbättrade antitumöreffekter *in vivo* med låg toxicitet. Sedan designades med hjälp av en kombination av bionisk och prodrug-teknologi ett cancercellriktat läkemedelslevereringssystem baserat på mesoporösa kiseldioxidnanopartiklar inkapslade av cancercellmembran. Detta system visade synergistiskt förbättrade anticancereffekter i cellulära experiment. Sammanfattningsvis har denna avhandling kommit fram med nya idéer för att förbättra bristerna i traditionell kombinationskemoterapi och fotodynamisk terapi, samt förverkliga den samtidiga tillförseln och kontrollerade frisättningen av olika antitumörläkemedel, och därmed förbättra synergin mellan läkemedlen och hämning av tumörproliferation och metastasering .

Nyckelord

prodrog, läkemedelstillförsel, mesoporösa kiseldioxid nanopartiklar, stimuli-responsiv läkemedelsfrisättning, kombinationsterapi, tumörmålsökning, intracellulär målsökning, mikrofluidistik

TABLE OF CONTENTS

List of original publications

1. ***Fabrication of Redox- Responsive Doxorubicin and Paclitaxel Prodrug Nanoparticles with Microfluidics for Selective Cancer Therapy***

Xiaodong Ma, Ezgi Ozliseli, Yuezhou Zhang, Guoqing Pan, Dongqing Wang, Hongbo Zhang*. Biomaterials Science, **2019**. 7 (2), 634-644. (DOI: 10.1039/c8bm01333k)

2. Self-assembled Disulfide Bond Bearing Paclitaxel- Camptothecin Prodrug Nanoparticle for Lung Cancer Therapy

Jingyan Gao, **Xiaodong Ma**, Lirong Zhang, Jiaqi Yan, Huaguang Cui, Yuezhou Zhang, Dongqing Wang, Hongbo Zhang*. Pharmaceutics, **2020** 12(12), 1169. (DOI: 10.3390/pharmaceutics12121169)

3. Porphyrin Centered Paclitaxel Tetrameric Prodrug Nanoassembliesas Tumor-Selective Theranostics for Synergized Breast Cancer Therapy

Xiaodong Ma, Pengfei Wang, Qiwei Wu, Junnian Zhou, Dongqing Wang, Deependra Yadav, Hongbo Zhang*, Yuezhou Zhang*. Advanced Healthcare Materials, **2022**: 2202024. (DOI: 10.1002/adhm.202202024)

4. Combination of photothermal, prodrug and tumor cell camouflage technologies for triple-negative breast cancer treatment

Lirong Zhang, **Xiaodong Ma**, Wenhui Zhou, Qiwei Wu, Jiaqi Yan, Xiaoyu Xu, Bhawana Ghimire, Jessica M. Rosenholm, Jing Feng*, Dongqing Wang*, Hongbo Zhang*. Mater. Today Adv., **2022**, 13, 100199. (DOI: 10.1016/j.mtadv.2021.100199)

5. Minimally Invasive injection of Biomimetic Nano@Microgel for In Situ Ovarian Cancer Treatment Through Enhanced Photodynamic Reactions and Photothermal Combined Therapy

Xiaodong Ma, Wenhui Zhou, Rong Zhang, Cancan Zhang, Jiaqi Yan, Jing Feng, Jessica M. Rosenholm, Tingyan Shi*, Xian Shen*, Hongbo Zhang*. Mater. Today Bio, **2023**, 20, 100663. (DOI: 10.1016/j.mtbio.2023.100663)

This study was conducted between 2018 and 2023 under the supervision of Professor Hongbo Zhang, co-supervised by Prof. Jessica Rosenholm at Åbo Akademi University's Pharmaceutical Sciences Laboratory. Some parts of the study were conducted at the Jiangsu University and Wenzhou Medical University in China.

Contribution of the author

1. In PAPER I, the author synthesized and characterized all samples, and analyzed the data. Ezgi Ozliseli conducted the *in vitro* experiments and Yuezhou Zhang contributed to the initial draft writing, Guoqing Pan, Dongqing Wang and Hongbo Zhang provided financial support.

2. In PAPER II, the author synthesized and characterized materials, contributed to draft writing, while Jingyan Gao conducted *in vitro* experiments and Jiaqi Yan, Huaguang Cui analyzed data. Yuezhou Zhang also contributed to the initial draft writing, Lirong Zhang, Dongqing Wang and Hongbo Zhang provided financial support.

3. In PAPER III, the author prepared and characterized all samples, conducted *in vitro* and *in vivo* experiments, analyzed data, and wrote the first draft. Pengfei Wang, Qiwei Wu, assisted with the *in vivo* experiments and Yuezhou Zhang contributed to initial draft writing. Deependra Yadav and Junnian Zhou contributed to data analysis. Dongqing Wang and Hongbo Zhang provided financial support.

4. In PAPER IV, the author synthesized and characterized the samples, conducted the *in vitro* experiments, Lirong Zhang Jiaqi Yan, Xiaoyu Xu and Bhawana Ghimire analyzed the data, Qiwei Wu conducted the *in vivo* experiments. W. Zhou was responsible for the initial draft writing, Jessica M. Rosenholm and Jing Feng contributed to the revision of the manuscript.

5. In PAPER V, the author synthesized and characterized all samples, analyzed the data, conducted the *in vitro* and *in vivo* experiments, and contributed to draft writing. Cancan Zhang, Jiaqi Yan contributed to data analysis, W. Zhou was responsible for the initial draft writing, Jessica M. Rosenholm and Jing Feng contributed to the revision of the manuscript. Rong Zhang, Tingyan Shi, Xian Shen, Hongbo Zhang provided financial support.

Supplementary publications

1. An autocatalytic multicomponent DNAzyme nanomachine for tumor-specific photothermal therapy sensitization in pancreatic cancer

Jiagi Yan, **Xiaodong Ma**, Danna Liang, Meixin Ran, Dongdong Zheng, Xiaodong Chen, Shichong Zhou, Weijian Sun, Xian Shen, Hongbo Zhang*. Nature communications, 2023, 14(1): 6905. (Co-first author) (DOI: 10.1038/s41467-023-42740-2)

2. Co-delivery CPT and PTX Prodrug with a Photo/thermo-responsive Nanoplatform for Triple Negative Breast Cancer Therapy

Wenhui Zhou, **Xiaodong Ma**, Jie Wang, Xiaoyu Xu, Oliver Koivisto, Jing Feng, Tapani Viitala, Hongbo Zhang*. Smart Medicine, **2022**, 1, 1, e20220036. (Co-first author) (DOI: 10.1002/SMMD.20220036)

3. Co-delivery of Paclitaxel Prodrug, Gemcitabine and Porphine by micelles for pancreatic cancer treatment via chemo-photodynamic combination therapy

Qiwei Wu, **Xiaodong Ma**, Wenhui Zhou, Rong Yu, Jessica M. Rosenholm, Weizhong Tian, Lirong Zhang*, Dongqing Wang*, Hongbo Zhang*. Pharmaceutics, **2022**, 14(11), 2280. (Co-first author) (DOI: 10.3390/pharmaceutics14112280)

4. Reregulated mitochondrial dysfunction reverses cisplatin resistance microenvironment in colorectal cancer

Yonghui Wang, **Xiaodong Ma**, Wenhui Zhou, Chang Liu, Hongbo Zhang*. Smart Medicine, **2022**, e20220013. (DOI: 10.1002/SMMD.20220013)

Abbreviations

APTEOS	(3-aminopropyl)triethoxysilane
$AgNO_3$	Silver nitrate
ATP	Adenosine triphosphate
AuNRs	Gold nanopaticles
CRT	Recombinant Calreticulin
CPT	Camptothecin
CTAB	Hexadecyl trimethyl ammonium bromide
CTAC	Cetyltrimethylammonium chloride
Cy5.5	Sulfo-Cyanine5.5 NHS ester
DOX	Doxorubicin
DCM	Dichloromethane
DAPI	4′,6-diamidino-2-phenylindole
DCA	Dichloroacetic acid
DMF	N, N'-dimethylformamide
DTDPA	3,3′-dithiodipropionic acid anhydride
DLS	Dynamic light scattering
DMAP	4-dimethylaminopyridine
DCFH-DA	2',7'-Dichlorodihydrofluorescein diacetate
DMSO	Dimethyl sulfoxide
DTT	Dithiothreitol
DIO	3,3′-dioctadecyloxacarbocyanine perchlorate
EDCI	N-(3-dimethylaminopropyl)-N-ethylcarbodiimide hydrochloride
ER	Endoplasmic reticulum
EPR	Enhanced permeation and retention
FA	Folic acid
FT-IR	Fourier-transform infrared spectroscopy
FBS	Fetal bovine serum
GelMA	Gelatin Methacrylamide
GSH	Glutathione
HMGB1	High mobility group protein B1
H_2O_2	Hydrogen peroxide
ICD	Immungentic cell death
MSN	Mesoporous silica nanoparticle
MS	Mass spectrum
NHS	N-Hydroxy succinimide
MA	Methacrylic anhydride
MFI	Mean fluorescent intensity
NMR	Nuclear magnetic resonance spectroscopy
PTX	Paclitaxel
PBS	Phosphate-buffered saline
PEG	Polyethylene glycol
PTT	Photothermal therapy
PDT	Photodynamic therapy

PCC	Pearson correlation coefficient
PXRD	Powder X-ray diffraction
ROS	Reactive oxygen species
TEM	Transmission electron microscopy
TEOS	Tetraethoxysilane
THPP	Tetrakis(4-hydroxyphenyl)-porphine
WST-1	Cell proliferation assay Roche diagnostics reagent

1. Introduction

Although chemotherapy is a very important means for cancer treatment, the use of a single chemotherapy drug has low efficacy and the consequential high dose is prone to generate significant side effects. In addition, chemotherapy is likely to also cause drug resistance in cancer patients and, in the worst case, induce tumor recurrence and metastasis. In order to solve the problems faced by using single chemotherapy drugs, combination chemotherapy is used based on cocktail of drugs to treat tumors in the clinic. However, the traditional combination chemotherapy and the inherent defects of small molecule chemotherapy drugs lead to unsatisfactory clinical treatment effect of traditional combination chemotherapy, and even lead to increased drug toxicity. The combination of nanodrug delivery systems and traditional combination chemotherapy may improve the pharmacokinetic properties of each drug in combined chemotherapy and the distribution of different drugs in organisms, thus enhancing the drug synergy of combined chemotherapy and greatly improving the antitumor efficacy of combined chemotherapy (Li et al., 2020). However, despite this, there is still no actively targeted nanomedicine that has entered the market. The active targeting functionality of nanoparticles still needs improvement. Additionally, drug leakage of nanoparticles in the bloodstream can lead to side effects and pose a threat to human health (Chendi et al., 2022).

To address these issues, it is urgent to propose new concepts and develop low-toxicity, high-efficiency, tumor-targeting nanodrug delivery systems. Currently, prodrug molecules with microenvironment-responsive properties are being developed to overcome these challenges (Xie et al., 2020). These prodrug molecules self-assemble into nanoparticles that not only possess the ability to respond to the tumor microenvironment, but also have high drug loading capacity due to their carrier-free structure (Xiao et al., 2022). This enables targeted co-delivery, synergistic therapy, and controlled drug release combined into one system. In this context, mesoporous silica nanoparticles (MSNs), as highly modifiable nanocarriers, are well-suited for incorporating targeting and microenvironment-responsive functions into the same platform. Therefore, constructing a multifunctional MSN drug delivery system for targeted combination therapy of cancer has become a feasible strategy (Saman et al., 2022) that warrants further exploration for realizing its full potential.

2. Review of literature

2.1 Introduction and current situation of cancer treatment

The tumor is a lesion induced by cell division and proliferation disorders. Tumors are variously named according to their size, the origin of cells, and the type of tissue in which they first appeared. Generally, it is divided into benign, precancerous, and malignant tumors. Benign tumors are not cancers, do not spread, have clear borders, can always maintain their original forms, and have a low recurrence rate after resection. Most benign tumors are harmless to human health. Precancerous tumors are not cancerous yet, but they risk developing into cancer at any time, so we must closely monitor their development trend. Malignant tumors, also known as cancer, can proliferate malignantly, invade adjacent normal tissues, with unclear borders. They can spread to other organs and tissues through the blood or lymphatic circulation system and continue to grow rapidly at the metastases, worsening the body's state. But there is no clear line between the three, especially when the tumor is in the middle state or rapid change in the situation; it is forced to classify is only a general estimate of the current state. Some benign tumors may also become precancerous tumors and eventually evolve into malignant ones. Malignant tumor (Fidler and Kripke 1977; Luby et al., 2019) is one of the important diseases endangering human health. Especially after the 21st century, it has increasingly become the number one killer threatening human life safety.

As cancer incidence continues to rise, cancer treatment has become a hot topic for researchers. Conventional treatments include surgical resection, radiation therapy, and chemotherapy. Emerging therapeutic approaches include photothermal therapy, photodynamic therapy, and immunotherapy. Chemotherapy is the most commonly used and effective treatment. According to the period, antitumor drugs, including methotrexate (Winocur et al., 2006), 5-fluorouracil (Gailani 2015), cisplatin (Olaussen et al., 2010), doxorubicin (Henderson et al., 2003), paclitaxel (Konecny et al., 2004), camptothecin (Hsiang et al., 1985), oxaliplatin (Alberts et al., 2003), gemcitabine, irinotecan, rituximab and imatinib appeared successively. Their anticancer mechanisms are different: they affect the nucleic acid synthesis, destroy and affect DNA replication, interfere with transcription and hinder RNA synthesis, inhibit protein synthesis, and interfere with hormone balance.

2.1.1. Chemotherapy

Small molecule chemotherapy drugs are generally hydrophobic molecules, with poor solubility, systemic distribution after systemic administration, poor selectivity between tumor tissue and normal tissue, which damage the normal organs and tissues, and produce systemic toxicity. Moreover, drug resistance of tumors is particularly easy to occur after drug administration, so that the effective response of organisms to drugs is greatly reduced (Asiabi et al., 2019). To maintain effective drug concentration, patients must be given multiple

doses, which virtually aggravates the economic and health pressure on patients. The emergence of nanotechnology (Edis et al., 2021), greatly improves the above problems. Nanodrugs utilize nano-scaled carriers to deliver active drug molecules. The advantages of nano-sized drugs over small molecule drugs are as follows: (1) The solubility of drugs is improved through excipients, and the drugs are protected from degradation in blood circulation; (2) prolonging blood circulation time, which may further increase the aggregation of nanodrugs in tumors; (3) passively or actively enhancing the aggregation of drugs in tumor tissues by the EPR (Enhanced permeation and retention) effect of the nano-sized material or introducing a targeting group; (4) regulating tissue infiltration and drug release; (5) common nanodrug carriers that can reduce the toxic and side effects of the original drug and improve the quality of life of patients. Nano-scaled carriers used for these purposes include liposomes, polymer nanoparticles, dendritic polymers, nano-micelles, polymer vesicles, nano-gels, exosomes, magnetic nanoparticles, carbon nanotubes, and gold nanoparticles. They are not perfect. Liposomes and polymers have been widely used due to their good biocompatibility, biodegradability and excellent mechanical properties (Chan and Kwok 2011; Mahmoudi et al., 2011; Manzoor et al., 2012; Mohammad et al., 2015; Vikash et al., 2013). However, the mechanisms of action of nanoparticles on tumor cells and tumor microenvironment are still unclear, so further investigation is needed on the toxic and side effects of nanoparticles and the effect of prolonging the survival time of patients. For liposomes, its greatest advantage is to reduce the toxic and side effects rather than increase the efficacy, which may be due to the degradation of liposome carrier, so that the internal release of the active drug is required for some time. In addition, balancing the stability of liposomes and the bioavailability of drugs in tumor tissue is also a very big challenge (Cheng et al., 2014; Konecny et al., 2004; Robert et al., 2006).

It has been only a few decades since the emergence of nanodrugs, but they have already profoundly impacted human health. Since 1964, liposome-based doxorubicin (Doxil), protein-bound paclitaxel (NAb-paclitaxel), polymer micelle-encapsulated paclitaxel (Genexol-PM), siRNA-targeted polymer nanoparticles (CALAA-01) and iron-based inorganic nanoparticles have been successively introduced to the clinic. The research of nanodrugs has also promoted the booming development of industries including medicine, diagnostic imaging reagents, *in vitro* diagnosis and physiotherapy devices. However, many obstacles and difficulties must be overcome for the nanodrugs to translate from the laboratory to the clinic. From material design to cell-level evaluation, to *in vivo* test of mice, to validation of efficacy in large animals such as monkeys, and finally to clinical trials of patients, Phase I assessment of safety and pharmacokinetic profiles in healthy humans to determine the appropriate dose administration. Secondly, the curative effect is evaluated on a few patients; Phase III is performed in a wider range of patients to further evaluate safety and efficacy; Phase IV followed by long-term safety assessment. Few drugs have been able to get through these evaluations until they finally hit the

market (Gratton et al., 2008; Rosemary et al., 2013; Winocur et al., 2006; Wong et al., 2011).

Although many nanomedicines have been clinically approved, they are not perfect. Doxil is a typical example. Although it reduces the accumulation of drugs in the heart and the side effects of doxorubicin, it does not increase the drug's efficacy, so it only prolongs the patient's survival to a certain extent. In addition, although Genexol-PM increases higher doses of paclitaxel without additional systemic toxicity, its anticancer effect is not satisfactory. Such cases are common in clinical practice. Nanomaterials can accumulate more in tumors than small molecule prodrugs and reduce systemic toxicity. However, high concentrations of systemic administration cannot bring high efficacy returns. Building a smart nanocarrier system that simultaneously achieves low toxicity and high efficiency requires careful consideration and continuous exploration. (Matsumoto et al., 2016; Minchin and Martin 2010; Müller et al., 2004; Net et al., 2009; Vikash et al., 2013; Wang et al., 2014).

2.1.2 Photodynamic therapy

Photodynamic therapy (Lo et al., 2020), (PDT) is an emerging cancer treatment method following the three traditional surgery methods, radiotherapy and chemotherapy. PDT mainly contains three elements: photosensitizer (PS), the excitation light and oxygen molecules in tissue, all of which are indispensable (Zhang et al., 2019). The principle is as follows (Sekar et al., 2022): under the illumination of specific wavelength, the photosensitizer molecule can absorb photons to change from the ground state to a short-lived excited singlet state (Liu et al., 2020). On the one hand, the excited singlet state can decay to the ground state and emit fluorescence, which can be used for fluorescence imaging. On the other hand, it can be transformed into a long-lived excited triplet state through the system-to-system crossing. There are two reaction types at this time: Type I, the photosensitizer in the excited triplet state can transfer an electron or a proton to the matrix to form a cation or anion. If this matrix is oxygen, $O_2^{\bullet-}$, OH-, and H_2O_2 will be formed (Wang et al., 2021). The second type is that the photosensitizer that excites the triple state can also directly react with the ground state oxygen of the triple state to generate $^1O_2$. These reactive oxygen species can kill cancer cells and be used for cancer treatment, as shown in Figure. 1 (Sai et al., 2021). In the actual treatment process, when nanoparticles accumulate at the tumor site, the use of a laser to irradiate the tumor can achieve the therapeutic effect. Different photosensitizers require different excitation wavelengths, for example, the typical excitation wavelength for porphyrin-based photosensitizers is 650nm, and the excitation wavelength for indocyanine green is 808nm.

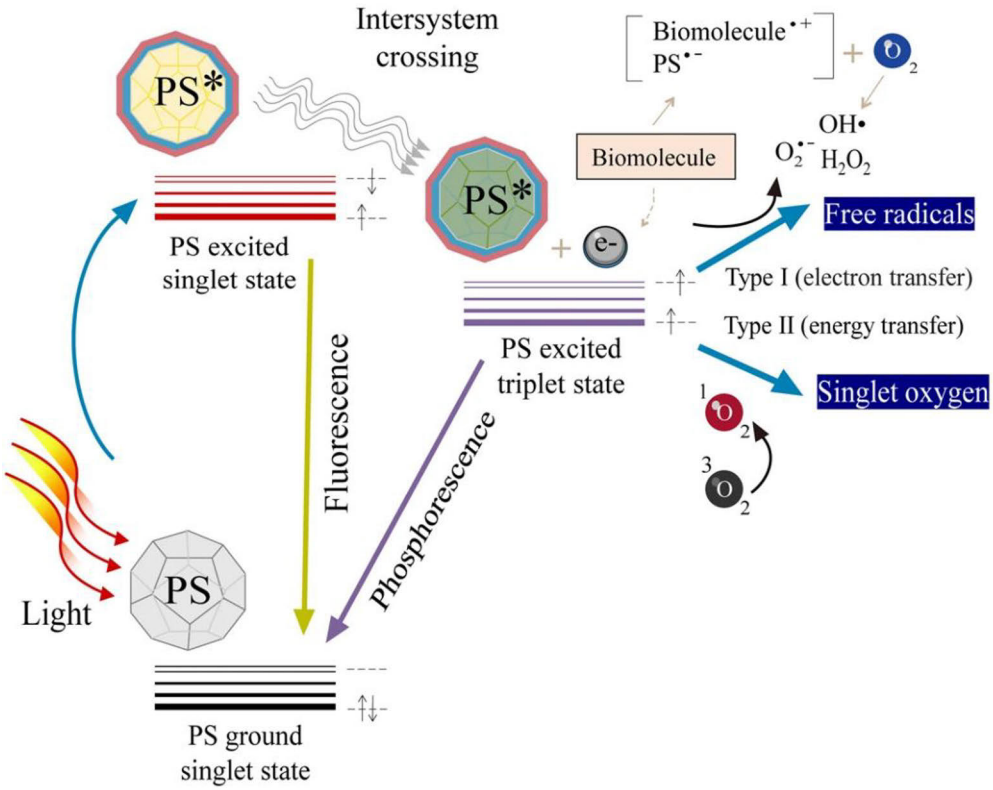

Figure 1. *Schematic illustration of photodynamic reactions. (Copyright 2021, Springer Nature)*

2.1.3 Photothermal therapy

Photothermal therapy (PTT) is also an emerging cancer treatment (Doughty et al., 2019; Huang et al., 2008; Yang et al., 2010; Yang et al., 2022; Zhang et al., 2021; Zhi et al., 2020). It uses nanomaterials with photothermal conversion capability to generate heat and the temperature is increased under the illumination condition. When the temperature inside the cell reaches 42 degrees Celsius or higher, it can destroy bioactive molecules in cells (such as protein degeneration and enzyme inactivation), destroy the normal physiological and metabolic functions of tumor cells, and lead to tumor cell injury, necrosis or thermal ablation of tumor tissue, to achieve the purpose of cancer treatment (Gao et al., 2022). PTT has the advantages of short irradiation time; rapid treatment process; repeatable operability; no drug resistance and good treatment effect (Figure 2) (Han and Choi 2021).

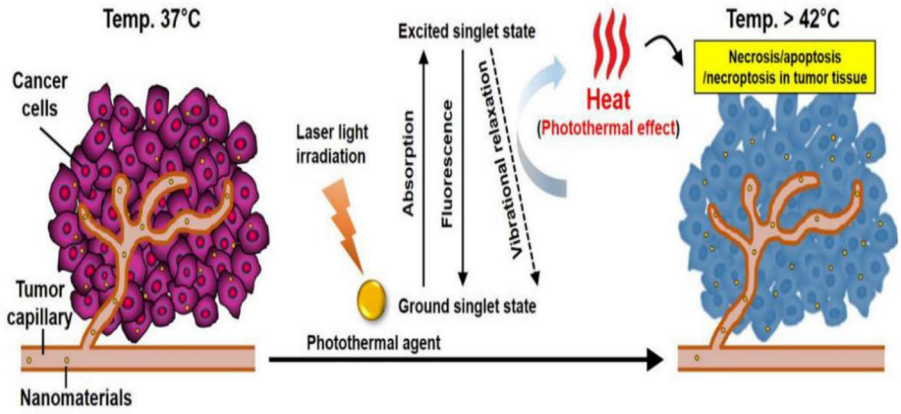

Figure 2. *Schematic illustration for PTT platforms. (Copyright 2021, Multidisciplinary Digital Publishing Institute)*

The greatest weakness of PTT is its poor tumor specificity. PTT does not have tumor selectivity, and accurate photothermal therapy relies on the accurate targeting of materials to tumors. However, the materials used for photothermal therapy generally do not have tumor targeting, and even though the targeting group is connected through surface modification, the targeting efficiency is not satisfactory. Once the photothermal conversion material enters the normal cells, illumination will cause damage to the normal tissue and produce side effects (Durr et al., 2007; Han and Choi 2021; Kang et al., 1996; Lin et al., 2014; Link and El-Sayed 1999; Liu et al., 2020; Plouffe et al., 2011). Therefore, the current research focus of photothermal therapy is on designing and modifying novel photothermal materials to enhance the efficacy of PTT and reduce side effects. Second, there is a thermal protection mechanism in cells, that is, when the cell temperature is too high, the expression of heat shock proteins will be increased, to protect the high temperature from protecting the active molecules, such as intracellular proteins, which will reduce the effect of PTT to a certain extent.

The nanomaterials used for PTT have the photothermal conversion ability. They can be divided into different categories: precious metal nanomaterials such as gold nanoparticles (gold nanorods, gold nanocages, gold nanoclusters, etc.), silver nanoparticles, and platinum nanoparticles. Among them, gold nanomaterials are the most widely used. It realizes efficient photothermal conversion through surface plasmon resonance (SPR), and has the advantages of high photothermal conversion efficiency, easy modification, and adjustable absorption wavelength, but the cost is high. Yujuan et al. designed a light-controlled photothermal therapy nano-system based on gold nanorods. The targeting adaptor folic acid (FA) was modified on the surface of the gold nanorods. This nano-system can target cancer cells, has a strong killing effect on these under light and verify the different apoptosis modes of cancer cells at different temperatures of particles (Yujuan et al., 2018).

2.1.4 Combination therapy based on prodrugs

While monotherapy has shown some success in treating certain tumors, its effectiveness remains limited, and achieving complete tumor eradication remains a challenge. This limitation arises from several factors. Firstly, tumors exhibit a high degree of heterogeneity, not only among different types of tumors and patients but also within the same tumor. Secondly, tumors have developed various mechanisms to evade the immune system's surveillance. Monotherapy struggles to address both tumor heterogeneity and the diverse immunosuppressive mechanisms simultaneously. Thus, a pivotal approach in treating tumors lies in simultaneously targeting these mechanisms to counteract tumor immune escape, potentially leading to significant anticancer effects. This can be achieved through the synergistic or enhancing effects of combining compounds that target different pathways (Liu et al., 2022; Wei et al., 2022; Yuan et al., 2022; Zeng et al., 2022; Zhu et al., 2022).

In the context of cancer treatment, chemotherapy can serve as an adjuvant treatment for early-stage cancer, aiming to shrink tumor size and reduce the risk of recurrence. However, systemic chemotherapy often results in side effects such as bone marrow suppression, nausea, vomiting, hair loss, and damage to normal tissues. Furthermore, chemotherapy can lead to the development of cellular resistance, significantly diminishing its effectiveness. Currently, laser therapies, including PDT and PTT, offer promising alternatives. While PDT and PTT exhibit high selectivity due to targeted infrared laser irradiation, they may not achieve complete tumor eradication when used in isolation.

Consequently, combining chemotherapy with laser therapies presents a compelling solution. This approach not only mitigates the issues associated with separate chemotherapy and infrared laser therapy but also offers synergistic effects that have been experimentally and clinically proven to be more effective in treating tumors.

In the realm of combination therapy, prodrugs play a vital role. Prodrugs involve chemically linking chemotherapy drugs with various photosensitizers to create chemically defined and stable prodrug combinations. These prodrugs possess a high drug loading capacity after self-assembly into nanoparticles, outperforming other drugs that require carrier delivery. Moreover, prodrugs can utilize different sensitive chemical linkers to target distinct disease microenvironments, making them a crucial strategy in drug delivery. (Cai et al., 2022; Guo et al., 2022; Li et al., 2021; Yang et al., 2021; Yu et al., 2021; Zhang 2021). Xie et al. designed a multifunctional prodrug by covalently linking the EGFR-tyrosine kinase inhibitor gefitinib (G) with a cleavable disulfide bond (SS) and a near-infrared (NIR) chromophore. This resulted in the main molecule of the prodrug, denoted as G-SS-NIR. In an aqueous medium, this main molecule (G-SS-NIR) readily self-assembles into nanoparticles, driven by the insertion of the disulfide bond and intermolecular π-π interactions. Akt inhibitor CEL is encapsulated into the nanoparticles, forming the CEL@G-SS-NIR. The prodrug accumulates in the tumor region and reacts with

overexpressed glutathione (GSH), releasing both inhibitors to combat cancer resistance while activating the NIR chromophore for fluorescence and multispectral photoacoustic tomography imaging (Xie et al., 2020) (Figure. 3).

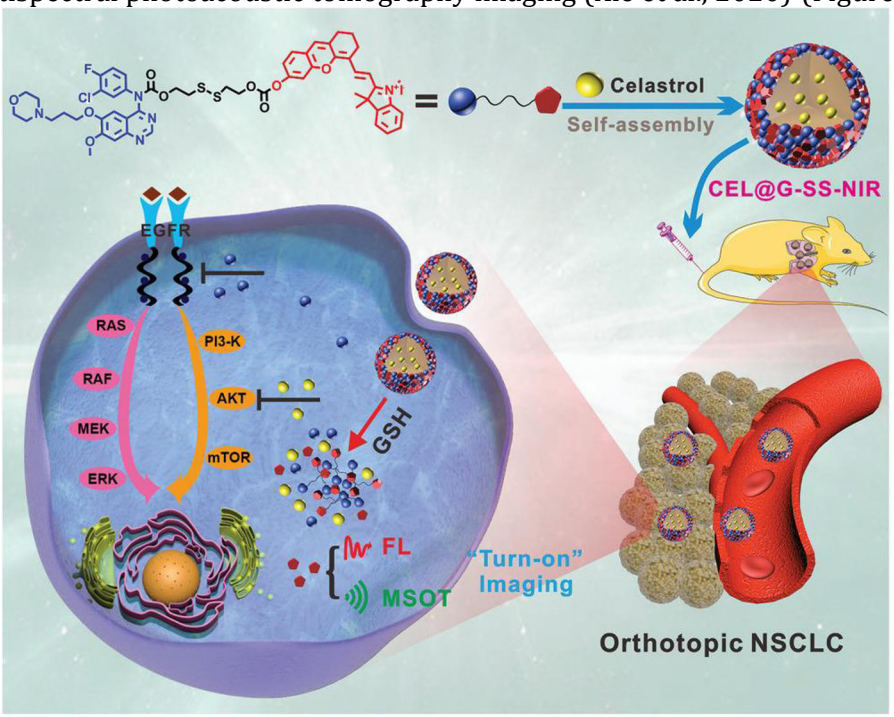

Figure 3. *Schematic diagram of self-assembled prodrug nanoparticles. (Copyright 2020, John Wiley & Sons)*

2.2 Application status of nano-materials in cancer treatment

In recent years, nanotechnology has made great progress (Zhou et al., 2022). It has played an important role in solving the current problems in biology and medicine, profoundly impacting these fields (Kaur et al., 2022). At the same time, with the continuous improvement of nanotechnology, more and more nanomaterials are applied to clinical cancer treatment (Adeel et al., 2020; Bian et al., 2021; Mazraedoost and Behbudi 2021; Tan et al., 2021).

A nanomaterial is a material whose three-dimensional space has at least one dimension in the nanoscale range (1-1000 nm) or is composed of them as basic units. Nanomaterials have large specific surface area characteristics, many active surface groups, easy modification, controllable morphology and size, and special chemical and physical properties (Gupta et al., 2017; Mrówczyński and interfaces 2017; Zare-Zardini et al., 2016). When designing nanomaterials for cancer treatment, several aspects should be generally considered: (1) good stability and biocompatibility with a long half-life *in vivo*; (2) large drug loading capacity; (3) has an accurate target function, and can realize accurate delivery of drugs; (4) controllable and continuous release of drug can be realized; (5)

having special physical and chemical properties such as light, electricity, magnetism and heat; and (6) is biodegradable and has low toxic and side effects (Massadeh et al., 2016; Singh and Nehru 2008).

2.2.1 Type of nano-materials in cancer treatment

At present, the commonly used nanomaterials for cancer treatment mainly include:

1. Self-assembled nano prodrugs

Because of no external auxiliary materials, the drug molecules form the self-assembled nanodrug through self-assembly (Cheng and Ji 2020; Lin et al., 2021; Mamuti et al., 2021). Its advantages cannot be underestimated: (1) simple synthesis, simple and clear structure, can be large-scale quantitative production; (2) its aggregation state can be regulated to prevent it from being rapidly cleared in the blood or metabolized by the kidney; (3) no additional auxiliary materials are added, so the drug loading amount and the drug loading efficiency are greatly improved, and troubles caused by short-term/long-term toxic reaction and immunogenicity of a body caused by a carrier are avoided; (4) the function of the nano self-assembly body (Jiang et al., 2016; Ren et al., 2016) is easily regulated and controlled by introducing functional groups (such as a targeting unit and an imaging unit); (5) controlled release of drugs can be achieved by regulating internal stimuli (such as pH, redox and enzyme), external stimuli (temperature, light) and combined stimuli and (6) with proper size and shape, long circulation and enhanced tumor aggregation of the nano system can be realized. They have many building units, which can be biocompatible molecules, such as oligomers, peptides, lipids, phospholipids, metal atoms; it can also be functionalized molecules, such as antitumor drugs, targeted ligands, imaging reagents, etc. These biocompatible or functionalized building blocks can prepare nano-dosage forms for tumor therapy via a double-self-assembly or nano-precipitation mechanism (Chhabra et al., 2010; Ding et al., 2013; Fan et al., 2015).

2. Mesoporous silica nanoparticles (MSNs)

Mesoporous silica nanoparticles refer to silicon dioxide (SiO_2) nanomaterials with ordered mesoporous channels. Due to its unique structural properties, it is one of the most commonly used nanodrug carriers, with good application potential in the field of biomedicine (Jafari et al., 2019; Kankala et al., 2020; Knežević and Durand 2015; Watermann and Brieger 2017). Mesoporous silica nanoparticles have the following advantages: (1) high drug loading capacity (Karaman et al., 2021; Niculescu 2020). Mesoporous silica nanoparticles have very large specific surface area and pore volume, and can be used for loading drug molecules by a covalent modification or non-covalent loading method, so that the loading amount of the drug is greatly improved; (2) having good biocompatibility and low damage to normal cells; (3) easy to modify. The Mesoporous silica nanoparticles are easy to introduce active groups such as an amino group, a carboxyl group, a mercapto group and the like. These

nanoparticles can be further modified with targeting moieties, dye molecules, proteases, and other biomolecules to achieve specific functions such as cellular targeting and labeling (Mai and Meng 2013; Pandey et al., 2014); (4) various drug release mechanisms can be constructed to achieve controlled and specific release of drugs (Li et al., 2012; Slowing et al., 2010; Wu and Yamauchi 2012).

3. Gold nanomaterials

Gold nanomaterials, including gold nanospheres, nanorods, and nanocages, have been extensively applied in cancer treatment due to several advantages. Firstly, they possess stable properties (Jahangiri-Manesh et al., 2022; Kalashgrani and Javanmardi 2022; Li et al., 2022) and can be easily modified with functional molecules through gold-sulfur bonding. This reaction is simple, convenient, and easy to operate (Yang et al., 2022; Yang et al., 2022). Secondly, their optical properties can be adjusted through surface plasmon resonance effect, where the maximum absorption peaks of gold nanospheres and gold nanorods regularly change based on size and length-diameter ratio. Gold nanospheres and nanorods can be selectively used as fluorescence quenching agents, exhibiting excellent quenching effects (Doghish et al., 2022; He et al., 2022). Thirdly, gold nanospheres, nanorods, and nanocages can efficiently convert light energy into heat, making them ideal for photothermal therapy of cancer (Chow 2022; Chuang et al., 2022). Gold nanorods can serve as contrast agents in magnetic resonance imaging and two-photon emission imaging (Al-Khedhairy and Wahab 2022; Aldahhan et al., 2022).

4. Liposomes

Liposomes are vesicle-like nanostructures formed by a lipid bilayer. Liposome is generally used as a carrier for chemotherapeutic drugs or exogenous genes to deliver drugs and genes for chemotherapy and gene therapy (Zhao et al., 2022; Zhu et al., 2022). It has the following advantages: (1) liposome nanomaterials are mostly formed by phospholipid molecules, and have good biocompatibility (Wang et al., 2022; Yasuoka et al., 2022), low immunogenicity and biodegradability; (2) having good membrane permeability and can be rapidly taken up by cells (Nikolova et al., 2022; Shen et al., 2022); (3) high loading capacity as a drug and gene carrier; (4) surface modifications such as targeted modification and fluorescent labeling can be performed. At present, liposome nanomaterials have entered the clinical research stage. For example (Liang et al., 2022; Mukherjee et al., 2022), treating liver cancer, breast cancer with breast recurrence, colorectal liver metastasis, and bone metastasis tumor treated by liposome-coated chemotherapy drug doxorubicin has entered the second stage of clinical research (Ashrafizadeh et al., 2022; Cao et al., 2022; Hussein and Abdullah 2022).

5. Magnetic nanomaterials

Magnetic nanomaterials are mainly magnetic iron oxide nanomaterials (Curcio et al., 2023; Diwakar et al., 2023; Yang et al., 2022). The most important

application of magnetic nanoparticles is achieving magnetic targeting in the body (Toro-Córdova et al., 2022; Wang et al., 2022; Włodarczyk et al., 2022). Based on this, the magnetic nanomaterials can rapidly respond to an external magnetic field and a magnetic signal, so the magnetic nanomaterials have the advantage of easy separation and purification in the preparation process, and the magnetic targeting function (Kumar et al., 2022; Lin et al., 2022; Mohsin et al., 2022) and the controllable drug release of magnetic response as well as the magnetothermal property in an alternating magnetic field can be used for thermal therapy of cancer (Eslami et al., 2022; Huang et al., 2022).

6. Rare-earth metal upconversion nanomaterials

The upconversion luminescent material follows the anti-stokes law, that is, it absorbs low-energy excitation light and emits high-energy emission light (Naher et al., 2023; Zhang et al., 2022; Zhang et al., 2022). At present, the main matrix of upconversion materials is generally Sodium yttrium fluoride ($NaYF_4$), which is internally doped with rare earth ions, such as Yb^{3+} as a sensitizer and Er^{3+} and Tm^{3+} as an activator (Zhang et al., 2022; Zhang et al., 2022; Zhang et al., 2022). Upconversion nanomaterials are mainly used for photodynamic cancer therapy because traditional photosensitizers' molecular excitation light is generally ultraviolet or visible light, with poor penetration ability. They can only be applied to surface, esophageal, and oral cancers and can do nothing for tumors in deep tissues (Ding et al., 2022; Ding et al., 2022; Gerelkhuu et al., 2022). The upconverted nanomaterials can be excited by near-infrared light to emit ultraviolet or visible light, and combine with photosensitizer molecules to realize photodynamic therapy excited by near-infrared light and effectively solve the problem of light penetration. Moreover, the wavelength of the emitted light of the upconversion nanomaterials can be adjusted by doping different rare earth ions to meet different requirements (Bing-Shuai et al., 2022; Chintamaneni et al., 2022).

7. Semiconductor nanomaterials

Semiconductor nanomaterials have unique optical and electrical properties (Yin et al., 2022; Zhang et al., 2022). For example, titanium dioxide and carbon nitride nanomaterial can generate electron-hole separation under that illumination condition, and then can react with wat and oxygen to generate a large amount of active oxygen for photodynamic therapy of cancer (Qi et al., 2022; Wang et al., 2022; Wei et al., 2022). Nanomaterials such as copper sulfide, tungsten oxide, and black phosphorus can absorb near-infrared light to generate heat for photothermal treatment of cancer (Hu et al., 2022; Li et al., 2022; Li et al., 2022).

8. Carbon-based nanomaterials

Carbon-based nanomaterials mainly comprise carbon nanotubes (Lai et al., 2023; Pandey and Chauhan 2023; Wang et al., 2022) and graphene nano material (Mazzaglia and Piperno 2022; Salve et al., 2022; Tang et al., 2022).

Carbon nanotubes are one-dimensional tubular carbon nanostructures, divided into single and multi-walled carbon nanotubes. Graphene is a two-dimensional nano-flake structure consisting of a single layer of carbon atoms separated from graphite material. They mainly have the following advantages: (1) good stability, high biocompatibility, and no biological activity (He et al., 2022; Kang et al., 2022; Kearns et al., 2022); (2) carbon nanotubes and graphene have larger specific surfaces (Azevedo et al., 2022; Fahmy et al., 2022).

2.2.2 The bottleneck of the development of antitumor nanodrugs

The ultimate goal of nanodrug delivery is the presentation of small molecule active drugs into the interior of tumor cells. Take intravenous administration as an example; to exert the efficacy after intravenous administration, the drug enters into the tumor cells and undergoes five steps: blood circulation, which accumulates in the tumor tissue through the leakage of blood vessels, permeates from the tumor tissue to the tumor cells, is ingested by the tumor cells, and finally releases the drug in the cells (Zhao et al., 2020) (Figure. 4). To maximize the overall efficiency of delivery (drugs within tumor cells/injected drugs), each of the above steps must be brought to a higher level, and the inefficiency of any of them will greatly reduce the final effect. For example, Doxil did not improve efficacy, although it reduced toxic and side effects. This is because, although Doxil has a long blood circulation, the accumulation in tumor tissue is much more than small molecule doxorubicin. Still, it stays in the tumor around the blood vessels (Matsumoto et al., 2016), and does not further penetrate the tumor tissue, or reach the tumor cells, therefore, relative to small molecules, its efficacy has not improved.

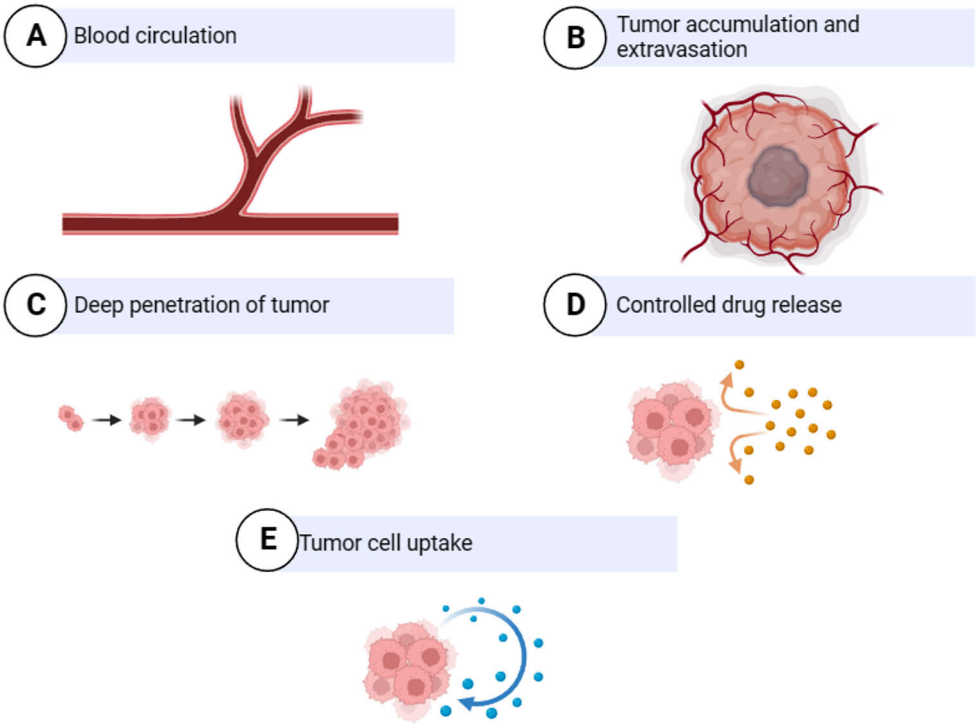

Figure 4. *Intravascularly administered therapeutics encounter serial biological barriers.*

2.2.2.1 Blood circulation

When nanodrugs enter physiological environments such as blood, plasma, and tissue fluid, the body's immune system recognizes these foreign substances and eliminates them through filtration by the kidneys or liver. (Lungu et al., 2019; Zhang et al., 2021). Apolipoprotein and albumin can help the nanoparticles put on the "invisibility cloak", and inhibit their recognition by the mononuclear phagocyte system (MPS). Proteins with specific targeting capabilities can increase nanoparticle aggregation in target organs. Based on the above strategies, we hope to increase the drug delivery efficiency in the blood circulation stage: on the one hand, the interaction between proteins and nanoparticles can be used to reduce the phagocytosis of macrophages and reduce the systemic clearance; on the other hand, the adhesion of proteins with targeting ability (such as transferrin) can be used to improve the positioning of the target by the nano system. The success of albumin-bound violacene lies in that the nano-preparations are coated with a layer of endogenous proteins, which endows them with anti-removal ability and extended blood circulation performance. In addition, the EPR effect of the nanoparticles themselves and the specific combination of albumin and gp60 on tumor cells can also promote the aggregation of the nanoparticles in tumors (Heeke et al., 2019).
Prolonged circulation is a prerequisite for the accumulation of nanomedicines in tumors. A short circulation time is not sufficient to achieve effective drug

accumulation in the tissue (Filipów and Łaczmański 2019). There are many methods to extend the blood circulation of nanodrugs, and the most commonly used strategy is to reduce the adsorption of proteins. The albumin binding method mentioned above uses the endogenous protein HSA wrapped outside the nanoparticles to achieve a long cycle by reducing the uptake of phagocytes. The method of encapsulating drugs with polyethylene glycol (PEG) polymers is another popular strategy. It is generally accepted that PEG is modified on the surface of the nanodrug through covalent bonding, encapsulation or adsorption. This highly hydrophilic polyether chain can establish a barrier between the nano-particles and plasma opsonin to block the adsorption effect, to disguise the nanodrug to escape from the phagocytosis of macrophages, and achieve the purpose of long-term circulation and change its distribution in the body (AlQahtani et al., 2019).

2.2.2.2 Tumor accumulation and extravasation

The influencing factors of systemic perfusion of nanomaterials into tumor tissues are: distorted tumor blood vessels, blood vessels, tumor microenvironment around and nanoparticles themselves. Tumor cells rapidly divide and proliferate, promoting angiogenesis to provide nutrition and oxygen, so the tumor's vascular endothelial cells are not like normal vascular endothelial cells to update once every 1000 days, it can almost double every 10 days (Zhou et al., 2022). Such rapid proliferation results in hasty formation of these vessels with imperfect structures, leaks, and lack of arterioles, venules, and capillaries in the microvessels. The defects of this structure provide a hotbed for EPR effect (Kostarelos 2022). Sufficient blood half-life gives the dynamic jets sufficient time to capture the nanomaterials to improve drug delivery to the tumor tissue. In addition, vascular media such as nitric oxide and angiotensin II can enhance the penetration of tumor blood vessels to achieve high-efficiency extravasation of nanodrugs (Huang et al., 2021). In different stages, the blood viscosity and expansion pressure of the tumor microenvironment around the tumor blood vessels are not identical, or even have significant differences, which also affect the movement of the nanomaterials and the access to the tumor stroma in an invisible manner. We need to further study the mechanism of nanoparticle extravasation into tumor tissue and further improve the design of materials to construct nanocarriers that can achieve efficient tumor aggregation and penetration. The physicochemical properties of nanomaterials can also affect their extravasation and aggregation in tumors to a certain extent. For example, polymer micelles with 30, 50, 70, and 100 nm diameters have similar spillover and anticancer effects in the hypertonic murine colon cancer model. However, in the low permeability model, micelles with a diameter of 30 nm had the most effective tumor aggregation (Hua et al., 2021; Peng et al., 2020; Zhou et al., 2020). This study shows that the heterogeneity of tumors has a very important impact on the anticancer efficacy. Compared with nanospheres, some nanostructures with elongated morphology (such as nanowires and nanorods

are more conducive to achieving the aggregation of nanomaterials in tumors (Ghimire et al., 2020; Vu et al., 2019).

2.2.2.3 Deep penetration of tumor

The aggregation of nanoparticles in the tumor is very important. The deep and uniform penetration of the loaded chemotherapeutic drugs into the tumor tissue is also crucial to achieve the optimal therapeutic effect. The particle size and binding affinity can affect some macromolecules' diffusion kinetics (Peng et al., 2022; Wang et al., 2023; Xu et al., 2021) and deep penetration (such as dextran and antibody). The tissue infiltration after the antibody with higher affinity combines with the target antigen on the tumor is not as good as the tissue infiltration after the antibody with lower affinity identifies with the same target antigen (Huang et al., 2021; Lin et al., 2021; Wan et al., 2021). This is because low-binding antibodies can penetrate deep tissues through target antigens, while high-binding antibodies are directly internalized by binding to antigens too tightly. Therefore, we should weigh the advantages and disadvantages of deep tumor infiltration and high cell uptake in the material design process. After all, the nanomaterials are much larger than the antibodies. Due to the inherent physiological barrier of the tumor microenvironment, the nanodrugs are very easily trapped in the extracellular matrix of the tumor microvessels. The physiological barriers of tumor microenvironment include collagen fibers and some tight interstitial stroma composed of proteins, abnormal blood vessels and elevated interstitial fluid pressure caused by lack of functional lymphatic vessels in the deep layer of tumor tissue (Xiong et al., 2020). These natural barriers reduce the efficiency of nanoparticle conduction from the vessel wall to the tumor stroma. In addition, tumor-related giant thiazole cells have non-specific cellular uptake of nanomaterials and negatively affect the diffusion of nanomaterials (Cheng et al., 2020). One of the solutions to overcome the delivery bottleneck is to regulate the physicochemical properties of the nanomaterials so that they can penetrate the diffusion barriers of the interstitial tumor matrix. The nanomaterials with small particle size can stably diffuse across the tumor tissue, and its specific surface area is large. The particle size of the nanodrug cannot be too small, and when the particle size is less than 5 nm, it will be quickly cleared by the kidney. Tumor-targeting punch-through peptides may also enhance deep delivery of the nanodrug to the solid tumor. Nanorods (15 nm x 54 nm) have a better effect on deep tumor penetration than nanospheres with a size of 35 nm, because the nanorods have a lower dimension (Cheng et al., 2020). We can design materials to make them more adaptive to the tumor microenvironment and try to change the tumor microenvironment to serve the materials. For example, the interstitial components are reduced by degrading the extracellular matrix of the tumor and inhibiting the activity of tumor-related fibroblasts, thereby weakening the restriction of the intercellular matrix on the penetration of nanomaterials, which can also help the nanodrugs to achieve the goal of deep penetration into tumor tissues (Feng et al., 2019).

2.2.2.4 Tumor cell uptake

The active sites for drug uptake by tumor cells are typically located intracellularly, especially for prodrug-type medications. Target cells must fully internalize and efficiently release the active drug within the cell to exert the drug's biological activity (Zhao et al., 2020). One of the ways to improve cell uptake is to modify the nanoparticles with targeting ligands (Wang et al., 2020). Unlike EPR effect, active targeting can actively cross physiological barriers such as intestinal mucosa and blood-brain barrier to enhance the accumulation of nanodrugs in tumors. Due to its unparalleled advantages, there have been clinical examples of active targeting. For example, liposomes with targeting ability can also regulate the uptake behavior of nanodrugs by cells by adjusting the size and shape of nanoparticles. After the nanomaterials are ingested by cells, the loaded prodrugs must be released to reach the target by diffusion. Or by intracellular pathways to the appropriate subcellular organelles. Lysosomal escape of nanoparticles is critical for the intracellular delivery of prodrug. Cationic liposomes and cationic polymer-based nanocarriers have great potential for drug delivery (Zhong et al., 2019). However, their lysosomal escape efficiency is still very low. Therefore, designing nano-sized preparations with higher lysosomal escape efficiency is urgent. The research on targeted organelles (nucleus, mitochondria, endoplasmic reticulum and Golgi apparatus) is also underway in an orderly way (Mayer et al., 2019). Many articles have confirmed that specific organelles can indeed ingest nanoparticles. However, exploring potential obstacles to organelles/membranes is insufficient and further research is needed.

2.2.2.5 Controlled drug release

The effective anticancer components it carries after reaching the tumor microenvironment may not be enough. To achieve optimal anticancer effects, the pharmacokinetics (PK) of nanoparticles, their permeability to tumor tissues, and the release of stimulation-responsive drugs need to be optimized. This requires an in-depth understanding of the relationship between several complex parameters, including nanoparticle PK and small molecule drug PK, encapsulated and released drugs in plasma, maximum blood concentration (Cmax) and maximum concentration of nanoparticles in blood after a single dose administration, and the drug-time curve (AUC) of small molecule drugs and AUC of nanoparticles. Traditional small molecule drugs reach their Cmax soon after intravenous infusion, followed by slowly decreasing drug concentrations. After intravenous administration of the nanodrug, it takes a period for the released small molecule drug to reach its Cmax. Therefore, Cmax is not accurate for evaluating the toxicity of nanodrugs. The AUC of small-molecule drugs and nanodrugs in tumors are very different, mainly because the EPR effect greatly enhances the aggregation of nanodrugs in tumors, and then the small-molecule drugs are released at tumor targets, resulting in high drug concentration in tumor areas (Bayer 2020; Zhao et al., 2019). Many studies have shown that nanodrugs can significantly improve the Cmax, PK and AUC of

drugs in tumor areas compared with traditional small-molecule drug delivery. However, drug enrichment in the tumor area did not improve the patient's survival. This involves whether the drugs can be released in the tumor cells and whether the released drugs can play a role in treating tumors. One of the ways to regulate the drug release is to construct an intelligent nanodrug loading system with stimulation response. These nanosystems can respond to the characteristics of the tumor microenvironment, or can be activated by external stimuli to release their loaded drugs. To some extent, external stimuli can regulate the release behavior of drugs in time and space, and they are more widely used (Lu et al., 2019; Sun et al., 2019).

2.3. Design of nano prodrug

To enhance the circulation time of nano prodrug in the body, some polymers such as PEG or HA are commonly used in the design of nano prodrug. Drugs are directly connected to the polymer through chemical bonds or physically embedded in polymer nanoparticles. In order to respond to the functional requirements of the internal environment and avoid early release of antitumor drugs during circulation in the body, chemotherapy drugs are typically modified by chemical bonds that respond to the biological microenvironment, such as disulfide bonds, diselenide bonds, etc., to achieve drug release under various conditions (Noor et al., 2023; Shen et al., 2022). Compared with normal tissues, tumor tissues have special physiological structure and physicochemical property differences, including vascular insufficiency, weakly acidic tumor tissue, higher temperature than normal tissue, specific overexpression of some enzymes, and low tissue oxygen content (Masserini 2013). The microenvironment in tumor cells differs from that of normal cells, which mainly includes high GSH content in most tumor cells, overexpression of some enzymes, and high concentration of H_20_2 in mitochondria. Among them, the acidic environment (pH 4.5-6.5) of lysosomal inclusions in tumor cells is often used to achieve drug release (Zhang, 2021) (Figure. 5).

In recent years, multiple smart response type nanodrug delivery vehicles (Mustafa et al., 2023) and cancer cell targeting have become major research hot spots. The nanodrug delivery system with multiple stimulation responses can simultaneously coordinate environmental stimulation (Hoare and Pelton 2004; Nakayama et al., 2011) substances of the nano particles in different stages, overcome multiple physiological barriers encountered by the nano particles in the delivery process, and realize efficient targeting and controllable drug release (Da 2020; Klochkov et al., 2021).

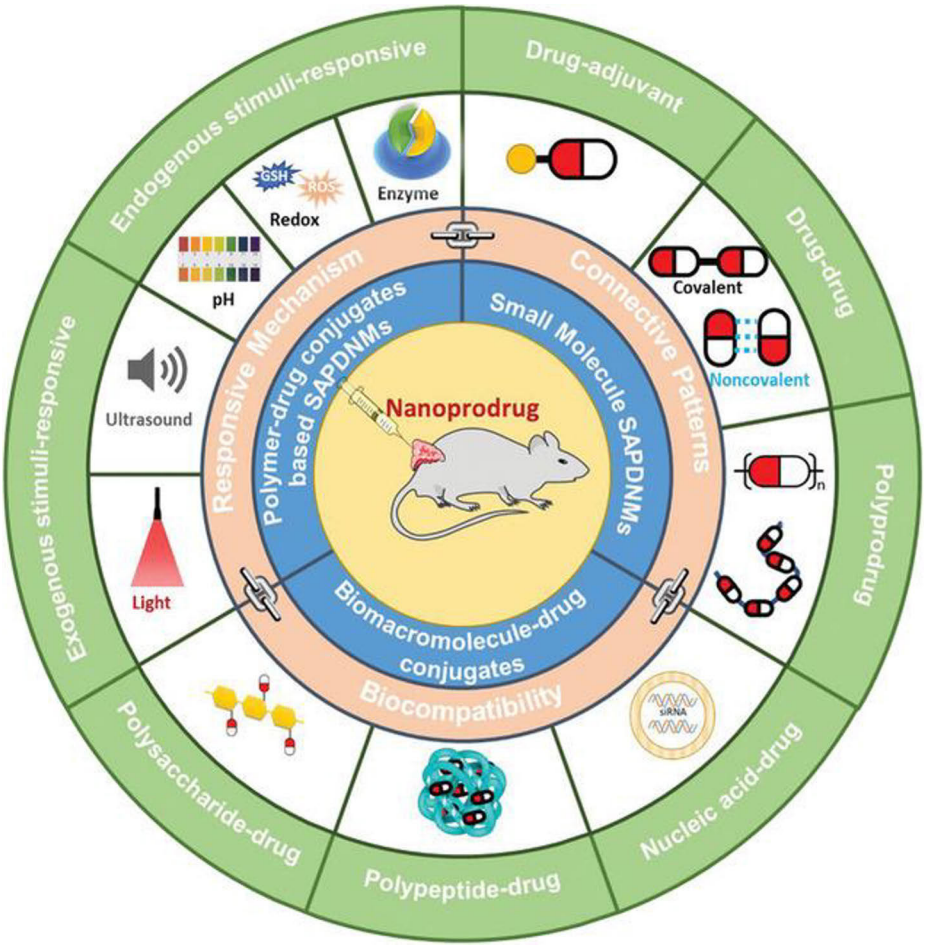

Figure 5. *Schematic illustration for multi functionalized nano prodrug (Copyright 2021, John Wiley & Sons)*

2.3.1 Nano prodrug targeting

The application of nanoparticles in tumor treatment has gradually become a hot topic. One of the main reasons is that the drug-loaded nanoparticles can realize the targeted delivery of drugs in tumor tissues. The targeting of nanoparticles in tumor tissues can be divided into two major categories: passive targeting and primary targeting. Passive targeting mainly refers to the EPR effect of nanoparticles in tumor tissue. Active targeting refers to modifying specific ligands on the surface of nanoparticles to identify the overexpression of receptors on the surface of tumor cells, thereby increasing the internalization of cells through receptor-mediated endocytosis (Sushnitha et al., 2020).

2.3.1.1. Passive targeting

Initially, the nanodrug-loaded particles were passively targeted to the tumor tissue mainly through the tumor vascular imperfection. The particle size, morphology and surface charge of the passive targeting is mainly affected by the nanoparticles., the size of nanoparticles is a key factor affecting passive targeting. The nanoparticle size in the range of 5 to 200 nm is considered the optimal particle size range for the passive targeting of nanoparticles to tumor tissue (Alavi et al., 2019; Attia et al., 2019; Bertrand et al., 2014). If the particle size is too small, it will be filtered by the glomerulus, while if size is too large, it cannot enter the tumor tissue through the tumor blood vessels (Bazak et al., 2014; L Arias 2011; Perrault and Chan 2010). Despite the fact that the EPR targeting theory has been widely used in preclinical studies, it appears to be very ineffective in more complex and larger systems such as the human body. Therefore, active targeting will become a research goal for nanomedicine.

2.3.1.2 Active targeting

Active targeting, also referred to as ligand-mediated targeting, involves the modification of nanoparticles with ligands such as antibodies, nucleic acid aptamers, polypeptides, polysaccharides, or cell membranes. This modification enables the nanoparticles to be specifically recognized by tumor cells that overexpress the corresponding receptors, thus achieving high specificity. Targeted molecular strategy is an important mechanism for intracellular endocytosis (Stine et al., 2022; Yang et al., 2020). The nanoparticles enter the tumor tissue through EPR action and are endocytosed by tumor cells through targeted molecular mediation. Among many ligands, folic acid is a small molecule with carboxyl group. Folate receptors are overexpressed on the surface of tumor cells, while they are scarcely expressed or expressed in small amounts in normal cells. Folate receptors can serve as targets for tumor identification and targeted delivery of anticancer drugs. Due to its simple structure, it can be easily grafted onto nanoparticles, making it the most widely studied one. Arginylglycylaspartic acid (RGD) protein is another widely used ligand that specifically binds to overexpressed receptors on the surface of tumor cells. The latest cancer targeting strategy involves encapsulating nanoparticles with various biological membranes, leveraging the abundant protein characteristics found on different biological membranes to achieve in vivo circulation and tumor targeting (Bazak et al., 2015; Kievit and Zhang 2011; Pearce and O'Reilly 2019). Currently, although active targeting strategies have made some progress, there are still many challenges waiting for researchers to explore due to the lower targeting efficiency (Figure. 6).

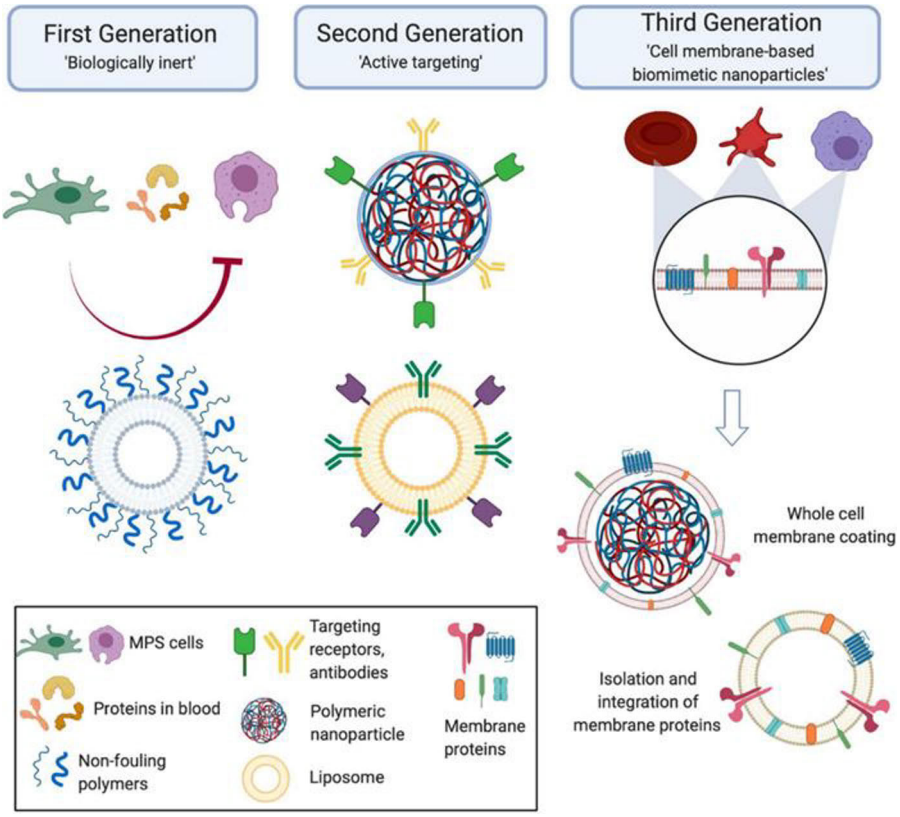

Figure 6. *Schematic illustration for targeting strategies of nanoparticles in different periods (Copyright 2020, Frontiers Media SA)*

2.3.1.3 Organelle targeting

The ligands targeting the tumor cells are beneficial to increasing the endocytosis of the tumor cells on the nanoparticles, better accumulating drugs to the tumor tissue and reducing the toxicity of the nanoparticles. Despite these advantages of targeting tumor cells, the results of further enhancing the activity of antitumor drugs have not been satisfactory (Liew et al., 2021; Zhan et al., 2022; Zheng et al., 2021). Many drug delivery systems assume that the internalization of regulatory cells or even cytoplasm is required to ensure the interaction between drug molecules and action targets, relying on the simple diffusion of drug molecules into organelles and their random interaction with organelles. This results in that some drug molecules must have sufficient metabolic stability before finally interacting with organelles, but not all drug molecules can meet this requirement. Therefore, solving the subcellular assignment of drug molecules can more effectively enhance the antitumor effect of drugs (Chen et al., 2021; Li and Huang 2020; Wang et al., 2020). The emergence of organelle-targeted nanodrug-loaded particles has become a new focus of targeted delivery research. Some methods for targeting organelles are to chemically graft anticancer drugs onto organelle-targeting ligands. Cell

penetrating peptides and triphenylphosphine cation (TPP) were all good organelle targeting ligands. However, not all drugs can graft organelle-targeting ligands in this way and do not change the antitumor activity of the drugs; more organelle-targeting is achieved by grafting the organelle-targeting ligands on the surface of the nanoparticles (Chen et al., 2019; Gao et al., 2019; Gao et al., 2019; Guo et al., 2020).

2.3.1.4 Mitochondrial targeting

Tumor cell growth requires a lot of energy, and mitochondria mainly produce adenosine triphosphate (ATP) that tumor cells require. Therefore, targeting mitochondria to inhibit ATP production can be an effective strategy for treating cancer. In addition, mitochondria also regulate calcium balance, cell growth and apoptosis, differentiation, and the synthesis and decomposition of secondary metabolites in the body. At the same time, mitochondria store various macromolecules and play an important role in the above physiological processes. Mitochondria also have the feature that mitochondrial DNA (mtDNA) is present in all mitochondria. Therefore, drugs targeting DNA damage, such as DOX and cis-molybdenum, can act on mitochondrial mtDNA and effectively kill tumor cells and cells resistant to traditional chemotherapy drugs. Lin et al. prepared self-assembling nanoparticles with mitochondrial targeting capabilities for precise mitochondrial delivery. Among these, DOX-TPP can release active DOX to disrupt mitochondria. Modifying the nanoparticles with TPP enables mitochondrial targeting within tumor cells. Glycyrrhetinic acid (GA), an extract from licorice, has been reported to interact with the mitochondrial respiratory chain, leading to hydrogen peroxide production and triggering the opening of mitochondrial permeability transition pores (MPTP). This effectively promotes mitochondrial apoptosis within tumor cells, ultimately leading to tumor cell death (Lin et al., 2021)(Figure. 7).

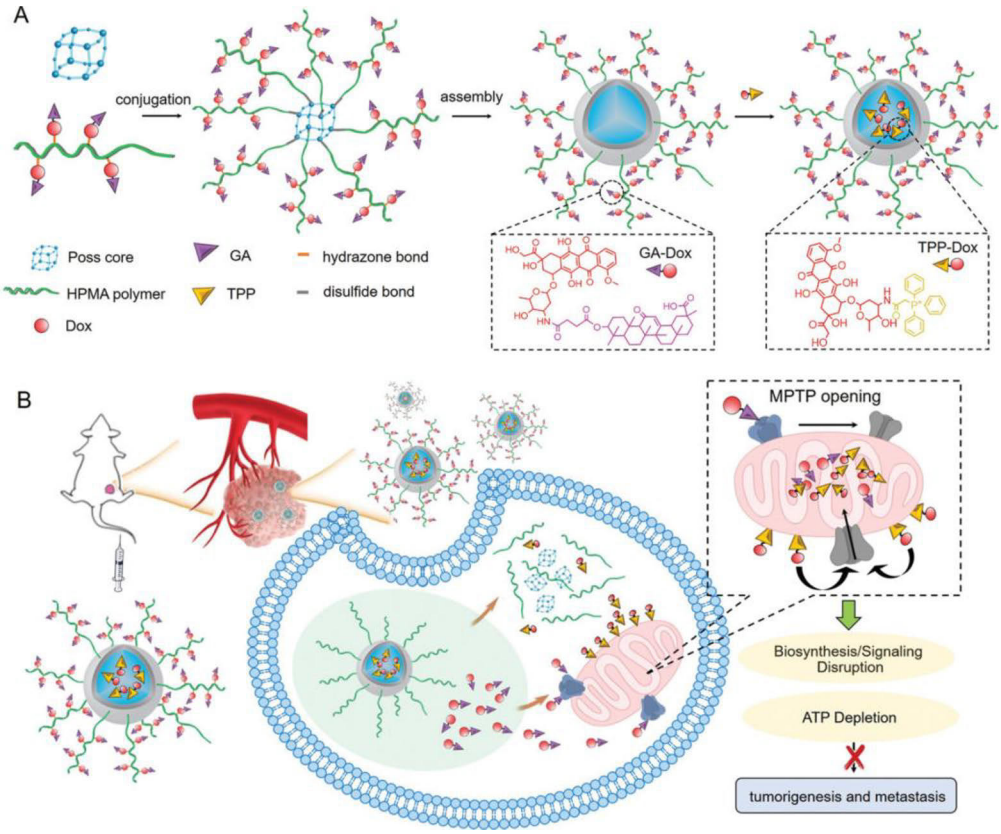

Figure 7. *Schematic diagram of mitochondrial target nanomedicine. (Copyright 2020, John Wiley & Sons)*

2.3.1.5 Endoplasmic reticulum targeting

In the common antitumor treatments, some chemotherapy drugs can cause the immunogenic death of cancer cells due to their unique mechanism of action. The same can be said of the singlet oxygen produced by photodynamic therapy (Li et al., 2022; Shi et al., 2021). One of the markers of immunogenic death, the HMGB1 protein, is stored in the endoplasmic reticulum of cancer cells. Therefore, targeting endoplasmic reticulum as an organelle can effectively promote immunogenic death (Deng et al., 2020; Yuan et al., 2019; Zhou et al., 2020). Li et al. encapsulated indocyanine green (ICG) into ER-targeting pardaxin (FAL) peptides modified hollow gold nanospheres. that could target the endoplasmic reticulum. These nanoparticles can be specifically accumulated in the endoplasmic reticulum after entering cancer cells. When irradiated with a near infrared laser at 808 nm, ROS will be locally generated in the endoplasmic reticulum to induce ER stress and amplify the immunogenic cell death (ICD) effect, thereby eradicating tumors (Figure. 8) (Li et al., 2019).

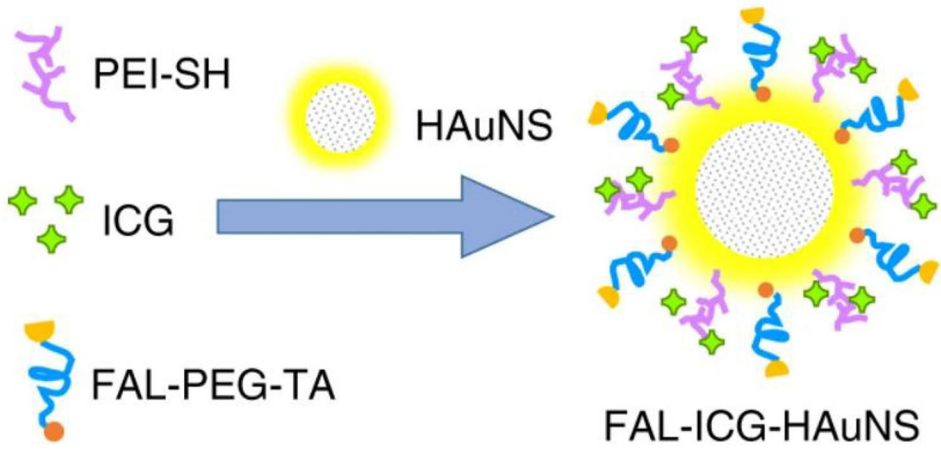

Figure 8. *Schematic diagram of Endoplasmic reticulum nanomedicine. (Copyright 2019, Springer Nature)*

2.3.2 Tumor microenvironment response type nano prodrug delivery systems

The triggering reactions of these vehicles are often used to control the controlled release of bioactive substances in time and space, or even to obtain more complex functions, such as regulating tissue infiltration and internalization. The chemical linkage mainly provides controlled drug release performance. At the same time, the responsive polymer backbone is often designed to adjust physical and chemical parameters, such as solubility, stability, conformation and hydration radius. Changes in physiological parameters are often important markers for different types of diseases. Due to the rapid proliferation of tumor cells, the expression levels of related factors in tumor sites are significantly different from those in normal tissues. Therefore, specific tumor microenvironment characteristics (such as acidosis, hypoxia and enzyme imbalance) are used to design endogenous stimulation-responsive nanodrug delivery vehicles for tumor targeted drug delivery. For biological systems, stimulation factors can be roughly divided into internal stimulation (pH, GSH, ROS, ATP, enzyme, etc.) (Bai et al., 2019; He et al., 2020; Hou et al., 2021; Li et al., 2020; Ma et al., 2023; Mirhadi et al., 2020; Shi et al., 2020) and external stimulation (such as light, ultrasound, electric field, magnetic field, and temperature)(Peng et al., 2022)(Figure. 9).

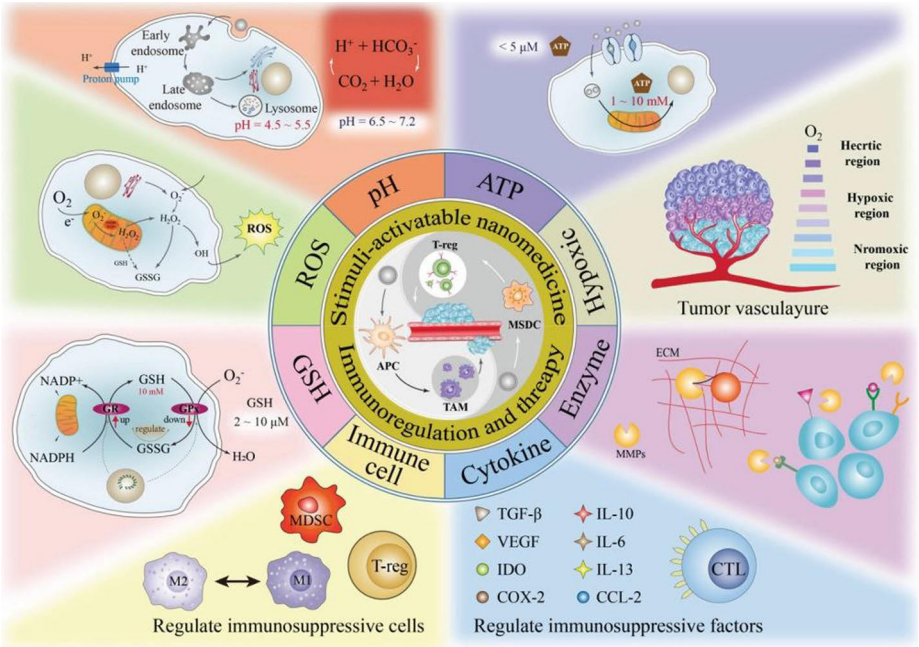

Figure 9. *Schematic diagram of tumor microenvironment response nanomedicine. (Copyright 2021, John Wiley & Sons)*

2.3.2.1 pH-responsive nano prodrug delivery systems

Due to tumor cells' rapid proliferation, tumor tissue pH is always weakly acidic. The pH in the extracellular matrix of normal tissues and blood is stable at about 7.4, while the pH in the extracellular microenvironment of the tumor cells is 6.5–7.2. When the nanodrug delivery vehicle is internalized by adsorption pinocytosis or receptor-mediated endocytosis, it is confined to a pinocytic vesicle, forming an unfavorable environment. After entering the cells, the vector would first encounter the endosome with pH 5.0-6.0, and then encounter the lysosome and multiple enzymes with pH 4.0-5.0 (He et al., 2021; Mu et al., 2021). Therefore, acid-unstable chemical bonds (such as hydrazone bonds, acetals, orthoesters, imines, oximes, and so on) or ionizable groups are often used to design pH-responsive nanodrug delivery vehicles to promote the rapid release of drugs within tumor cells or enhance internalization of drugs within tumor cells (Gannimani et al., 2020; Zhang et al., 2020). pH changes associated with pathological states have been widely used to trigger drug release (Liang et al., 2019; Sun et al., 2019) to specific lesion sites (such as the gastrointestinal tract, vagina, and tumor tissue) or cell lumens (cytoplasmic matrix, lysosome, mitochondria, and endoplasmic reticulum).

2.3.2.2 Redox response type nano prodrug delivery systems

Due to the strong metabolism in tumor cells, many reducing substances (such as divalent iron ions, cysteine, and thioredoxin reductase) are produced in tumor cells. Among them, GSH is abundant in the form of free mercaptan in

cells, which can produce a highly reducing tumor microenvironment and protect cells from free radical-induced oxidative damage (Kumar et al., 2020; Li et al., 2020; Tian et al., 2021). The concentration of GSH in tumor cells is about 2-10 mM, while that in normal cells is only 2-20 μM (Luo et al., 2019; Qu et al., 2019). Taking advantage of the difference between the concentration of reducing substances in cancer cells and normal cells, linking bonds with reduction responses has been widely used to design tumor-targeted drug delivery vehicles and nano prodrug with reduction responses, such as disulfide bonds, borate bonds, and double selenium bonds (Liu et al., 2019). Liu et al reported this redox-responsive Selenocystamine-modified mesoporous silica nanoparticle (MSN-SS-CEL) system through disulfide bonds. they employed poly β-cyclodextrin (PCD) as a gatekeeper to seal doxorubicin (DOX) inside the pores of MSNs, resulting in the desired nano-system (MSCP). The MSCP nano-system can efficiently deliver both of these molecules to the tumor site and release the active drug within the tumor tissue (Liu et al., 2019)(Figure. 10).

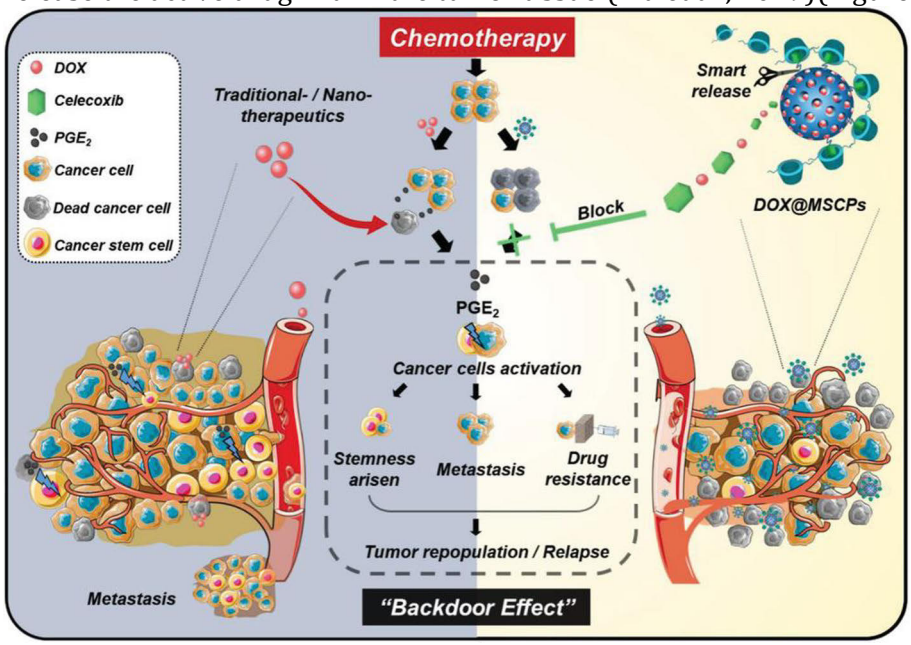

Figure10. *Schematic diagram of redox-sensitive nanoparticles (Copyright 2019, John Wiley & Sons)*

2.3.2.3 ROS-responsive nano prodrug delivery systems

Reactive oxygen species (ROS) are a group of organisms that contain various highly oxidative substances, including H_2O_2, O_2, and NO (Yang et al., 2020; Zhu et al., 2020). A study has shown that 90% of intracellular ROS are derived from mitochondria (Na et al., 2020; Xia et al., 2020). Under normal circumstances, intracellular ROS is in a very low balance state. However, in many tissues such as tumors, inflammation, and chronic diseases, the level of ROS in mitochondria is much higher than in normal tissues (Chu et al., 2020; Ding et al., 2020). A large amount of ROS will damage cell DNA, protein and lipids (Jin et al., 2019).

ROS-based cancer treatment often fails to achieve the expected results due to the very short effective cycle of ROS, limited diffusion range and relatively insufficient endogenous ROS levels in cells. In recent years, using excessive ROS in tumor cells as a trigger point for drug release to design ROS-responsive nanodrug delivery vehicles for controlling the drug release rate and targeting cancer therapy has aroused great interest (He et al., 2019).

Drug-loaded sulfide-containing polymers can be oxidized to sulfoxides or even sulfones by reactive oxygen species, resulting in the cleavage of the polymers or vesicles, which release the loaded drugs. In recent years, various functional materials targeting subcellular organelles have also played an increasingly important role in tumor treatment. By specifically destroying the function of organelles, they can not only have fatal effects on cells, but also reduce the random diffusion and efflux of drugs in the cytoplasm. Subcellular organelle compartments had stronger drug retention effect and could effectively increase drug concentration. For example, Hao et al. developed an active oxygen-responsive prodrug nanoparticle system loaded with Pt nanoparticles, which enhances the efficacy of PDT therapy. Under 660 nm laser irradiation, this prodrug generates ROS and controls the release of camptothecin (CPT) within the prodrug. Additionally, Pt nanoparticles can catalyze hydrogen peroxide (H2O2) within cancer cells to generate oxygen for alleviating the hypoxic conditions in tumor tissue, thereby enhancing the efficiency of PDT (Hao et al., 2020) (Figure. 11).

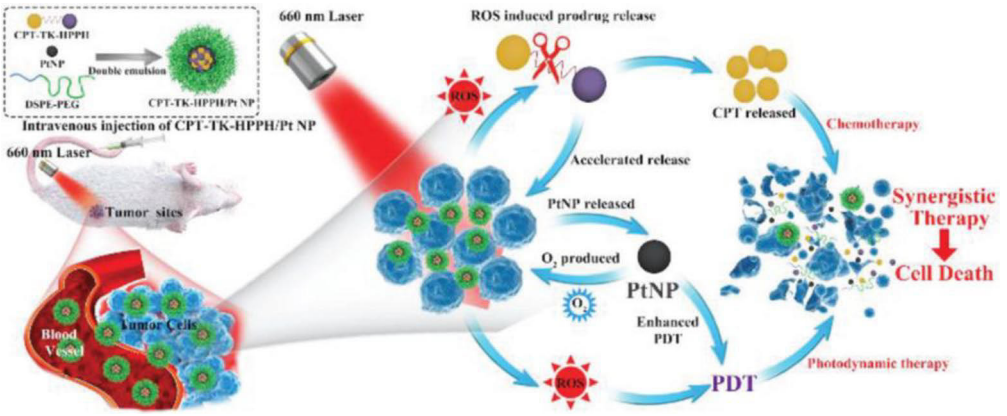

Figure 11. *Schematic diagram of ROS-sensitive nanoparticles (Copyright 2020, John Wiley & Sons)*

3. Objectives of the work

Although traditional chemotherapy drugs such as paclitaxel (PTX) and doxorubicin (DOX) have broad-spectrum antitumor activity and stable efficacy, they still have several drawbacks. These include severe toxicity and side effects on normal cells and tissues during blood circulation, inadequate selectivity, poor water solubility, and the development of resistance with long-term use. To address these issues, we propose designing PTX and DOX as prodrugs to overcome the aforementioned limitations. Prodrugs, by bridging reactive chemical bonds between two functional groups, significantly enhance the stability of drug molecules in the bloodstream compared to physically encapsulated drugs, reducing non-specific drug release behavior. Moreover, prodrugs can rapidly degrade under specific tumor microenvironment conditions, facilitating efficient release of free drug molecules. This can effectively reduce the toxic side effects on normal tissues and organs while achieving efficient drug accumulation at the site of the lesion, consequently enhancing the therapeutic efficacy. Furthermore, due to the high chemical modifiability of prodrugs, there is a wide range of formulation possibilities. For example, prodrug molecules can be designed for simultaneous delivery of two drugs, effectively overcoming the resistance to single drugs. Alternatively, chemotherapy drugs can be chemically conjugated with photosensitizers for combination therapy involving chemotherapy and photodynamic therapy. Regarding the carrier design for prodrugs, we can not only use microfluidic techniques to prepare self-assembled prodrug nanoparticles but also explore the modification of prodrugs onto organic polymers or inorganic carriers. Subsequently, these nanoparticles can be further modified using tumor cell membrane camouflage techniques to achieve tumor cell targeting. In summary, the objective of this study is to construct a series of tumor microenvironment-responsive prodrug nanomedicines based on the anticancer drug paclitaxel and thoroughly explore the different formulation approaches and *in vitro* antitumor performance of these prodrugs.

4. Materials and methods

This section outlines the materials and synthetic methods utilized in the thesis work. The materials section provides a comprehensive overview of the main materials involved in the synthesis of prodrugs and modified MSNs. The methods section highlights the key characterization techniques employed. For a more detailed account of the experimental procedures, please refer to the relevant sections of Papers I-V. The goal is to provide readers with a thorough understanding of the materials and methods utilized in the research presented in this thesis.

4.1. Materials

All chemicals used in this study were purchased from well-known commercial suppliers such as Sigma-Aldrich, Abcam, Novex, and VWR. No additional purification steps were performed before their use in the experiments.

4.2. Preparation approaches

4.2.1. Synthesis of prodrug

Synthesis of PTX prodrugs (I, II, III, IV)

To synthesize the pure intermediate, a mixture of PTX (2.0 g), dithiodipropionic anhydride (DTDPA) (590.94 mg), (3-dimethylaminopropyl) ethyl-carbodiimid monohydrochloride (EDCI) (537.02 mg), and 4-dimethylamino-pyridine (DMAP) (343.36 mg) was added to 40 mL of dichloromethane and stirred for one night. The final mixture was purified by silica gel column chromatography, which provided the desired intermediate with a yield of 58.8%.

Synthesis of PTX and DOX prodrugs (I)

The synthesis of PTX-S-S-DOX involved the use of amide coupling. Initially, DOX (0.28 mmol), PTX-S-S-COOH (0.2 mmol), EDCl (0.28 mmol), and triethylamine (TEA) (39.1 µl) were dissolved in DMSO. The reaction mixture was stirred overnight, followed by removal of DMSO through lyophilization. The residue was purified using silica gel column chromatography to yield 56% red powder of the desired product.

Synthesis of PTX and CPT prodrugs (II)

To synthesize the final product, PTX-S-S-COOH (0.24 mmol), CPT (0.285 mmol), 4-dimethylaminopyridine (0.05 mmol), and N, N′-dicyclohexylcarbodiimide (0.285 mmol) were dissolved in DMSO. After stirring overnight, the DMSO was removed by lyophilization, and the resulting residue was purified using silica gel column chromatography to yield yellowish pure products with a 59.7% yield.

Synthesis of PTX and THPP prodrugs (III)

The target compound was synthesized by dissolving 6,6',6'',6'''-((porphyrin-5,10,15,20-tetrayltetrakis(benzene-4,1-diyl)) tetrakis(oxy)) tetrakis(hexan-1-ol) (THPCC6-OH) (0.18 mmol), PTX-S-S-COOH (0.92 mmol), EDCl (0.92 mmol), and DMAP (0.38 mmol) in 40 mL of anhydrous methylene chloride and stirring

the resulting mixture at 25°C for 2 days. The residue was purified using silica gel column chromatography.

4.2.2. Synthesis of Modified MSNs

Preparation of AuNRs (IV, V)

The synthesis process involves the following steps:
1. Mixing a 0.1 M hexadecyl trimethyl ammonium Bromide (CTAB) solution (3.75 mL) and a 0.01 M $HAuCl_4$ solution (0.125 mL) for 5 min to form gold seeds. 2. Adding a rapid injection of 0.01 M $NaBH_4$ solution (0.3 mL, ice-cold) to the mixture under vigorous stirring to form gold seeds. 3. After 4 hours, stirring a solution containing 0.1 M CTAB (200 mL), 0.01 M $HAuCl_4$ (10 mL), 0.01 M $AgNO_3$ (2.4 mL), and 1 M HCl (3.8 mL) at 30°C for 10 min. 4. Adding 0.1 M ascorbic acid (2 mL) quickly to the growth solution, which immediately turned colorless. 5. Adding the gold seeds solution (0.48 mL) and stirring for 5 min, followed by an overnight standing.

Preparation of Au@MSNs (IV)

1. A purified solution of AuNRs was prepared. 2. Aqueous CTAB solution (1 mM, 50 mL) was added to the AuNRs solution. The pH was adjusted to 10-11 with 0.1 M NaOH. 3. A 20 v/v% TEOS ethanol solution (0.33 mL) was added to the mixture. 4. The reaction mixture was stirred overnight at 30 °C. 5. The resulting Au@MSN NPs were collected by centrifugation at 13,000 rpm for 10 minutes. 6. The collected NPs were washed with 0.6 wt% ammonium nitrate (NH_4NO_3) ethanol solution to remove the CTAB. 7. The activated modification of APTES in ethanol was carried out overnight. 8. The final product, Au@MSN-NH_2 NPs, was obtained (Zhang et al., 2012).

Preparation of Au@PTXSS-MSN/DOX@CM (IV)

The synthesis process involved adding Au@MSN-NH_2 NPs and PTX-SS-COOH to a solution of dichloromethane, using DMAP and EDCI as catalysts, and stirring the mixture overnight. After the reaction, the NPs were washed with dichloromethane. Next, Au@PTXSS-MSN NPs and DOX were mixed and stirred overnight in an aqueous solution. The cancer cell membrane extract was then added to the mixture and stirred in an aqueous solution overnight.

Preparation of Au@MSN-Ter/THPP@CM (V)

The cancer cell membrane (CM) was mixed with the tetrahydroxyphenyl porphyrin (THPP) loaded and tosyl ethylenediamine (Ter) modified NPs in MilliQ water at 4°C, and the mixture was stirred overnight. The resulting mixture was then subjected to centrifugation to obtain the desired NPs.

Au@MSN-Ter/THPP@CM@GelMA/CAT microgel preparation(V)

A microfluidic chip with two channels was utilized. The inner channel contained a mixture solution of methacrylic anhydride gelatin (GelMA), photoinitiator, Catalase (CAT), and nanoparticles. The outer channel contained mineral oil with Span 80. Microgels were obtained by the flow of different phases at varying speeds. After UV curing, the microgels were obtained through centrifugation and ethanol washing.

4.3. Characterization methods

4.3.1. Composition and structure analysis

Nuclear magnetic resonance (NMR) analysis

The NMR was measured by Bruker AV-500 NMR, the solvent was $CDCI_3$, and the test temperature was 25℃. NMR used 0.01% tetramethylsilane (TMS) as internal standard.

Mass spectrometric analysis

Linear ion trap (LTQ) mass spectrometer test with electrospray source.

Transmission electron microscopy

The TEM images were acquired using a JEM-1400 Plus TEM microscope (JEOL Ltd., Japan).

Dynamic light scattering (DLS) and zeta-potential

The size distribution and zeta-potential of the nanoparticles were analyzed using a Zetasizer Nano ZS instrument (Malvern Instruments Ltd., UK).

4.3.2. *In vitro* cell studies

Cell proliferation assay for cytotoxicity

The *in vitro* cytotoxicity of the sample was characterized by WST-1 assay. Breast cancer cell line (MDA-MB-231), non-tumorigenic epithelial cell line (MCF-10A), human ovarian cancer cell line (SKOV3), human ovarian adenocarcinoma adherent cell line (OVCAR3) and normal human skin fibroblasts (NHDF) were used to determine the toxicity of different samples. In short, different cells (5×10^3 cells/well) were inoculated in a plate. The samples to be tested were co-cultured with cells for 24 h or 48h respectively. Then WST-1 testing kit was added, co-cultured with cells for 2 hours, and the absorbance was measured by enzyme-labeled instrument.

Confocal laser scanning microscopy (CLSM)

To detect cell uptake of NPs, laser confocal scanning microscope (CLSM) was used. SKOV3 cancer cells were inoculated in a Petri dish at a density of $2X10^5$ cells per well, and cultured for 24 hours to allow cell adhesion. Next, the culture medium was replaced with a fresh medium containing NPs at an appropriate concentration, and the cells were cultured at 37℃ for a specific time. After incubation, the supernatant was discarded, and the cells were washed with PBS buffer. Then, the cells were fixed with 1 mL of 4% paraformaldehyde for 5 minutes, followed by washing with PBS buffer and incubation with 4',6-Diamidino-2-Phenylindole, Dihydrochloride (DAPI). For evaluating lysosomal co-localization, lyso-tracker green was added to stain lysosomes for 1 hour prior to another staining, and the cells were then observed with CLSM (Zhang et al., 2012).

Flow cytometric analysis of cellular uptake

Cancer cells were inoculated into 12-well plates with 1 ml culture medium in each well, and the inoculation density was $2X10^5$ cells in each well, so that the cells adhered to the wall for 24 hours. Then suck out the culture medium and

replace it with NPs solution diluted with medium. The cells were cultured at 37℃ for 2 hours, 4 hours and 6 hours. Subsequently, the supernatant was thrown away, the cells were washed with PBS and digested. The digested cells were dispersed in PBS, then centrifuged (1000 r/min, 5 min) and collected. The above centrifugal cleaning process was repeated three times. Finally, the supernatant was removed, and the cell mass at the bottom was redispersed with 0.5 ml PBS, and then the endocytosis was analyzed by flow cytometry (Rao et al., 2019).

Living/dead cell detection

Inoculate cancer cells in a Petri dish. Then, the cells were co-cultured with different samples for 24 h. Cells were stained with calcein and propidium iodide, incubated at 37°C for 0.4 h, and then observed by CLSM.

Apoptosis

The apoptosis detection kit was utilized to investigate the apoptosis pathway. The cancer cells were incubated with the test sample for 12 hours, then washed with culture medium thrice, and exposed to 650/980 nm NIR laser for 5 minutes. After 12 hours, PBS cleaning, incubated with kit dye at room temperature for 15 minutes. Subsequently, flow cytometry was utilized to analyze the apoptotic cells.

Intracellular detection of O_2• production

Cancer cells were cultured in confocal Petri dishes. The sample to be tested was dissolved in DMEM medium and added to the cells for 12 h. After incubation, the cells were washed with PBS buffer. Next, the medium containing 2',7'-Dichlorodihydrofluorescein diacetate (DCFH-DA) was added, and the cells were exposed to 650 nm laser irradiation for 5 minutes. Finally, cell imaging was obtained using CLSM.

Statistical Analysis

All data were collected from three independent experiments conducted in triplicate. Quantification of confocal images was performed using Image J software. Data analysis and graphical work were carried out using GraphPad and SPSS 20.0 software. A significance level of $P < 0.05$ was considered statistically significant.

4.3.3. *In vivo* evaluation assay

Evaluation of *in vivo* toxicity

The animal experiment protocol was approved by the Research Ethics Committee of Jiangsu University, and was conducted in accordance with the Guidelines for the Care and Use of Laboratory Animals. All mice were subjected to scheduled injections and laser irradiation according to the expected treatment regimen. After 15-20 days of treatment, during which mouse body weight and tumor size were measured, the mice were euthanized at the conclusion of the treatment. Major organs and tumors were removed for various types of histological analysis.

***In vivo* imaging system (IVIS)**

The sample solution was injected intravenously into tumor-bearing mice. Then, the mice were anesthetized at specified time intervals (6, 12, 24 h) and scanned with CRi MaestroTM automatic *in vivo* imaging system (C.R. International Inc. USA).

5. Results and discussion

5.1. Overview of the thesis work

The main objective of this study is to explore the potential of self-assembled prodrug nanoparticles through the chemical bonding of two drugs for delivering drugs and achieving a synergistic therapeutic effect under stimulus response. Additionally, a multifunctional drug delivery system was developed by modifying the MSN matrix material. Moreover, the use of microfluidic technology to encapsulate nanoparticles with GelMa material was investigated to achieve better control over the construction of a drug sustained-release system.

The following workflow was adopted in this thesis:

(I) Preparation of Redox-Responsive Doxorubicin and Paclitaxel Prodrug Nanoparticles for Breast Cancer Therapy Using Microfluidics.

(II) Preparation of Self-assembled Disulfide Bond Bearing Paclitaxel-Camptothecin Prodrug Nanoparticle for Lung Cancer Therapy.

(III) Preparation of Porphyrin Centered Paclitaxel Tetrameric Prodrug Nanoassembliesas Tumor-Selective Theranostics for Synergized Breast Cancer Therapy.

(IV) The Combination of Photothermal Therapy, Prodrug, and Tumor Cell Camouflage Technology Applied to MSN Carrier For the Treatment of Triple-Negative Breast Cancer.

(V) Minimally Invasive Injection of Biomimetic Nano@Microgel for In Situ Ovarian Cancer Treatment Through Enhanced Photodynamic Reactions and Photothermal Combined Therapy.

5.2. Self-assembled nano prodrugs for cancer treatment (papers I, II, III)

This section describes the use of similar synthetic methods to prepare prodrug compounds with different structures, which were then characterized by NMR and MS spectra. Using solvent exchange methods, the compounds were subsequently used to prepare nanomaterials for cancer treatment. The release capacity of the nano prodrug and its treatment effect were evaluated *in vitro* and *in vivo*.

Specifically, prodrug molecules CPT-S-S-PTX and DOX-S-S-PTX were synthesized to deliver two chemotherapeutic drugs, while THPP-$(S\text{-}S\text{-}PTX)_4$ was synthesized for combined photodynamic/chemotherapy. Nano prodrugs were prepared using various methods, such as microfluidic or dialysis, and subjected to stimulation response release testing. The antitumor effects of the nano prodrugs, including cytotoxicity and cellular uptake, were subsequently evaluated. Additionally, the targeting ability and *in vivo* therapeutic effect of the nano prodrug were investigated.

5.2.1. Synthesis and characterization of the self-assembled nano prodrugs

5.2.1.1. Characterization of the synthesized PTX prodrugs (I, II, III)

PTX-SS-COOH prodrug was synthesized in accordance with Figure 12A. The chemical structure of the prodrug was confirmed by ^1H NMR spectroscopy and mass spectrometry. It can be seen from Figure 12B and C that the hydrogen shift of the disulfide linker is within the range of 2.6–2.9 ppm, and the number of hydrogen atoms is 8. The other peak types are consistent with PTX. The mass number of PTX-SS-COOH prodrug was 1044.3259 based on the mass spectrum results, consistent with the calculated results. The above results verified the correctness of the chemical structure of the PTX-SS-COOH prodrug.

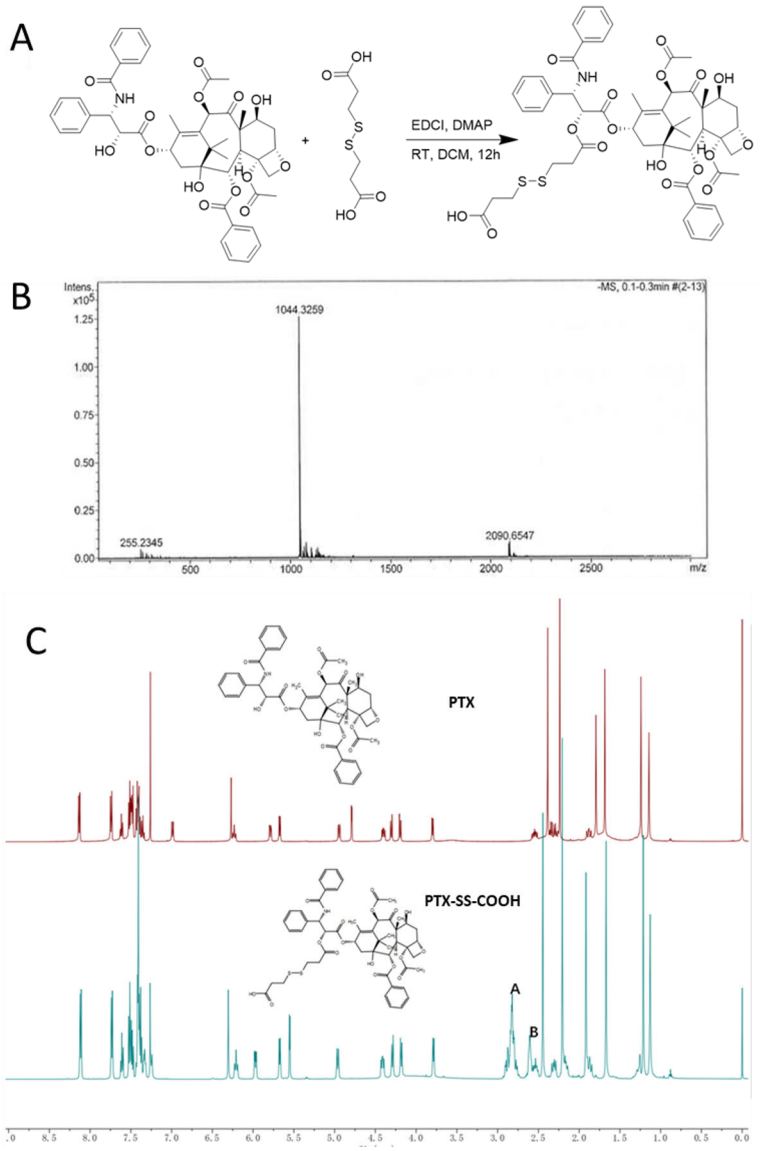

Figure 12. Characterization of the PTX-SS-COOH*. Synthetic route (A), MS results (B), NMR results (C).*

5.2.1.2. Characterization of the synthesized PTX and DOX prodrugs (I)

The prodrug of PTX-SS-DOX was synthesized according to Figure 13A. As seen from the NMR spectrum, the amino shift of DOX is 8.03, which disappears after esterification with PTX-SS-COOH, and the characteristic peaks of PTX and DOX both appear in the molecular spectrum of prodrug. According to the mass spectrometry results, the M+Na peak of PTX and DOX prodrug is 1593.4910, which is consistent with the calculated results. The above results verify the correctness of the chemical structure of the prodrug (Figure 13B and C).

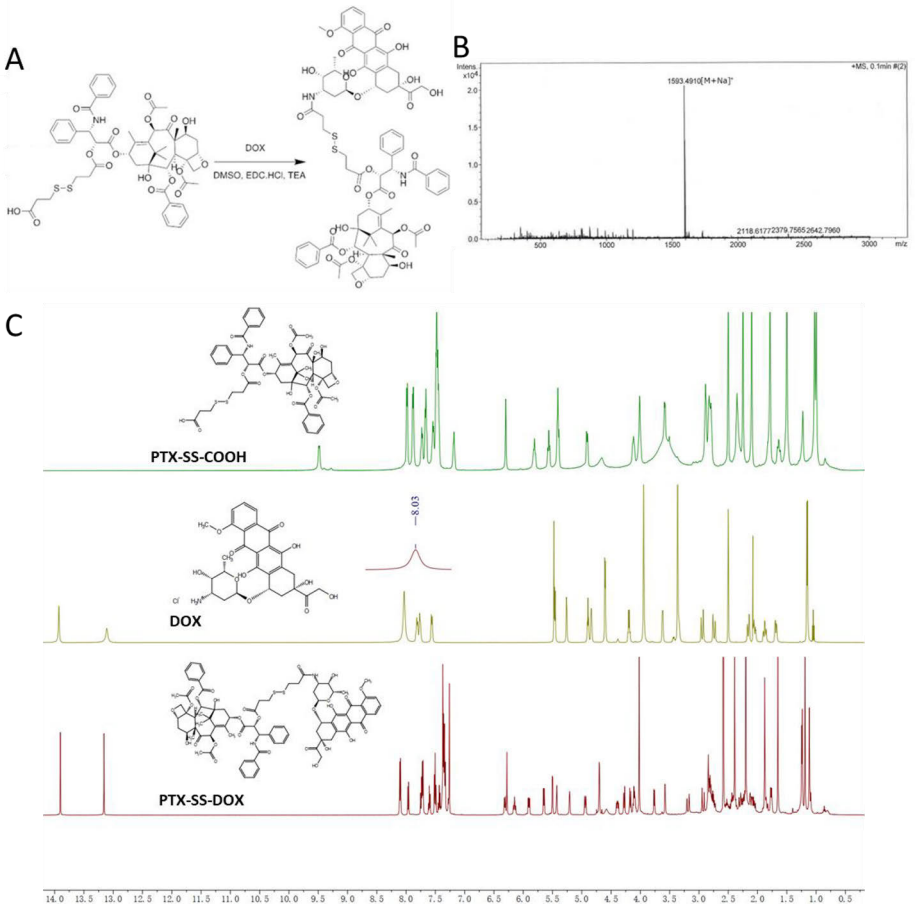

Figure 13. Characterization of the PTX-SS-DOX*. Synthetic route (A), MS results (B), NMR results (C).*

5.2.1.3. Characterization of the synthesized PTX and CPT prodrugs (II)

PTX-SS-CPT prodrug was synthesized as shown in Figure 14A. The hydroxyl shift of CPT was 8.68. After the hydroxyl group reacted with the carboxyl group of paclitaxel prodrug, the hydroxyl peak disappeared. At the same time, the characteristic peaks of paclitaxel and camptothecin appeared in the molecular spectra of the prodrug (Figure 14B). According to the mass spectrum results (Figure 14C), the M+Na peak of the PTX and CPT prodrug was 1398.4105. The results above verified the correctness of the chemical structure of the prodrug.

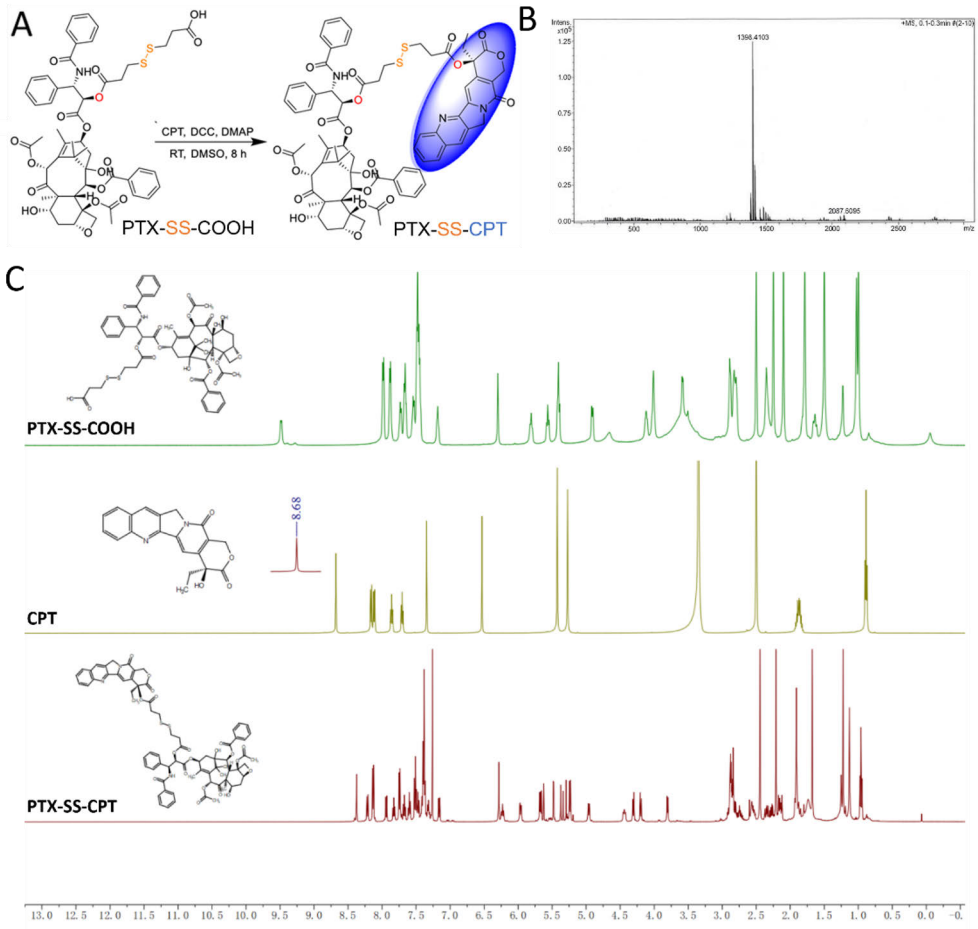

Figure 14. Characterization of the PTX-SS-CPT*. Synthetic route (A), MS results (B), NMR results (C).*

5.2.1.4. Characterization of the synthesized PTX and THPP prodrugs (III)

THPP-(S-S-PTX)$_4$ prodrugs were synthesized as shown in Figure 15A. The hydroxyl shift of THPP was 9.92. After the hydroxyl group underwent halogenation reaction with 6-chloro-1-hexanol, the hydroxyl peak disappeared. The newly generated THPP-(CH$_2$)$_6$-(OH)$_4$ hydroxyl peak shift was 4.42, and the hydroxyl group disappeared after reaction with paclitaxel prodrug (Figure 15B). Based on the mass spectrum results (Figure 15C), the (M+Na)/3 peak of the paclitaxel and THPP prodrugs was 1753.2957. The results above verified the correctness of the chemical structures of the prodrugs.

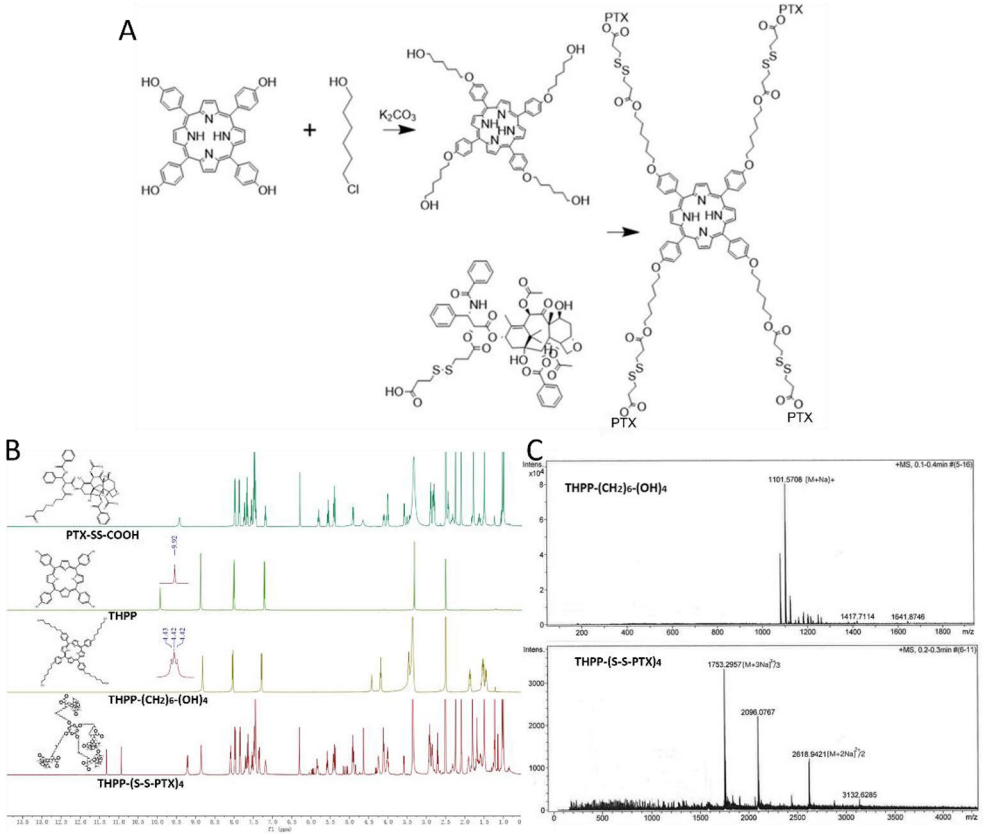

Figure 15. Characterization of the THPP-(S-S-PTX)$_4$. *Synthetic route (A), NMR results (B), MS results (C).*

5.2.2 Preparation of nanoparticles and stimuli-responsive release (I, II, III)

5.2.2.1 Preparation and characterization of prodrug nanoparticles (I, II, III)

Nanoparticles with different particle diameters were prepared by a microfluidic device. Different particle size results can be achieved by adjusting the drug concentration and the outward/inward flow rate ratio. In summary, when the drug concentration is fixed and the internal/external flow rate ratio is increased, the particle size of the nano prodrug will continuously decrease (Figure 16 A and B). When the flow rate ratio was fixed, the drug concentration in the inward solution was changed, and the particle size of the nanoparticles would be continuously decreased with the decrease of the drug concentration (Figure16A and B). The average particle size of PTX-SS-DOX self-assembled nanoparticles was about 150 nm (Figure 16A), and PTX-SS-CPT nanoparticles were about 200 nm (Figure 16B). For (III), THPP-(S-S-PTX)$_4$-RGD NPs have been prepared by dialysis with a mean particle size of 80 nm (Figure 16C).

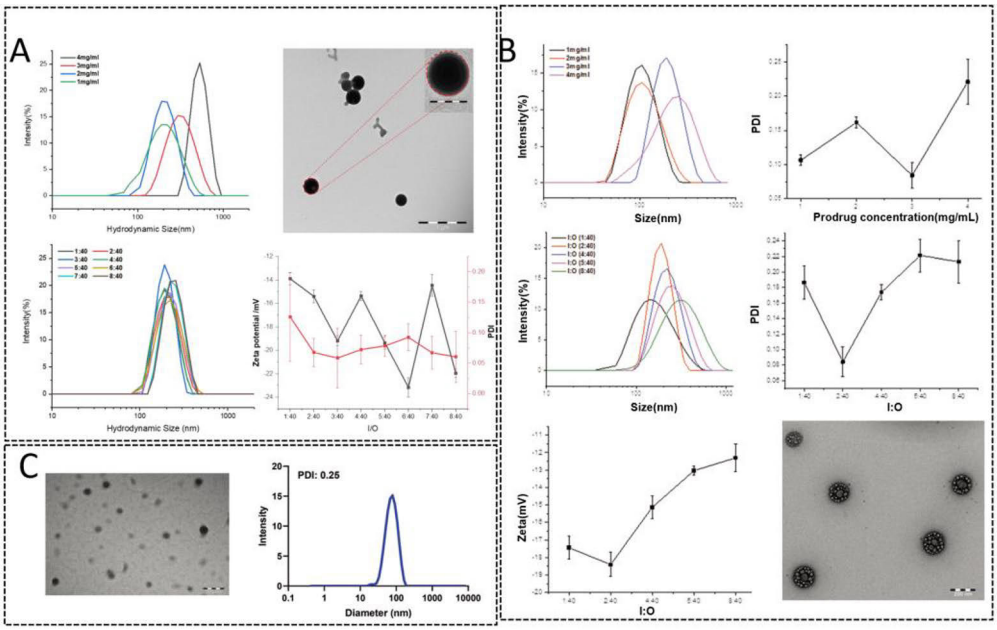

Figure 16. Characterization of prodrug nanoparticles*(A) PTX-S-S-CPT nanoparticles(B) PTX-S-S-DOX nanoparticles (C) THPP-(S-S-PTX)$_4$-RGD nanoparticles.*

5.2.2.2. *In vitro* drug release (I, II, III)

To test the duration of release of active drugs from prodrug nanoparticles in a reducing environment, we conducted experiments as shown in Figures 17A, B, and C. DTT was used as a reducing agent to simulate the environment in cancer cells, and the drug release was detected by HPLC. Since the synthesized prodrug is composed of two drugs, their molar ratio is determined by the molecular structure of the prodrug, and thus, the ratio is fixed. When the disulfide bond is cleaved, both drugs are simultaneously released. Therefore, only one of the drugs is chosen for release testing. Our results showed that DOX-S-S-PTX NPs, CPT-S-S-PTX NPs, and THPP-(S-S-PTX)$_4$-RGD NPs could gradually release PTX within 48 hours. Furthermore, the release performance of these three prodrug nanoparticles was weak in non-reducing conditions, with only a small amount of the drug being released.

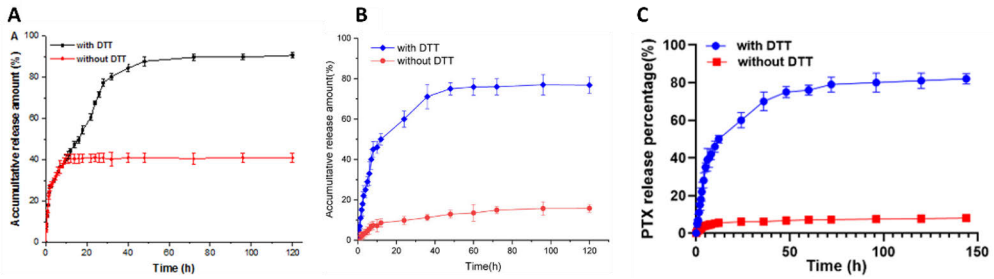

Figure 17. *(A) The in vitro release of DOX from DOX-S-S-PTX NPs; (B) The in vitro release of PTX from CPT-S-S-PTX NPs; (C) The in vitro release of PTX from THPP-(S-S-PTX)$_4$-RGD NPs;*

5.2.3. Evaluation of antitumor effect *in vitro* (I, II, III)

5.2.3.1. Cellular uptake (I, II, III)

To evaluate the cellular uptake behavior of prodrug NPs, we examined the red fluorescence of the NPs group over time. We observed that the fluorescence intensity was weaker than that of the free drug DOX group (Figure 18A). This may be due to the prodrug structure affecting the fluorescence of DOX. Furthermore, multiple cell lines treated with CPT-S-S-PTX NPs showed blue fluorescence (Figure 18B). To verify the targeting ability of cancer cells, we compared the THPP-(S-S-PTX)$_4$-RGD NPs and THPP-(S-S-PTX)$_4$ NPs groups. The confocal images showed a stronger red fluorescence over time in the THPP-(S-S-PTX)$_4$-RGD NPs group than in the THPP-(S-S-PTX)$_4$-NPs group (Figure 18C and D). To quantify the cell uptake behavior more accurately, we measured the uptake efficiency of different samples using flow cytometry. As shown in Figure. 18E and F, the uptake efficiency of cells was significantly improved by the nano-preparations with RGD protein compared to those without RGD protein. The nano prodrugs with targeting ability demonstrated a better promotion effect, resulting in an approximately 21% increase in cell uptake efficiency.

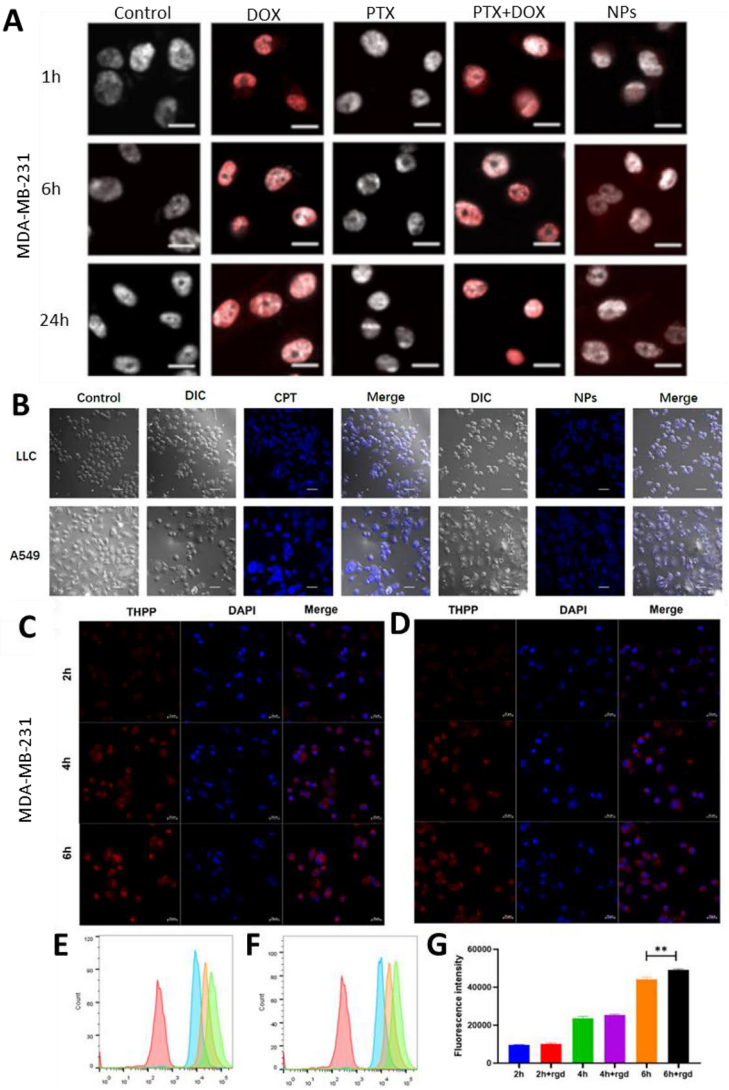

Figure 18. *A) The fluorescence microscopy images of cellular uptake of DOX, PTX, DOX+PTX and prodrug NPs (scale bar, 10 μm). B) Confocal microscope image of LLC, and A549 cell lines when incubated with CPT and CPT-S-S-PTX prodrug NPs (scale bar, 50 μm). C) Confocal microscopy images of MDA-MB-231 cells incubated with THPP-$(S\text{-}S\text{-}PTX)_4$-RGD NPs at different intervals with an equivalent THPP concentration of 1 μM. D) Confocal microscopy of MDA-MB-231 cells incubated with THPP-$(S\text{-}S\text{-}PTX)_4$ NPs for different time intervals (scale bar, 20 μm). E) Time-dependent quantitative analysis of fluorescence intensity of THPP-$(S\text{-}S\text{-}PTX)_4$-RGD NPs and F) THPP-$(S\text{-}S\text{-}PTX)_4$ NPs in MDA-MB-231 cells measured by flow cytometry. G) Quantification of fluorescence positive cells analyzed by flow cytometry.*

5.2.3.2. Cellular lysosome escape (III)

Effective intracellular distribution is crucial for the efficacy of nano-preparations. To study nano prodrug distribution within cells, we used lysosomal probes (LysoTracker, green) to investigate the co-localization of lysosomes and THPP-(S-S-PTX)$_4$-RGD NPs in cells. Since many nanoparticles are readily engulfed by lysosomes upon entry into cells, rendering them ineffective, we aimed to investigate if prodrug NPs (red) are transported to lysosomes after being internalized by cells. CLSM was used to detect the co-localization of nano prodrug and lysosomes. Results depicted in Figure 19 showed that NPs in the non-laser group had a high co-localization effect with lysosomes from 2 to 4 hours, indicating a weak escape from lysosomal phagocytosis. The co-localization began to decrease at 6 hours, implying that NPs could spontaneously escape under non-laser conditions. In the laser group, prodrug NPs showed a strong fluorescence signal in the cytoplasm from 2 hours, indicating that laser promoted prodrug NPs to effectively escape lysosomal phagocytosis. This implies that THPP-(S-S-PTX)$_4$-RGD NPs can overcome the main biological barrier of cancer cells, providing higher drug delivery capacity.

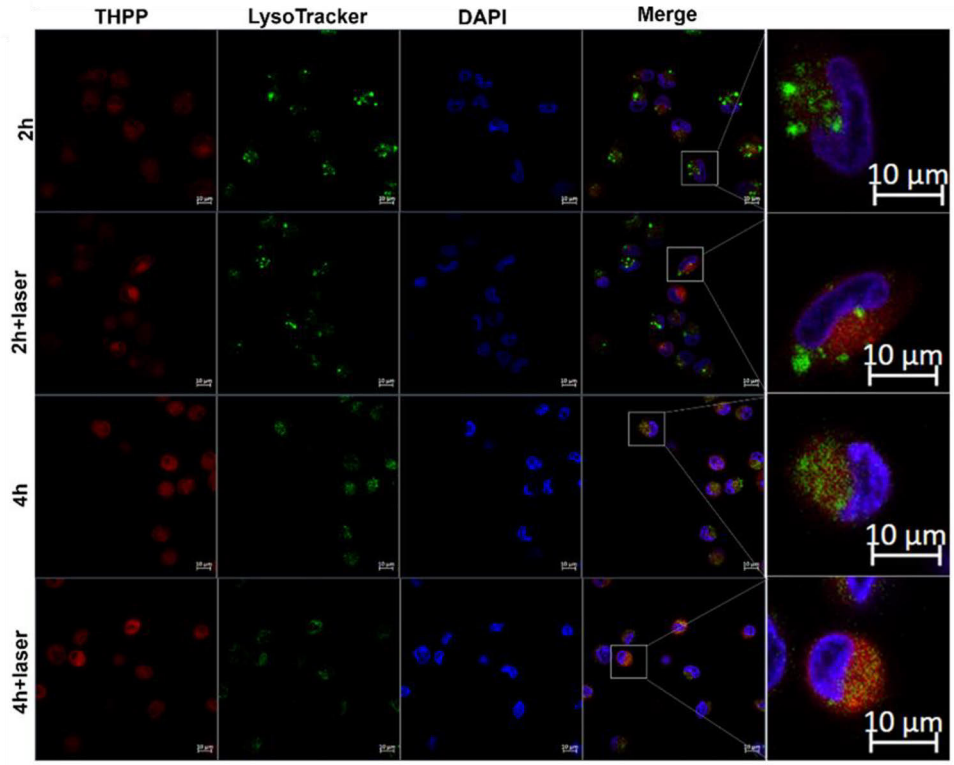

Figure 19. *Endosomal escape analysis of the intracellular untaken THPP-(S-S-PTX)$_4$ NPs-RGD NPs in MDA-MB-231 cells. Cells were selectively treated with laser for 5 min (0.5W/cm^2, 5 min; scale bar, 10 μm).*

5.2.3.3. Cytotoxicity assay (I, II, III)

As seen in Figure 20A, MDA-MB-231/ADR, MDA-MB-231, and MEF cell lines were used herein to demonstrate the anticancer activity of DOX-S-S-PTX NPs. After the cells were treated with different samples for 24 or 48h, the DOX and PTX groups showed weak anticancer abilities, and the DOX+PTX group showed stronger anti-cancer abilities, which indicated the therapeutic effect of the combination of two drugs. In contrast, the cancer cells in DOX-S-S-PTX NPs group showed the lowest viability. With the increase of the concentration of DOX-S-S-PTX NPs, the viability of cells was further decreased. Meanwhile, DOX, PTX and DOX+PTX groups also showed certain cytotoxicity to healthy cells. DOX-S-S-PTX NPs showed the lowest killing effect on healthy cells, indicating the selectivity of therapeutic effects of the nano prodrug with redox sensitive response. The drug combination of CPT and PTX has been tested to have a synergistic therapeutic effect on the lung cancer cell lines LLC and A549. As shown in the figure20 B, the CPT-S-S-PTX NPs group showed a more effective treatment with increased concentrations than the free drug group. The combination of chemotherapy and photodynamic therapy can effectively reduce the activity of cancer cells. As shown in the figure 20C, THPP can only produce cytotoxicity after laser irradiation. Compared with the THPP group and the PTX group. THPP-$(S\text{-}S\text{-}PTX)_4$-RGD NPs have better anticancer ability, especially after laser irradiation, reflecting the advantages of combined treatment.

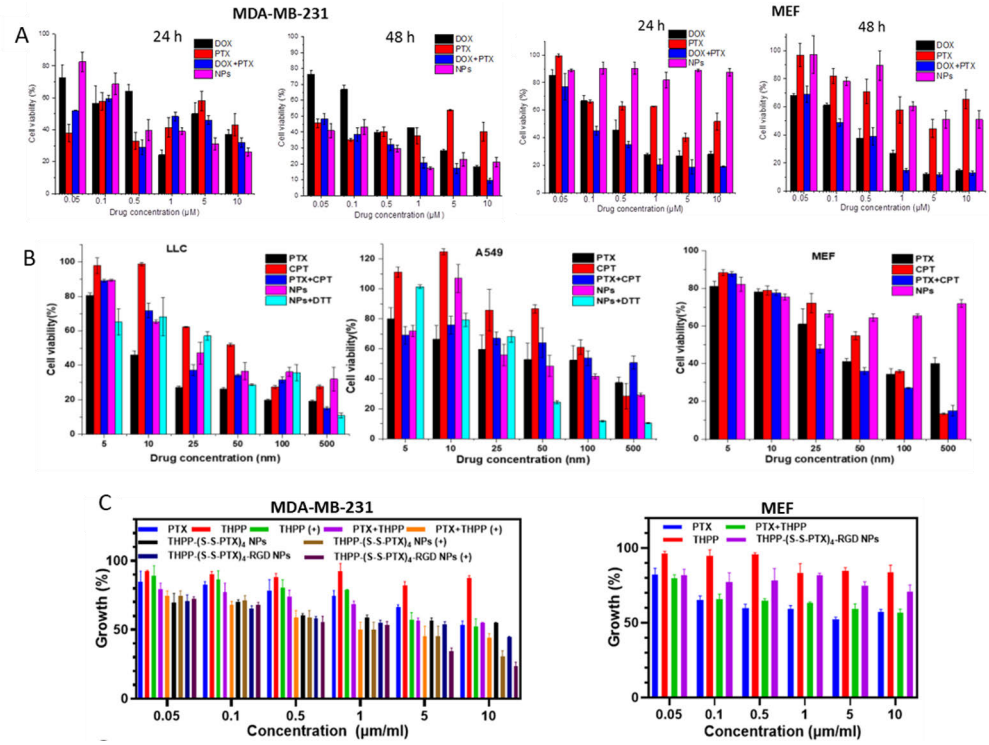

Figure 20. *(A). Cytotoxicity of DOX, PTX, DOX+PTX mixture and NPs. MDA-MB-231 cells incubated for 24 h and 48 h, MEF cells incubated for 24 h and 48 h. (B). Cytotoxicity of PTX, CPT, and PTX+CPT mixture in equal amounts NPs and NPs+dithiothreitol (DTT) against Lewis lung carcinoma (LLC), A549, and mouse embryonic fibroblast (MEF) cell lines within 48 h. (C). Cytotoxicity of THPP-(S-S-PTX)$_4$ -RGD NPs against MDA-MB-231 cells and MEF cells.*

5.2.4. Evaluation of antitumor effect *in vivo* (III)

The ultimate objective of achieving efficient cellular and tissue infiltration is to address the challenges posed by systemic chemotherapy for drug-resistant tumors. Accordingly, we utilized mice bearing MDA-MB-231 tumors as animal models to investigate the *in vivo* antitumor efficacy of the nano prodrug. PTX, THPP, and THPP-(S-S-PTX)$_4$-RGD NPs were set as the experimental group. The distribution of THPP-(S-S-PTX)$_4$-RGD NPs *in vivo* showed that after the tumor-bearing mice were injected, the fluorescence signals of THPP-(S-S-PTX)$_4$-RGD NPs group could be accumulated at the tumor site over time (6–24 h), which was not observed in the THPP group (Figure. 21A). As shown in Figure. 21G, the relative tumor volume of the THPP-(S-S-PTX)$_4$-RGD NPs + Laser group was significantly reduced, indicating that THPP-(S-S-PTX)$_4$-RGD NPs had good tumor elimination capacity. However, the weak tumor elimination capacity was observed in the PTX group and THPP+Laser group. During the experiment, all the mice in the nano prodrug group could maintain their body weight (Figure. 21F), while the body weight of the PTX group decreased slightly.

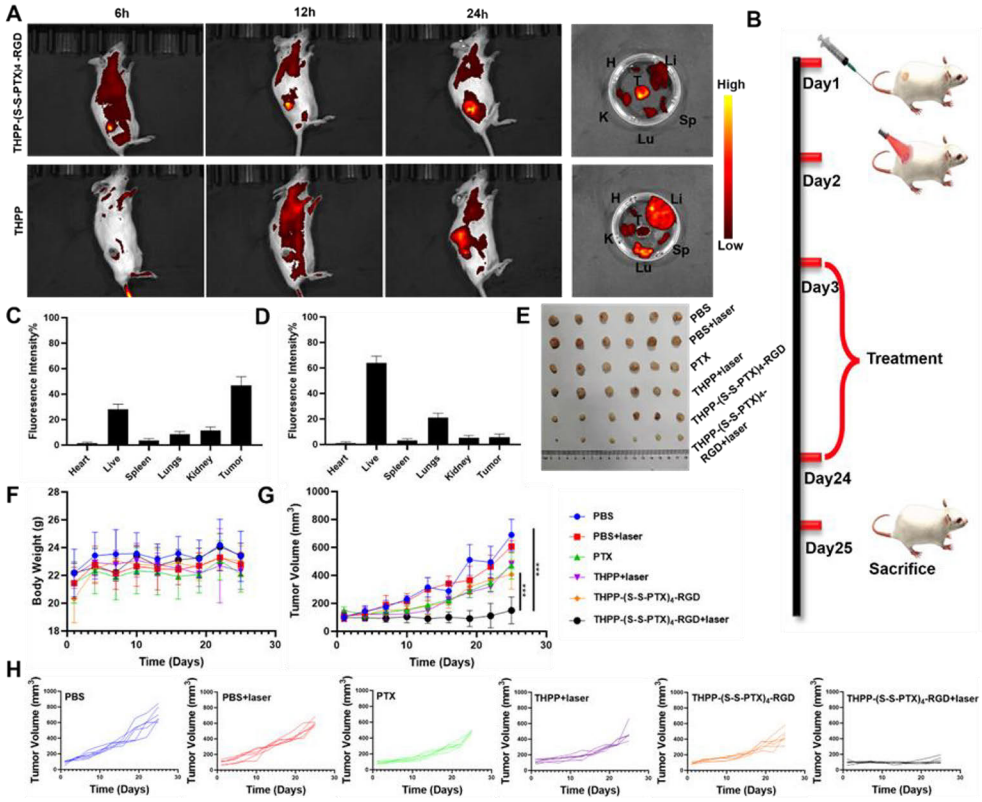

Figure 21. *In vivo time-dependent fluorescence image of tumors in MDA-MB-231 bearing NCG mice and ex vivo fluorescence images of the sacrificed tissues. In vitro imaging of the livers (Li), hearts(H), spleens (Sp), lungs (Lu), kidneys(K), and tumors(T) excised from MDA-MB-231 bearing NCG mice after THPP-(S-S-PTX)4-RGD NPs and THPP after 24 h tail-vein injection. B) Therapeutic schedule of THPP-(S-S-PTX)$_4$-RGD NPs for PDT against tumors. Quantitative fluorescence intensity of THPP-(S-S-PTX)$_4$-RGD C) and THPP D) measured by RIO value. (E) Digital pictures of the excised tumors from different groups; (F) Body weight change of mice and (G) Tumour growth curves at different groups for 24 days; H) The corresponding individual distant tumor growth curves of MDA-MB-231 bearing NCG mice after various treatments.*

In addition, immunohistochemical studies showed significantly fewer antigen kiel 67 (Ki-67) positive proliferating cells in the tumor tissues of the THPP-(S-S-PTX)$_4$-RGD NPs group. In contrast, far more terminal deoxynucleotidyl transferase dUTP nick end labeling (TUNEL) positive apoptotic cells were observed in the other groups, which showed markedly proliferating cells and few dead cells. The results of Hematoxylin and eosin (HE) staining showed that all the experimental mice could maintain their body weights and normal tissue structures of major organs during the experiment (Figure. 22).

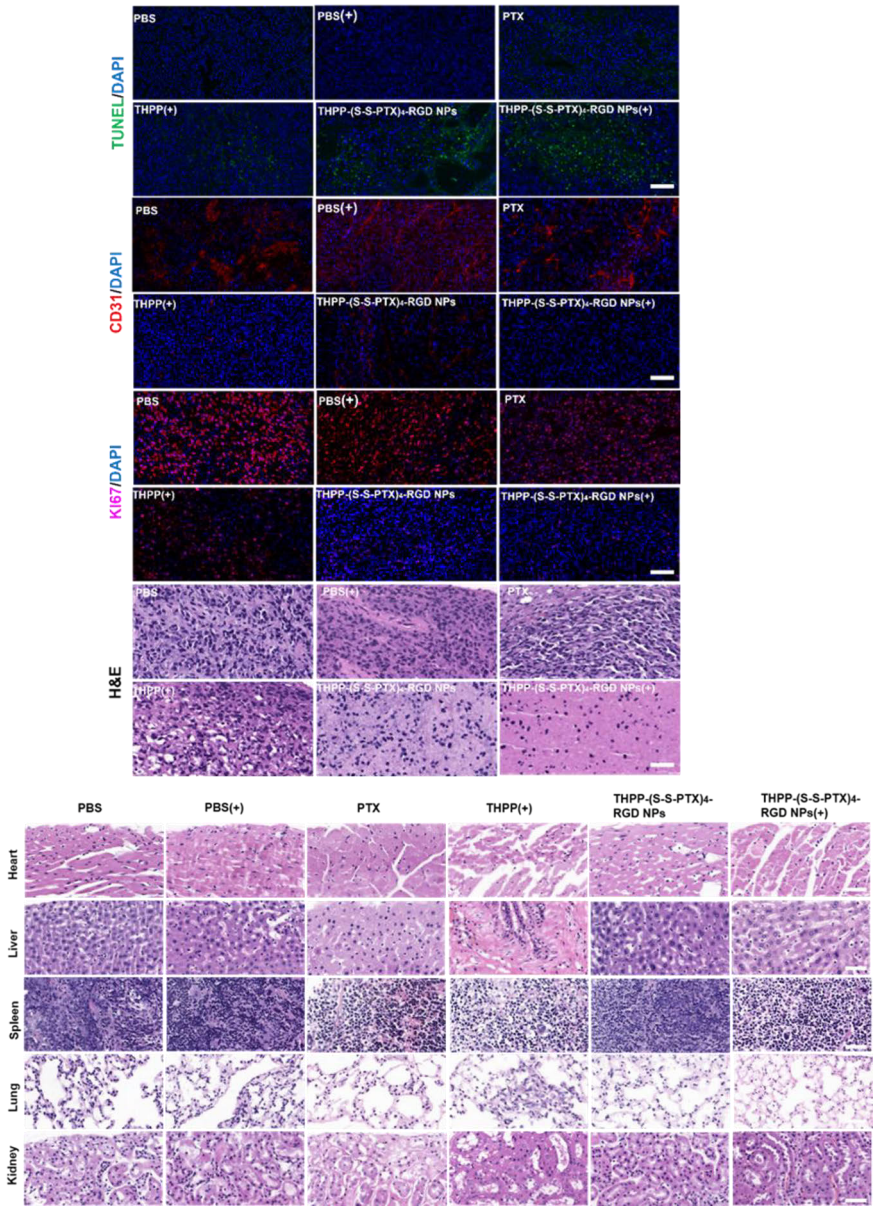

Figure 22. *Histological analysis of tumors for different groups. H&E stained photos and DLSM imaging of TUNEL, CD31, Ki-67 and DAPI stained tumor sections (scale bar: 20 μm).*

5.3. MSN-based nanomaterials for cancer treatment (papers IV & V)

In the previous section, we demonstrated the feasibility of self-assembled prodrug nanoparticles for cancer treatment. To achieve diversified functionalities in prodrug therapy systems, we combined prodrug technology with MSNs to explore novel delivery pathways for prodrugs. Firstly, we encapsulated a gold rod into an MSN material, then modified prodrug molecules or targeting ligands through functional groups on the surface of the MSN, encapsulated the drug molecule in an MSN pore canal, and finally encapsulated the whole MSN into extracted cancer cell membranes to achieve cancer cell targeting. Additionally, we encapsulated MSN NPs in GelMA microspheres, creating a temperature-controlled and sustained-release treatment system. At the cellular level, we evaluated the function of these nanomaterials, including cytotoxicity, cellular uptake and targeting, lysosomal escape, and organelle targeting. Lastly, we studied the combined therapeutic effects of different MSN nano-preparations on tumor cells.

5.3.1. Synthesis and characterization of the MSN-based nanomaterials (IV & V)

5.3.1.1. Characterization of the synthesized prodrug modified MSN (IV)

TEM photographs of the gold rod, Au@MSN, and Au@PTXSS-MSN/DOX@CM are shown in figure 23A-C. The gold rods exhibit a uniform rod structure of 56 nm. Au@MSN presented a regular elliptical shape, and was uniformly distributed, with a clear dendritic hollow mesoporous structure inside. Compared with Au@MSN, Au@PTXSS-MSN/DOX@CM exhibited significant drug loading in their internal voids and significant cell membrane coating with good overall dispersibility. From figure. 23D-F, we could find that the Zeta potentials of nanoparticles were positive. With the surface modification and cell membrane coating, the particle size and PDI increased to different degrees. The characteristic peak of paclitaxel appeared in the Au@PTXSS-MSN NPs infrared spectrum (Figure. 23G), indicating the successful synthesis of prodrug-modified MSN.

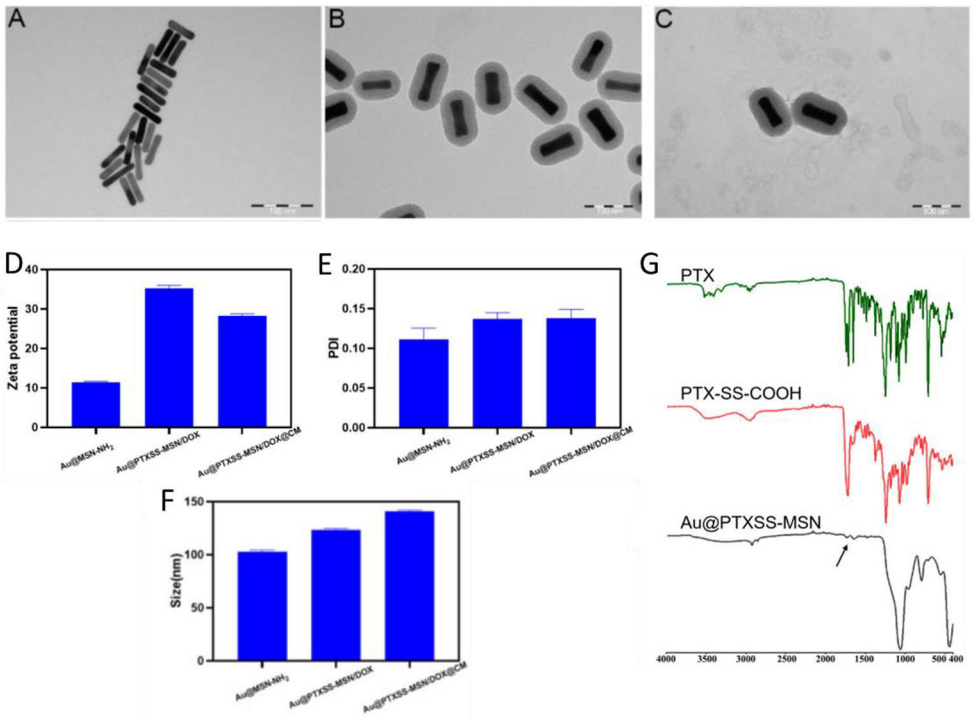

Figure 23. *Morphologies of different NPs. A-C. TEM images of Au NRs, Au@MSN NPs, Au@PTXSS-MSN/DOX@CM NPs (Scale bar = 100 nm); (D) Zeta-potential; (E) PDI; (F) Particle size; (G) FTIR analysis.*

5.3.1.2. Characterization of the synthesized ligand modified MSN (V)

From the results of TEM, we found that Au@MSN-Ter/THPP@CM is similar to Au@PTXSS-MSN/DOX@CM in structure (Figure. 24A). The particle size and Zeta potential test data for different NPs are shown in Figure. 24D and E, respectively. The particle size of Au@MSN was 121.1 nm, and the Zeta potential was -19.5 mV. In contrast, the particle size of Au@MSN-Ter was increased by about 20nm, but the potential changed to 20.8 mV. At the same time, a -CONH- peak appeared in the infrared spectrum, which proved the successful modification of Au@MSN-Ter(Figure. 24F). After loading with THPP, the Zeta potential became negative, which might be due to the fact that the negative charge part of hydroxyl in THPP structure shielded the positive charge on Au@MSN-Ter surface. Compared with Au@MSN-Ter/THPP, the membrane-coated Au@MSN-Ter/THPP@CM exhibited significantly increased particle sizes of 160.5 nm. At the same time, the Zeta potential also changed significantly to -19.4 mV. TEM, particle size, infrared spectrum and Zeta potential results showed that the nanoparticles fused with cell membrane Au@MSN-Ter/THPP@CM were successfully prepared. We also tested the stability of Au@MSN-Ter/THPP@CM in 10% FBS medium and the changes in particle size and particle size distribution within 10 days. Au@MSN-

Ter/THPP@CM did not exhibit significant changes in particle size and PDI after 10 d in 10% FBS, as shown in Figureure 24G. The above results indicated that the membrane coating strategy could significantly improve the *in vitro* stability of mesoporous silica nanoparticles.

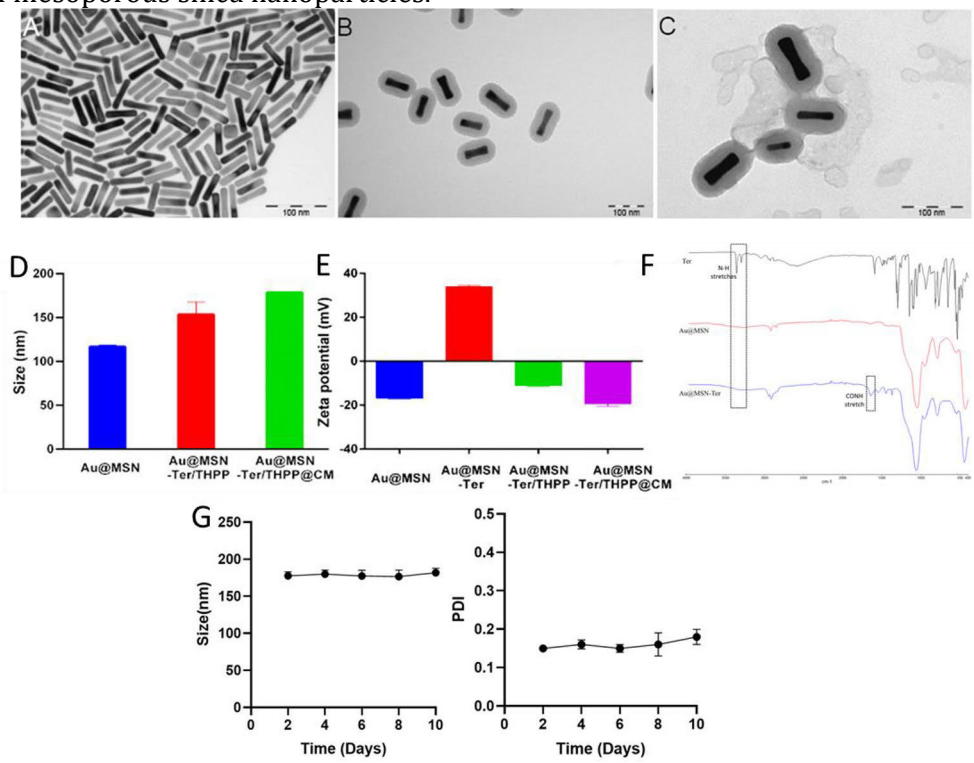

Figure 24. Morphologies of different NPs*. A-C. TEM images of Au NRs, Au@MSN NPs, Au@MSN-Ter/THPP@CM NPs (Scale bar = 100 nm); D. Particle size; (E), Zeta-potential; (F) FTIR analysis of Ter, Au@MSN and Au@MSN-Ter NPs (from up to down panel); (G) The stability of Au@MSN-Ter/THPP@CM NPs in culture medium.*

5.3.1.3. Characterization of the microspheres (V)

GelMa microspheres with different particle sizes were prepared by microfluidic device. Different particle size results can be obtained by adjusting the external/internal flow rate ratio (Figure. 25A). The degradation test of microspheres with different particle sizes showed that the drug retention time was longer only when the diameter of microspheres was larger (Figure. 25D and F), so we chose microspheres with particle size of 200 microns (Figure. 25C). After that, we used confocal microscope to analyze the uniformity of nanoparticles in the microspheres. The results showed that MSN nanoparticles could be evenly distributed in the microspheres (Figure. 25B), and nanoparticles and catalase could be released slowly within 30 days (Figure. 25D and E). The high temperature generated by photo-thermal could

effectively promote the release of nanoparticles and achieve a certain degree of temperature control and slow release.

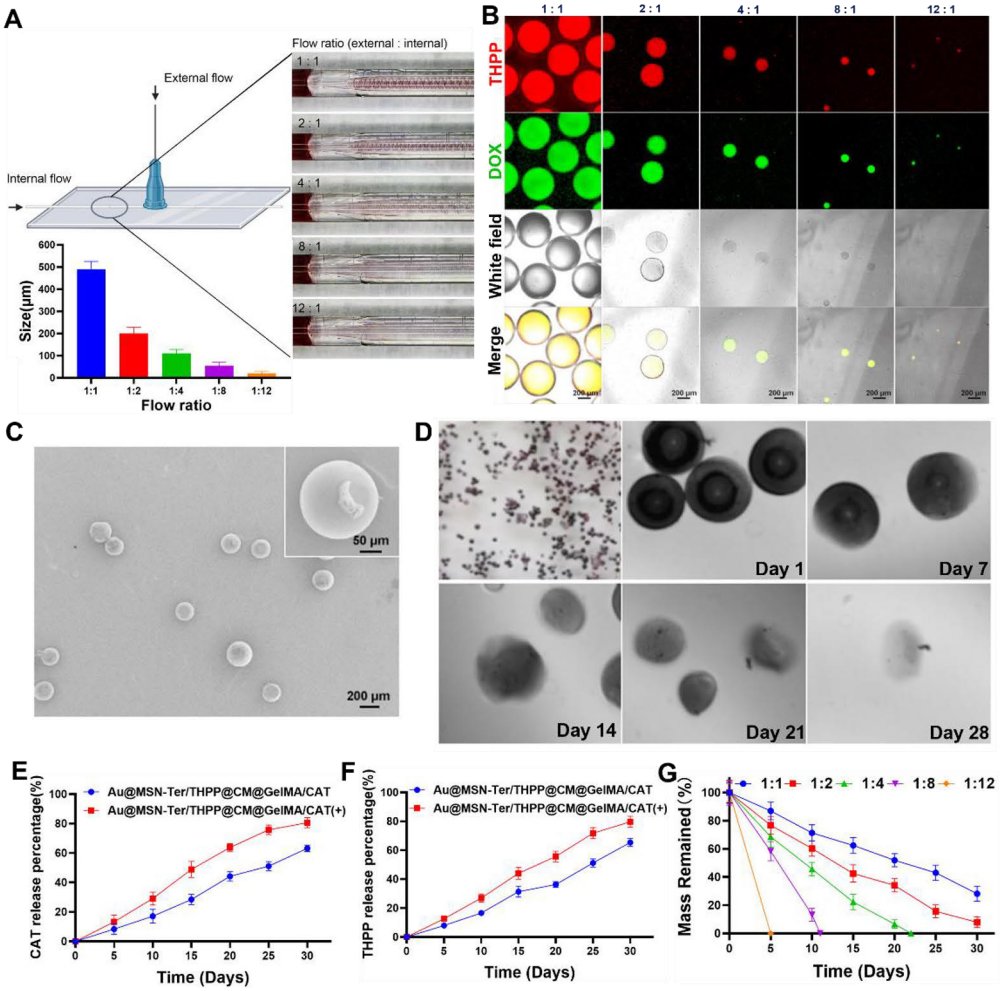

Figure 25. *Morphology and CAT/THPP releasing of Au@MSN-Ter/THPP@CM@GelMA/CAT microsphere. Illustration, particle size (A) and confocal microscope images (B) of Au@MSN-Ter/THPP@CM@GelMA/CAT microspheres with indicated external (5% Span 80 in mineral oil) and internal (mixture of NPs, DOX and GELMA) flow rate; C. SEM images of Au@MSN-Ter/THPP@CM@GelMA/CAT microsphere formed by external and internal flow rate of 2:1; D. Microscope images of Au@MSN-Ter/THPP@CM@GelMA/CAT microspheres at different time point; CAT (E) and THPP (F) releasing from Au@MSN-Ter/THPP@CM@GelMA/CAT microspheres in PBS buffer with or without laser (980 nm, 1 W/cm2, 10 min); G. The degradation curve of different Au@MSN-Ter/THPP@CM@GelMA/CAT microspheres formed by different flow ratio.*

5.3.1.4. *In vitro* photothermal/photodynamic efficiency and drug release evaluation (IV, V)

The thermal infrared imager was used to detect the temperature rise of Au@PTXSS-MSN/DOX@CM (IV) and Au@MSN-Ter/THPP@CM (V) NPs

solutions irradiated by near-infrared laser. The temperature change for each sample solution is shown in figure 26A-C and F-H. The temperatures of the two kinds of nanoparticles were increased to different degrees under the conditions of different concentrations and different laser powers, indicating that MSN with the gold rod as the core could produce better photothermal effect. The temperature of 1 mg/ml nanoparticles rapidly increased to about 62℃ when irradiated with laser for 5 min, and then gradually decreased to 34℃ when irradiated for 10 min. The heating rate was significantly affected by the change of laser power. When the concentration was the same, and the laser was applied for 5 min, the temperature of 0.5 W and 0.75 W was increased to 59℃ and 55℃, respectively. In addition, there was little difference in the highest achievable temperatures of the nanoparticles observed in the three warming cycles, indicating that Au@MSN-Ter/THPP@CM and Au@PTXSS-MSN/DOX@CM had good photothermal stability and potential for photothermal therapy.

We examined the ability of Au@PTXSS-MSN/DOX@CM (IV) and Au@MSN-Ter/THPP@CM (V) to release the drug DOX/THPP under different conditions using dialysis. As shown in figure. 26J, Au@MSN-Ter/THPP@CM and Au@PTXSS-MSN/DOX@CM both exhibited obvious photothermal responsive drug release characteristics, with a faster release rate under the laser irradiation at 980 nm. The nanoparticles without cell membrane also showed rapid drug release characteristics in the presence and absence of laser, indicating that the cancer cell membrane surface coating could avoid drug leakage and increase the stability of the drug. For Au@PTXSS-MSN/DOX@CM NPs, drug release was also affected by reducing conditions, so DTT was added to the experiment to mimic the reducing conditions in cancer cells. The results showed that DTT promoted the release of DOX and PTX, especially for PTX, the release amounts were 70.5% in the DTT condition and 4% in DTT-free condition, respectively (Figure. 26J). The experimental data above indicated that Au@PTXSS-MSN/DOX@CM had a redox/photothermal double-responsive release property.

The abilities of the blank control group, free THPP and Au@MSN-Ter/THPP@CM solution to trigger ROS generation under the irradiation of near-infrared laser were detected by using the active oxygen fluorescence probe singlet oxygen sensor green (SOSG). The enhancement of the fluorescence signal of SOSG indicated that the ROS level in the system was increased. As shown in Figure. 26I, no increase in ROS level in the blank solution was detected during the irradiation period. Within 5 min of laser exposure, the ROS levels of the free THPP and Au@MSN-Ter/THPP@CM groups rapidly increased and then tended to be flat, indicating that both had strong photodynamic efficiency. In contrast, the production of free THPP ROS was much higher, probably due to the enhanced optical stability of THPP after it was encapsulated and stacked on the internal void structure of MSN.

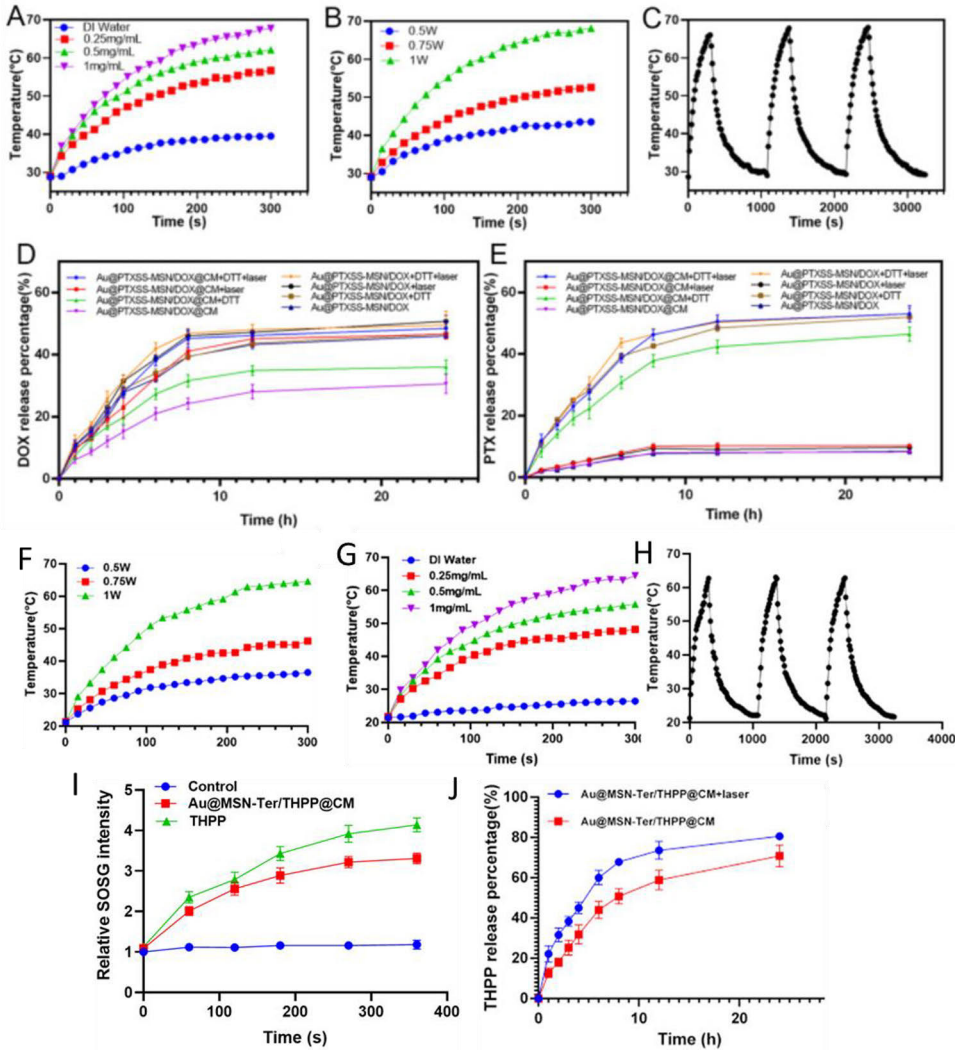

Figure 26. *(A) Photothermal heating curves of DI water and Au@PTXSS-MSN/DOX@CM NPs with different NPs concentrations (0.25, 0.5, and 1 mg/mL) under 1.0 W cm^{-2}, 980 nm laser irradiation. (B) The temperature profile of Au@PTXSS-MSN/DOX@CM (1 mg/mL) with different laser power intensities (0.5, 0.75, and 1.0 W cm^{-2}, 980 nm). (C)Temperature elevation of Au@PTXSS-MSN/DOX@CM NPs (1 mg/mL) over three times of NIR on–off irradiated cycles (1.0 W cm^{-2}, 980 nm). (D) DOX and (E) PTX Release behavior of Au@PTXSS-MSN/DOX@CM NPs under different conditions. Photothermal response of Au@MSN-Ter/THPP@CM NPs under 980 nm laser irradiation (F-H); (I)Time-dependent production of SOSG fluorescence upon light exposure (650 nm, 0.4 W/cm^2) for THPP and Au@MSN-Ter/THPP@CM NPs. (J)THPP releasing from Au@MSN-Ter/THPP@CM NPs in PBS buffer with or without laser (980 nm, 1 W/cm^2, 10 min).*

5.3.3. Evaluation of antitumor effect *in vitro* (IV & V)

5.3.2.1. Cellular uptake (IV, V)

Using the autofluorescence of DOX and THPP, we observed the uptake of different formulations of nanoparticles in different cell lines after 2–6 h co-incubation with confocal microscope. The results are shown in Figure. 27A and E. The red fluorescence of THPP and that of DOX are mainly located in the cytoplasm, and the nucleus shows blue fluorescence using DAPI staining. The fluorescence signal intensities of THPP and DOX in each group were increased with time. As shown in Figure. 27A and Figure. 27F, the intracellular fluorescence signals of the cell membrane-coated nanoparticles in the corresponding cancer cells were significantly higher than those of the cell membrane-free nanoparticles, because the homologous proteins on the membrane surface of cancer cells mediated the specific endocytosis. We also used the spontaneous red fluorescence of DOX and THPP to quantitatively investigate the phagocytosis of Au@MSN-Ter/THPP@CM and Au@PTXSS-MSN/DOX@CM after 2-6 h incubation by flow cytometry. The results also showed that the cancer cell membrane coating greatly promoted cell uptake (Figure. 27I).

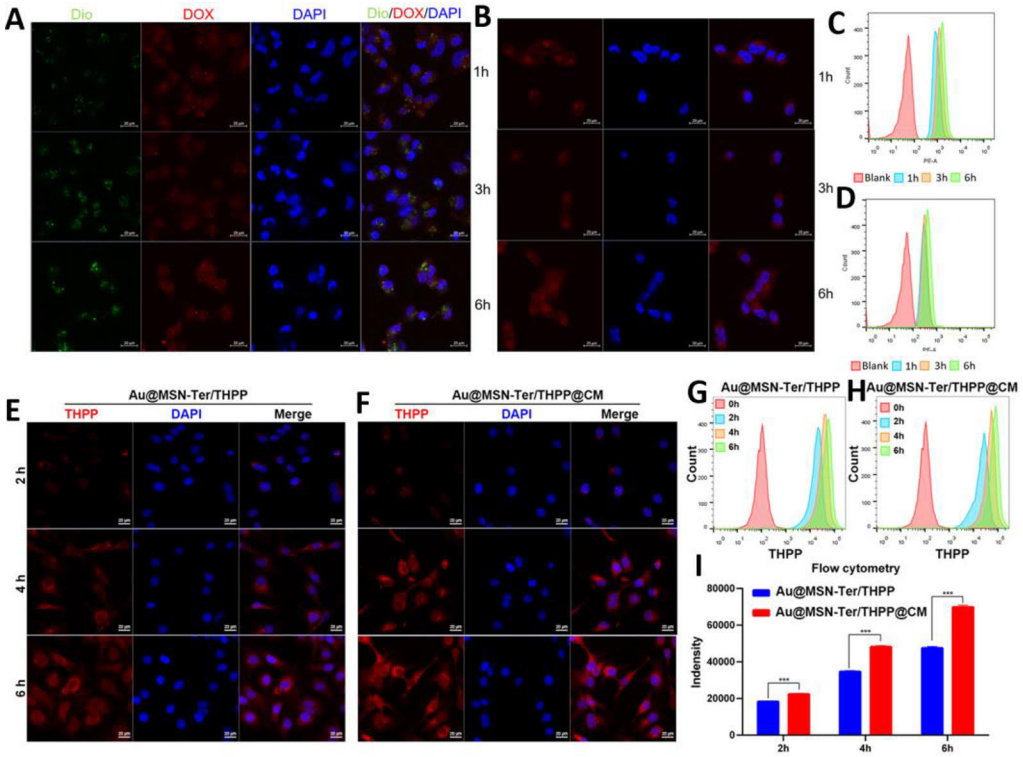

Figure 27. *Fluorescence images of MDA-MB-231 cells incubated with (A) Au@PTXSS-MSN/DOX@CM and (B) Au@PTXSS-MSN/DOX for 1–6 h and flow cytometry analysis (C and D). Confocal microscope images (E and F) and flow cytometry analysis (G, H and I) of Au@MSN-Ter/THPP@CM NPs or Au@MSN-Ter/THPP NPs after 2-6 hours co-incubation with SKOV3 (Blue channel: DAPI; Red channel: DOX or THPP; Green channel: DIO; Scale bar: 20 μm)*

To verify the specificity of Au@MSN-Ter/THPP@CM for cancer cell targeting, we used the normal human fibroblast NHDF cell line to compare. The cellular uptake of Au@MSN-Ter/THPP@CM and Au@MSN-Ter/THPP was tested like above. The results showed that the cancer cell membrane-coated nanoparticles did not exhibit higher uptake rates in healthy cells, suggesting that Au@MSN-Ter/THPP@CM could specifically target cancer cells rather than healthy cells (Figure. 28).

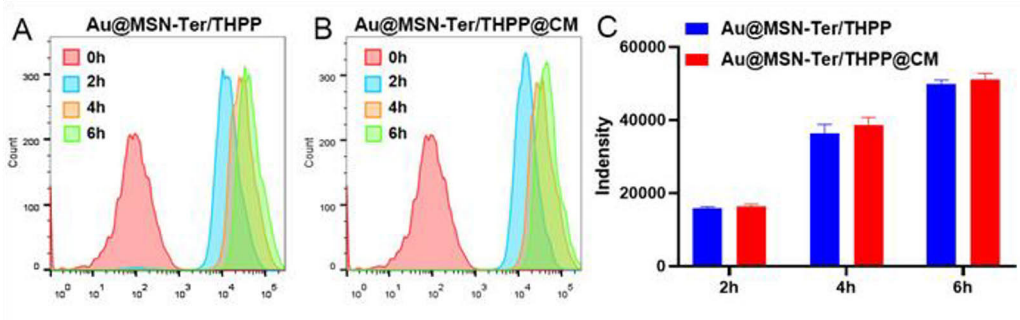

Figure 28. *Flow cytometry analyzing of THPP fluorescence signal positive NHDF cells after co-incubation with Au@MSN-Ter/THPP or Au@MSN-Ter/THPP@CM NPs for 48 hours.*

5.3.2.2. Cellular lysosome escape (IV, V)

We further evaluated the intracellular transport of this MSN material using CLSM. The effect of photothermal effect on lysosomal escape was verified in this experiment. Au@MSN-Ter/THPP@CM and Au@PTXSS-MSN/DOX@CM were incubated with 231 or SKOV3 cells for 2-6 h, respectively, with or without laser irradiation set as a variable. It could be seen that most of the nanomaterials were located in lysosomes at 2 h, wherein the lysosomes were stained with the lysosome-labeled dye lyso-tracker green. After the nano photosensitizer was incubated for 4 h, the green and red signals were gradually separated with the prolongation of incubation time (Figure 29A-C), which meant that the nanoparticles could spontaneously escape from the lysosome. Among them, the nanoparticles in the laser group had a faster escape velocity. They could escape from the organelles from 2 h onwards, due to the damage to the lysosomes by the temperature generated by the photothermal process.

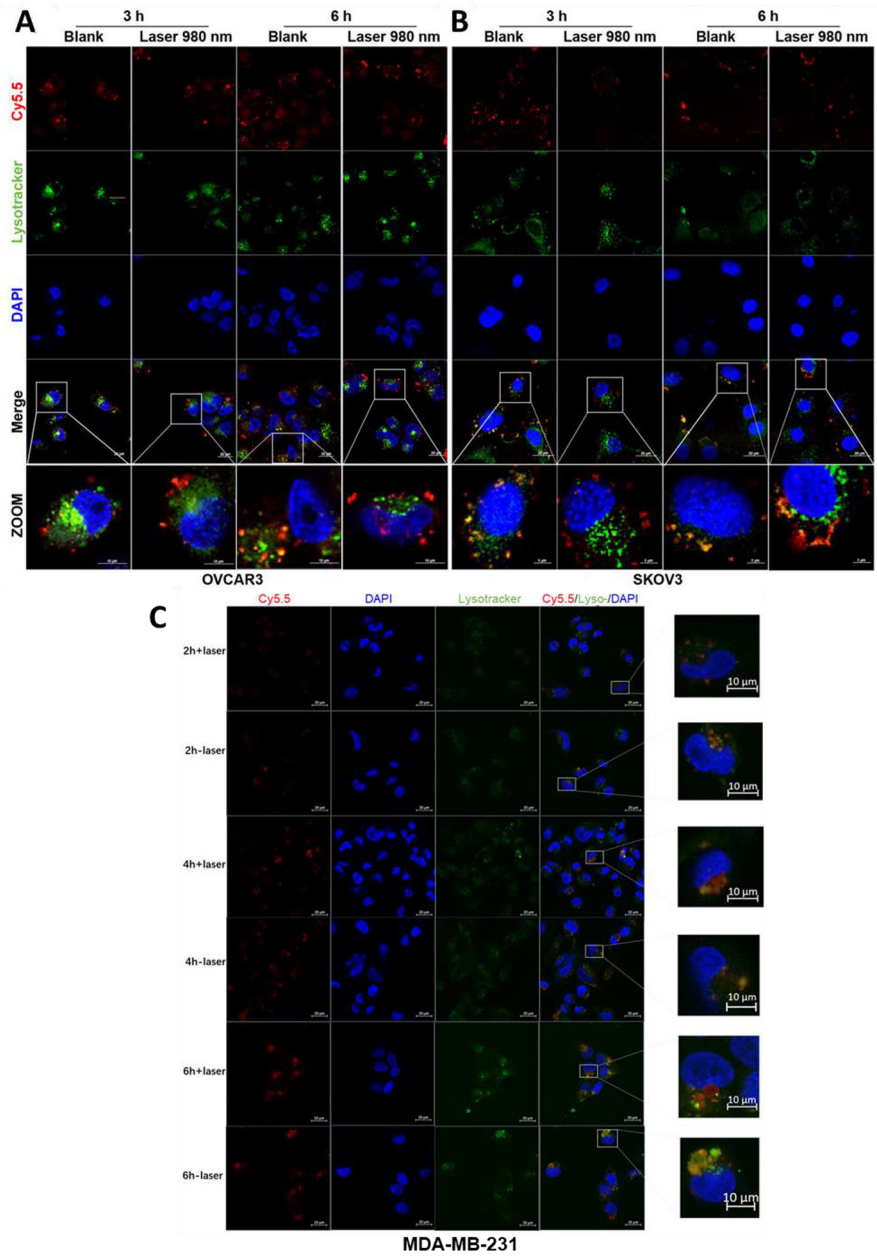

Figure 29. *Endosomal escape analysis of the intracellular uptaken. (A) and (B). Confocal microscope images of Cy5.5 labeled Au@MSN-Ter@CM NPs' lysosome escape in SKOV3 cells after 3-6 hours co-incubation and selectively treated with980 nm laser (1 W/cm², 10 min) irradiation. (C) Au@Cy5.5-MSN@CM NPs in MDA-MB-231 cells. Confocal microscopy images after cells culturing with Au@Cy5.5-MSN@CM NPs for 2 h, 4 h, and 6 h. And cells were selectively treated with laser for 5 min (Red: Cy5.5; Green: lysotracker; Blue: DAPI)*

5.3.2.3. Cytotoxicity assay (IV & V)

First, the WST-1 method was used to examine the synergistic effect of the combination therapy on the inhibition of the *in vitro* growth of mouse breast cancer MDA-MB-231 cells /skov3 cells. For (IV), the extent to which free DOX, free PTX, DOX/PTX mixture, Au@MSN, Au@PTXSS-MSN/DOX, and Au@PTXSS-MSN/DOX@CM NPs killed 231 cells in the presence or absence of laser light was tested. The experimental results are shown in Figure. 30 A. After 24 h of incubation, the inhibition of MDA-MB-231 cell growth by free DOX and free PTX was concentration-dependent, the cytotoxicity of DOX/PTX mixture was superior to that of single drug at the optimal drug ratio (Figure. 30 C). Au@MSN showed no significant toxicity to cells without laser irradiation even at elevated concentrations. The toxicity of Au@MSN was significantly increased after laser irradiation (980 nm, 10 min), indicating that the high temperature generated by laser irradiation could effectively kill cancer cells. Au@PTXSS-MSN/DOX and Au@PTXSS-MSN/DOX@CM NPs showed obvious concentration dependence without laser irradiation. After laser irradiation was added, the inhibition effect on MDA-MB-231 cells was significantly enhanced, and the cell growth inhibitory effect was stronger at the same concentration as that of free DOX+PTX and free single drug. In particular, the Au@PTXSS-MSN/DOX@CM NPs group exhibited higher cytotoxicity than the Au@PTXSS-MSN/DOX/CM NPs group after cell membrane addition. These results indicated that combining photothermal therapy and chemotherapeutic drugs could synergistically treat mouse breast cancer 231 cells. The free drug group was highly toxic in healthy cells MCF-10A, while the nanoparticle group was much less toxic due to the responsive design of the prodrug (Figure. 30 B).

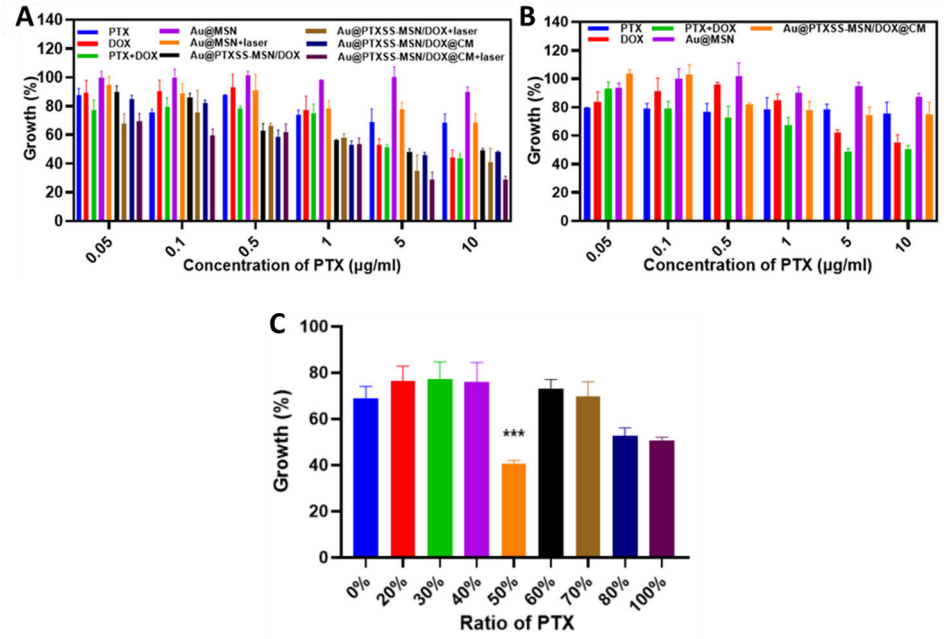

Figure 30. *Cell viability of (A) MDA-MB-231 cells and (B) MCF-10A cells after treatment with PTX, DOX, PTX+DOX, Au@MSN NPs, Au@PTXSS-MSN/DOX NPs, and Au@PTXSS-MSN/DOX@CM NPs for 24 hours and selectively treated with 980 nm laser irradiation. (C) Cell viability of MDA-MB-231 cells after treatment with 5mg PTX and DOX for 24 hours. (The indicated ratios were calculated by the weight of DOX in 5 mg of PTX and DOX.*

For (v), the extent to which the free THPP, Au@MSN, Au@MSN-Ter/THPP, and Au@MSN-Ter/THPP@CM NPS kill OVCAR3/SKOV3 cells in the presence or absence of laser irradiation was tested. The experimental results are shown in Figure. 31B. The inhibitory effect of free THPP on the growth of SKOV3 cells in the absence of laser irradiation was not concentration-dependent, but the cytotoxicity of free THPP was significantly increased under laser irradiation, indicating that the PDT effect of THPP under laser irradiation effectively inhibited the growth of SKOV3 cells. Similar to the above conclusion, Au@MSN exhibited certain cytotoxicity only under laser irradiation. To investigate the effect of cell membrane on Au@MSN-Ter/THPP@CM NPs, we selected Au@MSN-Ter/THPP and Au@MSN-Ter/THPP@CM NPs as the groups to investigate the inhibition effect on the growth of SKOV3 cells at different drug concentrations. Au@MSN-Ter/THPP and Au@MSN-Ter/THPP@CM NPs exhibited low inhibition without laser. In the absence of irradiation, the cytotoxicity of Au@MSN-Ter/THPP@CM NPs group was slightly higher than that of Au@MSN-Ter/THPP group. This was because the cancer cell membrane had the homologous targeting, and nanoparticles could enter cells to exert the inhibitory effect. In addition, after laser irradiation, since the increase in temperature also accelerated the release of THPP, PTT/PDT effect was exerted under laser irradiation and synergistic killing effect was generated on tumor

cells. Similar conclusions can be drawn in another cell line OVCAR3 (Figure. 31A).

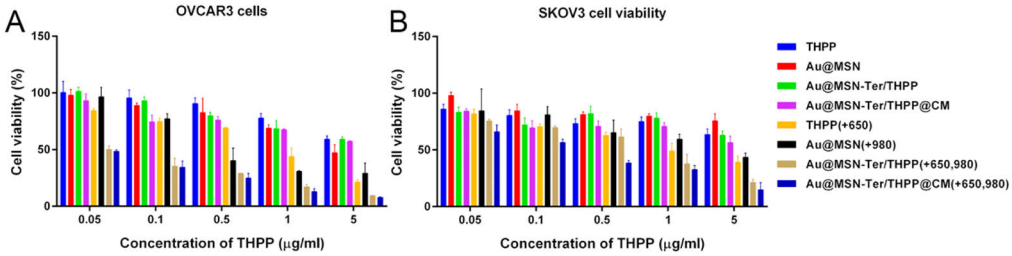

Figure 31. *Cytotoxicity of different NPs. OVCAR3 (A) and SKOV3 (B) cells viability after different concentrations of various NPs for 24 hours following with 650 nm laser (0.4 W/cm^2, 5 min) and / or 980 nm laser (1 W/cm^2, 10 min) irradiation.*

5.3.2.4. Live-dead cell staining (V)

We also used the live/dead cell staining kit to more intuitively detect the synergistic cytotoxic effects of Au@MSN-Ter/THPP@CM@GelMA and Au@MSN-Ter/THPP@CM@GelMA/CAT under different laser exposures condition. The dead cells showed red fluorescence after staining with PI. The living cells were stained with Calcein-AM and showed green fluorescence. Therefore, that live cells can be observed by fluorescence microscopy. The experimental results are shown in Figure. 32. After incubated with different groups for 48 h, partial cell death was observed after laser irradiation alone (980 nm or 650 nm). When both lasers are used simultaneously, most of the cells in the laser area are in a dead state. This further illustrates the effect of PTT/PDT synergistic treatment under laser irradiation. In addition, when CAT was contained in the microspheres, the inhibition effects on the growth of two kind of cancer cells were more significant. This is because CAT catalyzes the hydrogen peroxide in cancer cells to enhance the efficacy of PDT treatment.

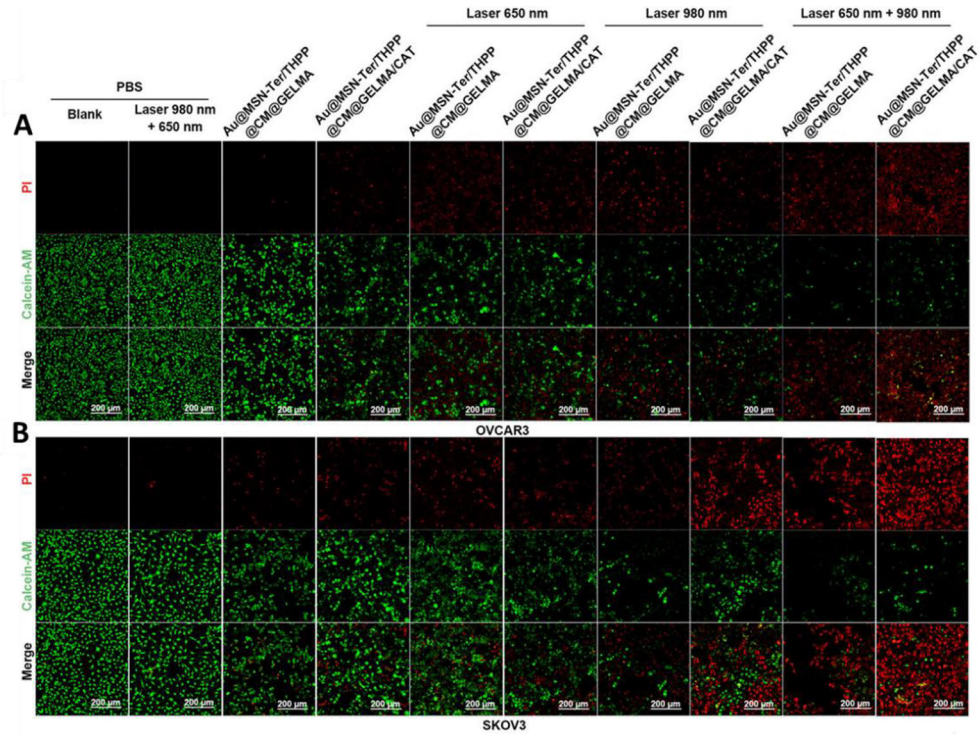

Figure 32. *Cytotoxicity of different GelMA microsphere formulations and treatments. A and B. Cell death analysis with confocal microscope after co-incubation with Au@MSN-Ter/THPP@CM@GelMA or Au@MSN-Ter/THPP@CM@GelMA/CAT for 48 hours and following 650 nm laser (0.4 W/cm², 5 min) and / or 980 nm laser (1 W/cm², 10 min) irradiation (Red: PI; Green: Calcein-AM; Scale bar: 200 μm).*

5.3.2.5. Cell apoptosis (V)

Next, using flow cytometry, we investigated the synergistic induction of apoptosis in SKOV3 /OVCAR3 cell lines by different microsphere preparations in the presence and absence of laser irradiation. Flow cytometry data (Figs. 33C and D) showed that near-infrared laser irradiation alone could hardly induce apoptosis, but significantly enhanced the induction of apoptosis by Au@MSN-Ter/THPP@CM@GelMA/CAT in SKOV3 cells /OVCAR3 cells, indicating that laser irradiation triggered the PTT/PDT effect in each treatment system, and CAT exerted the synergistic effect. Intra-group comparison showed that Au@MSN-Ter/THPP@CM@GelMA/CAT-treated cells exhibited higher apoptosis rates under laser conditions than the other treatment groups. This is similar to the results of the living and dead cell experiment. Figures. 33 A and B are the apoptotic columnar analysis views corresponding to the flow data in the non-laser and laser groups, respectively. The strong apoptosis induction effect shown by Au@MSN-Ter/THPP@CM@GelMA/CAT could be observed more clearly.

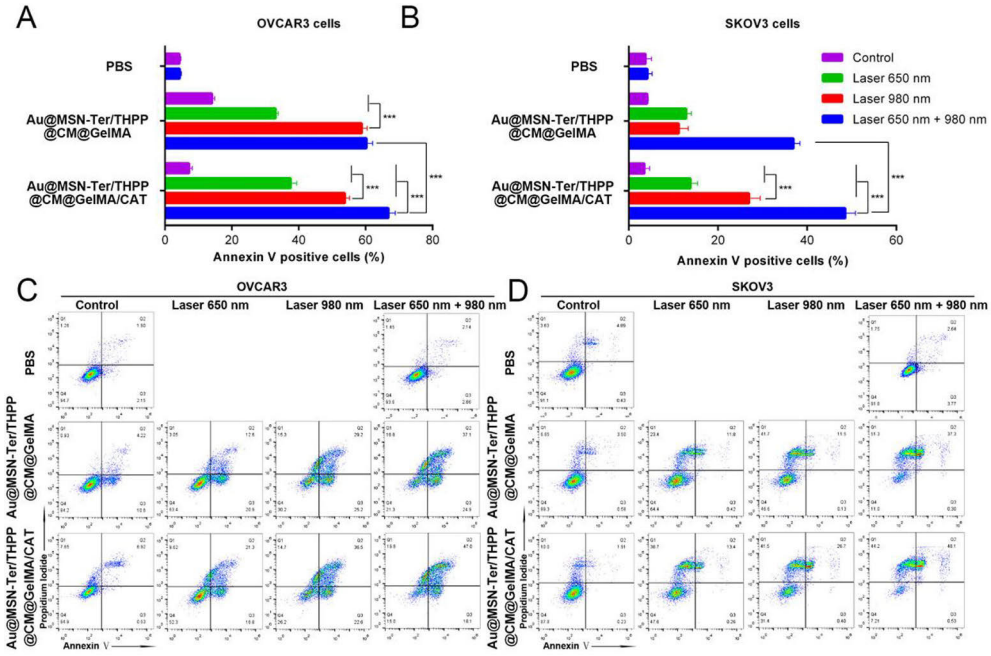

Figure 33. *Cytotoxicity of different GelMA microsphere formulations and treatments. A-D. Flow cytometry analysis of apoptotic cells by Annexin V-FITC/PI staining after co-incubation with Au@MSN-Ter/THPP@CM@GelMA or Au@MSN-Ter/THPP@CM@GelMA/CAT for 48 hours and following 650 nm laser (0.4 W/cm², 5 min) and / or 980 nm laser (1 W/cm², 10 min) irradiation.*

5.3.2.6. Detection of intracellular ROS (V)

We next examined intracellular ROS production by Au@MSN-Ter/THPP@CM@GelMA/CAT. To monitor the real-time dynamic changes of ROS, in this experiment, a probe DCFH-DA responding specifically to O_2· was used, and it could generate green fluorescence when reacting with ROS. SKOV3 cells were incubated with Au@MSN-Ter/THPP@CM@GelMA/CAT and Au@MSN-Ter/THPP@CM@GelMA for 20 min after the addition of probe DCFH-DA. Then laser irradiation was performed for 5 min, and confocal imaging was performed. As shown in Figure. 34, no obvious fluorescence signal was detected when no laser irradiation or photosensitizer was added. When both photosensitizer and laser irradiation existed simultaneously, a green fluorescence signal could be captured and the group filled with CAT had a stronger fluorescence signal. The experimental results showed that the photosensitizer in the microspheres could produce ROS as expected, and CAT could effectively promote ROS production. The fluorescence intensity was quantified by image J software and the results also showed a significant difference between Au@MSN-Ter/THPP@CM@GelMA/CAT and Au@MSN-Ter/THPP@CM@GelMA group

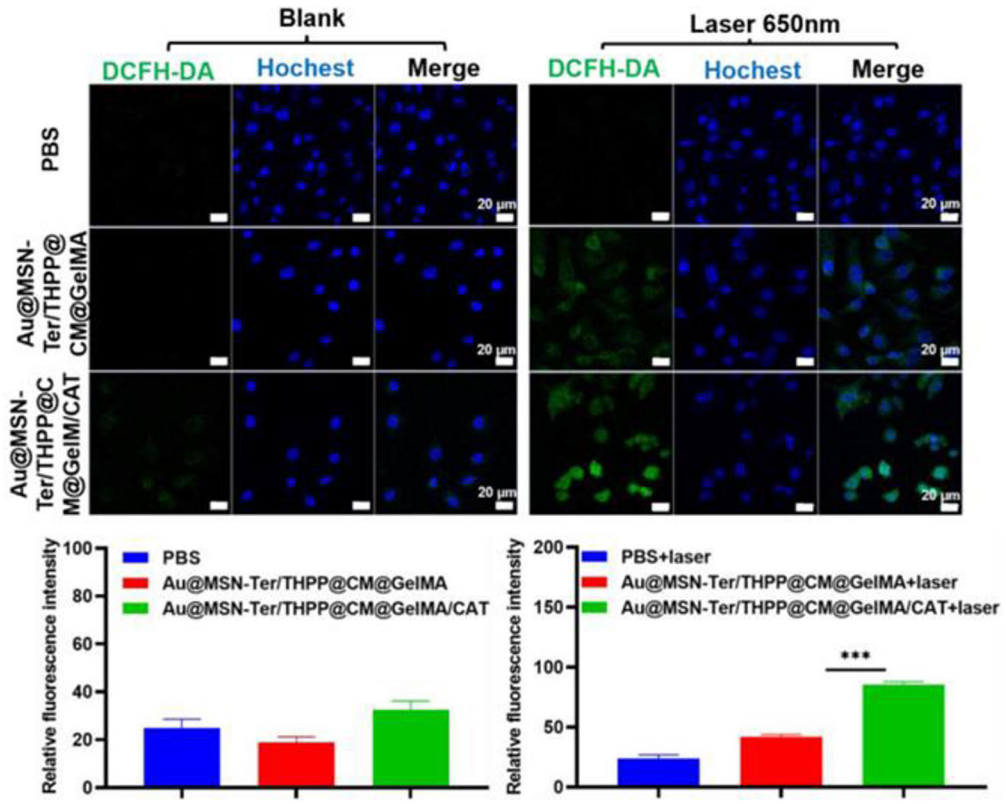

Figure 34. *Confocal microscope images of SKOV3 cell after co-incubation with Au@MSN-Ter/THPP@CM@GelMA or Au@MSN-Ter/THPP@CM@GelMA/CAT for 48 hours and selectively treated with 650 nm laser (0.4 W/cm^{-2}) for 5 min, Images of DCFH-DA stained SKOV3 cells and quantifications (Green: DCFH-DA; Blue: Hochest; Scale bar: 20 μm).*

5.3.2.7. Detection of immunogenic cell death (V)

To explore the mechanism of cell death induced by endoplasmic reticulum targeting nano-photosensitizer, fluorescence-labeled CAT and HMGB1 proteins were used for staining experiment. ICD-mediated apoptosis occurs in cells under ROS stimulation. CRT protein present in endoplasmic reticulum is released into cytoplasm and HMGB1 protein originally in nucleus. SKOV3 cells were incubated with different groups of preparations and then laser irradiated. The cells were fixed with 4% PFA for 5 min after cell treatment, washed and stained with CRT or HMGB1 antibody for 1 h, and finally stained with DAPI for 5 min for localization. As seen from confocal imaging, no fluorescence was observed in the CRT staining group and a small amount of fluorescence was observed in the nuclei of the HMGB1 staining group before exposure to NIR light. When irradiated with laser, CRT staining could be detected successfully in the cell images to enhance the green fluorescence. For HMGB1 protein, fluorescence was obviously released from the nucleus with a strong fluorescence signal in the cytoplasm, which confirmed the occurrence of ICD.

In particular, in the control group where cells were incubated with Au@MSN-Ter/THPP@CM, both CRT and HMGB1 detected stronger fluorescence intensities after irradiation with NIR light compared to Au@MSN /THPP@CM (Figure 35A and C). Subsequently, we quantified the fluorescence intensities of the two proteins using flow cytometry, and the results showed that the Au@MSN-Ter/THPP@CM+laser group exhibited the highest expression levels of both CRT and HMGB1 proteins (Figure 35B and D). The above experimental results have shown that under the stimulation of ROS, cells will undergo immunogenic death, and the nano-photosensitizer with the function of targeting endoplasmic reticulum can enhance the effect of ICD treatment.

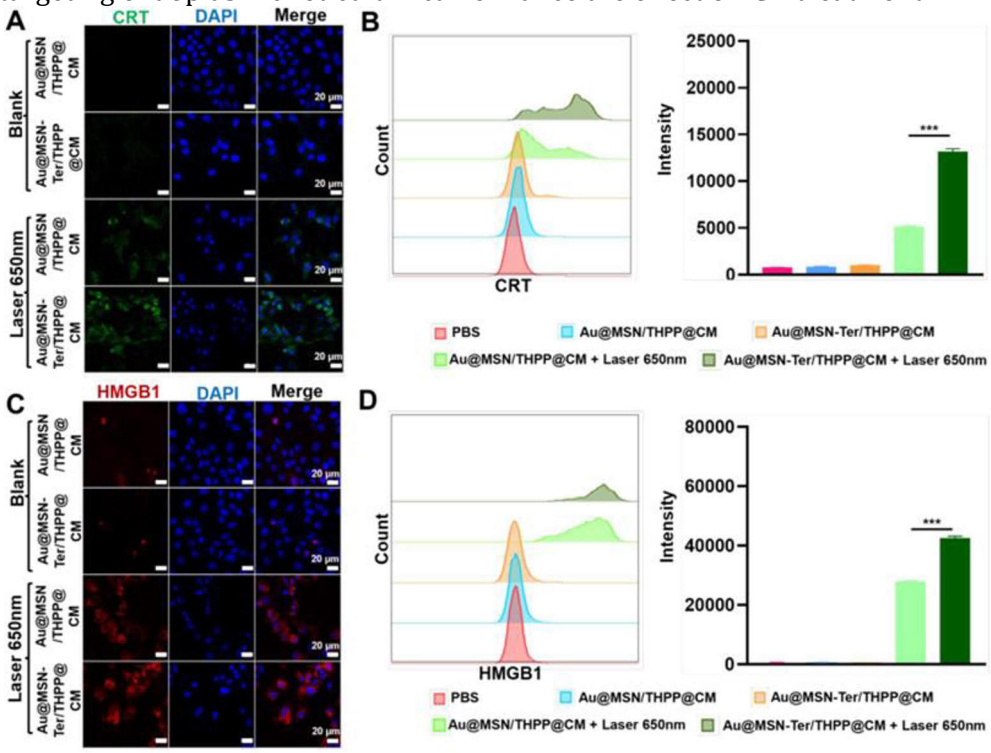

Figure 35. *Confocal microscope images of CRT and HMGB1 stained SKOV3 cells after Au@MSN-Ter/THPP@CM or Au@MSN-Ter/THPP@CM NPs treatment. Cells were stained with CRT (A) and HMGB1 (C) and imaged with confocal microscope after 24 hours of Au@MSN-Ter/THPP@CM or Au@MSN-Ter/THPP@CM NPs co-incubation and following 650 nm laser (0.4 W/cm^{-2}, 5 min) irradiation. Flow cytometry analysis and quantifications of CRT (B) or HMGB1 (D) positive cells after 24 hours of Au@MSN-Ter/THPP@CM or Au@MSN-Ter/THPP@CM NPs co-incubation and following 650 nm laser (0.4 W/cm^{-2}, 5 min) irradiation.*

To continue exploring the role of CAT in promoting PDT treatment, the same fluorescently labeled CAT and HMGB1 proteins were still used for staining experiments. The experimental operation method is consistent with the above. As observed from confocal microscope images, the fluorescence intensities of

both CRT and HMGB1 were higher in the CAT-added group than in the CAT-free group. Significant differences were also noted in the imageJ fluorescent quantitation results, demonstrating the synergistic effect of CAT on PDT treatment (Figure 36A and B).

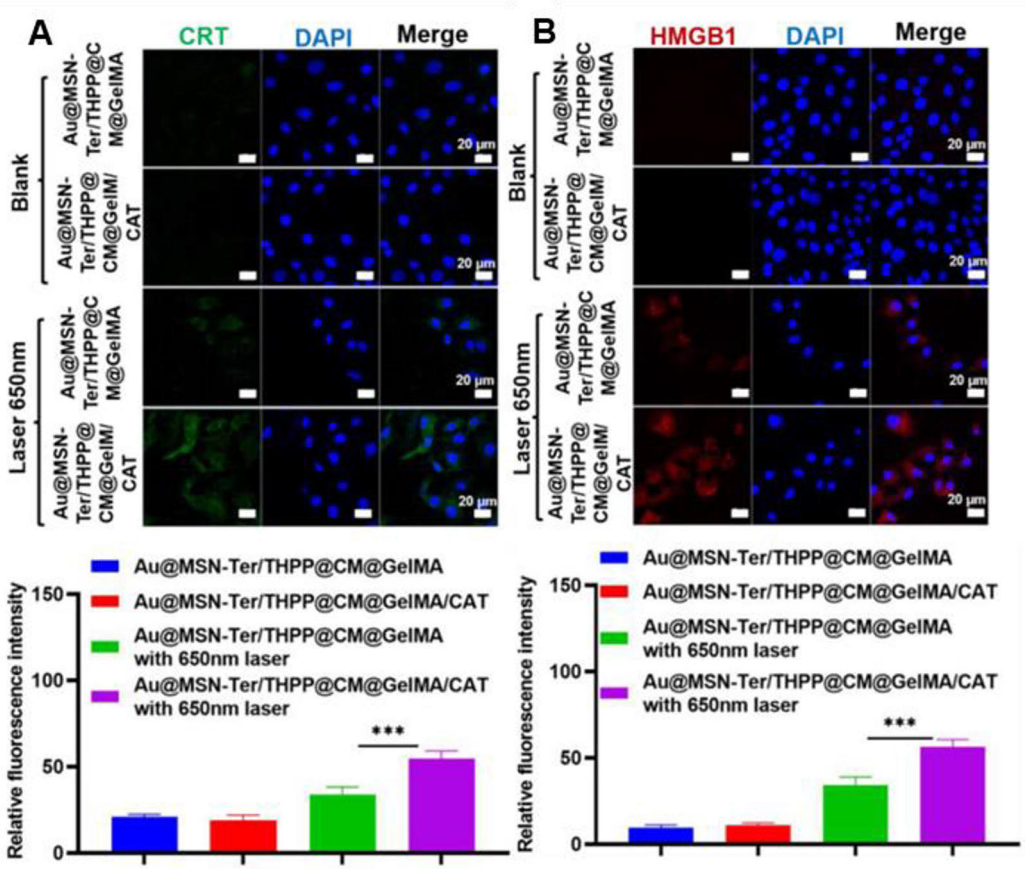

Figure 36. *Confocal microscope images of SKOV3 cell after co-incubation with Au@MSN-Ter/THPP@CM@GelMA or Au@MSN-Ter/THPP@CM@GelMA/CAT for 48 hours and selectively treated with 650 nm laser (0.4 W/cm^{-2}) for 5 min. Images of CRT (A) and HMGB1 (B) primary antibodies stained SKOV3 cells and quantifications (Green: CRT; Red: HMGB1; Blue: DAPI; Scale bar: 20 μm).*

5.3.4. Evaluation of antitumor effect *in vivo* (IV & V)

Due to the significant results *in vitro*, 4T1 tumor-bearing mice (IV) and SKOV3 ovarian tumor-bearing mice in situ (V) were used for *in vivo* antitumor experiments. For (IV), the mice were randomized into 4 groups: PBS, free PTX+DOX, Au@PTXSS-MSN/DOX@CM NPs, and Au@PTXSS-MSN/DOX@CM NPs with laser. Mice were treated for 18 days at three-day intervals and body weights and tumor size were recorded. The results showed that the Au@PTXSS-MSN/DOX@CM NPs+laser group had the best therapeutic effect, followed by Au@PTXSS-MSN/DOX@CM NPs group (Figure 37A). Subsequently,

H&E staining was performed on the tumor tissues and major organs of mice in different treatment groups to evaluate the nano-preparations' therapeutic effect and systemic toxicity. A large area of damage was observed in the tumor tissues of mice treated with nanoparticles with laser. In contrast, there were no significant changes in most tumor tissues in the control group. Eighteen days after injection of the nanomaterial, the health effects of the nanomaterial on five major organs (liver, lung, spleen, kidney, and heart) of the mouse were detected, and no histopathological abnormalities were found (Figure. 37D). Based on the above experimental results, it can be seen that the combination therapy of nanoparticle-mediated PTT and chemotherapy is very effective, and there is no toxic or side effect on normal tissues.

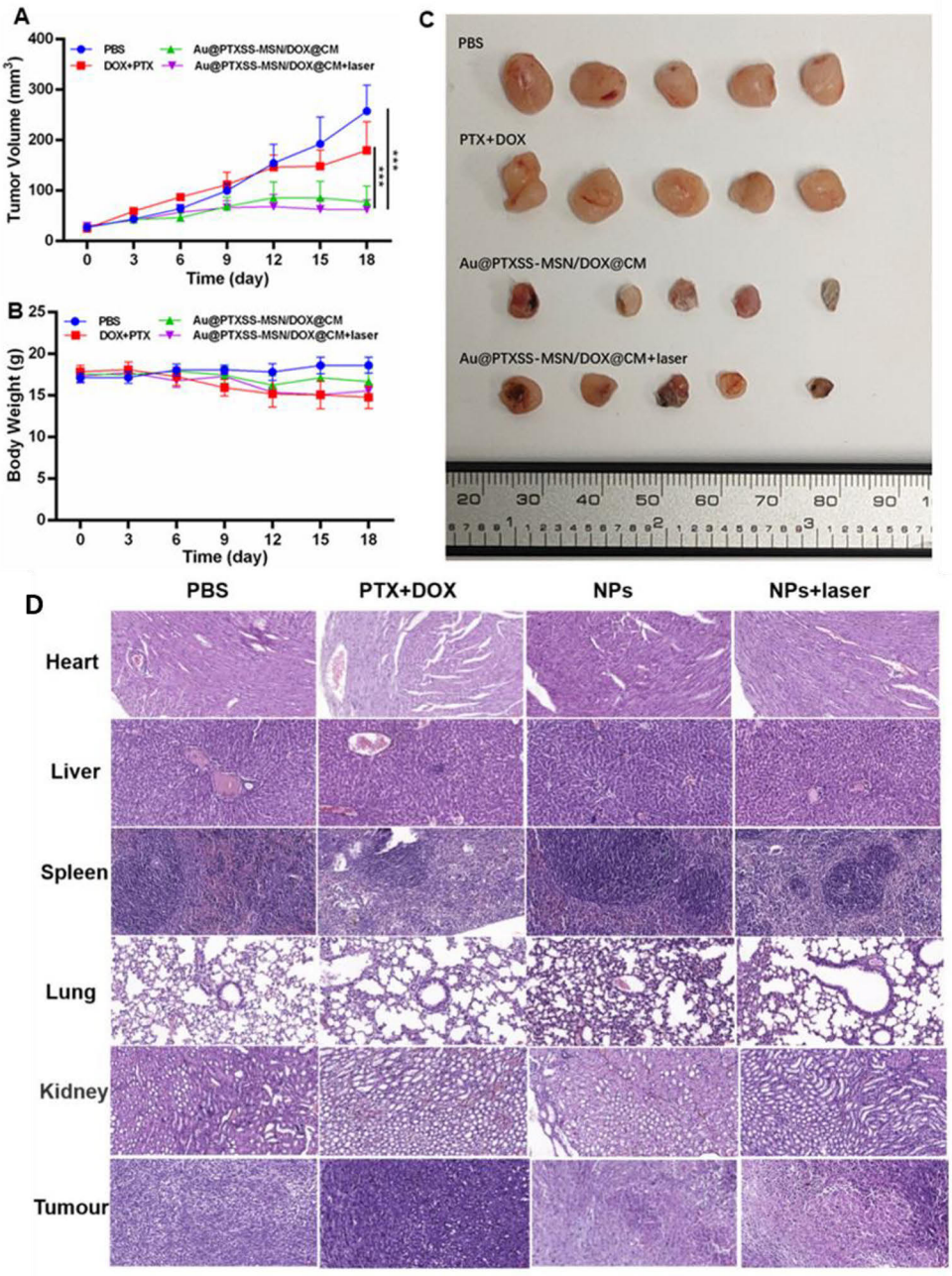

Figure 37. *Results of antitumor efficacy of Au@PTXSS-MSN/DOX@CM NPs in vivo. Recorded tumor volumes (A), body weight (B), photograph of isolated tumors from 4T1-tumor burden mice (C) and (D) HE staining images of different organs (scale bar: 100 μm).*

For (V), the mice were randomized into 4 groups: PBS, Au@MSN-Ter/THPP@CM NPs, Au@MSN-Ter/THPP@CM@GelMA/CAT, and Au@MSN-Ter/THPP@CM@GelMA/CAT with laser. Fluorescence imaging results (Figure

38B) showed that the fluorescence intensity in the NPs group was continuously increased in the tumor and liver from 6 h to 24 h. At 48 h, the fluorescence intensity in the tumor tissue was decreased, while a large amount of fluorescence was still retained in the liver. After 15 days of a single injection, fluorescence could be detected to retain the tumor site in the microsphere group, and the fluorescence intensity of the laser group was stronger. These results indicated that the microsphere groups had good drug retention capacity and the temperature generated by photothermal therapy could promote the release of drugs. This design also reduced the drug-induced metabolic pressure in the liver. After a single in situ injection, the tumor site was irradiated with a laser two days apart. The treatment cycle was 15 days, during which the body weight and tumor volume of mice in each group were measured and recorded daily. As shown in Figure. 38C, compared with the PBS group and NPs group, the microsphere laser treatment group had a more significant impact on the tumor weight but minimal impact on the body weight, showing the excellent treatment effect of microsphere preparation. To further study the therapeutic effect of tumor tissues, histological analysis was performed on the main organs (heart, liver, lung, kidney, and spleen) and tumor tissues of mice. As shown in Figure. 38D, compared with the organs of mice in the health group, there was no significant difference in the microsphere with laser treatment group, showing low biological toxicity. For tumor tissues, significant differences from PBS control groups were shown. Observation of H&E stained tumor sections revealed significant cytoplasmic leakage and karyomegaly in the Au@MSN-Ter/THPP@CM@GelMA/CAT+laser group (Figure 38D). Furthermore, TUNEL staining was used to locate the apoptotic cells in the tumor sections, and the same conclusion could be drawn. These results indicate that the combination of PTT and PDT has a significant tumor cell killing effect when compared to conventional chemotherapy and monotherapy regimens.

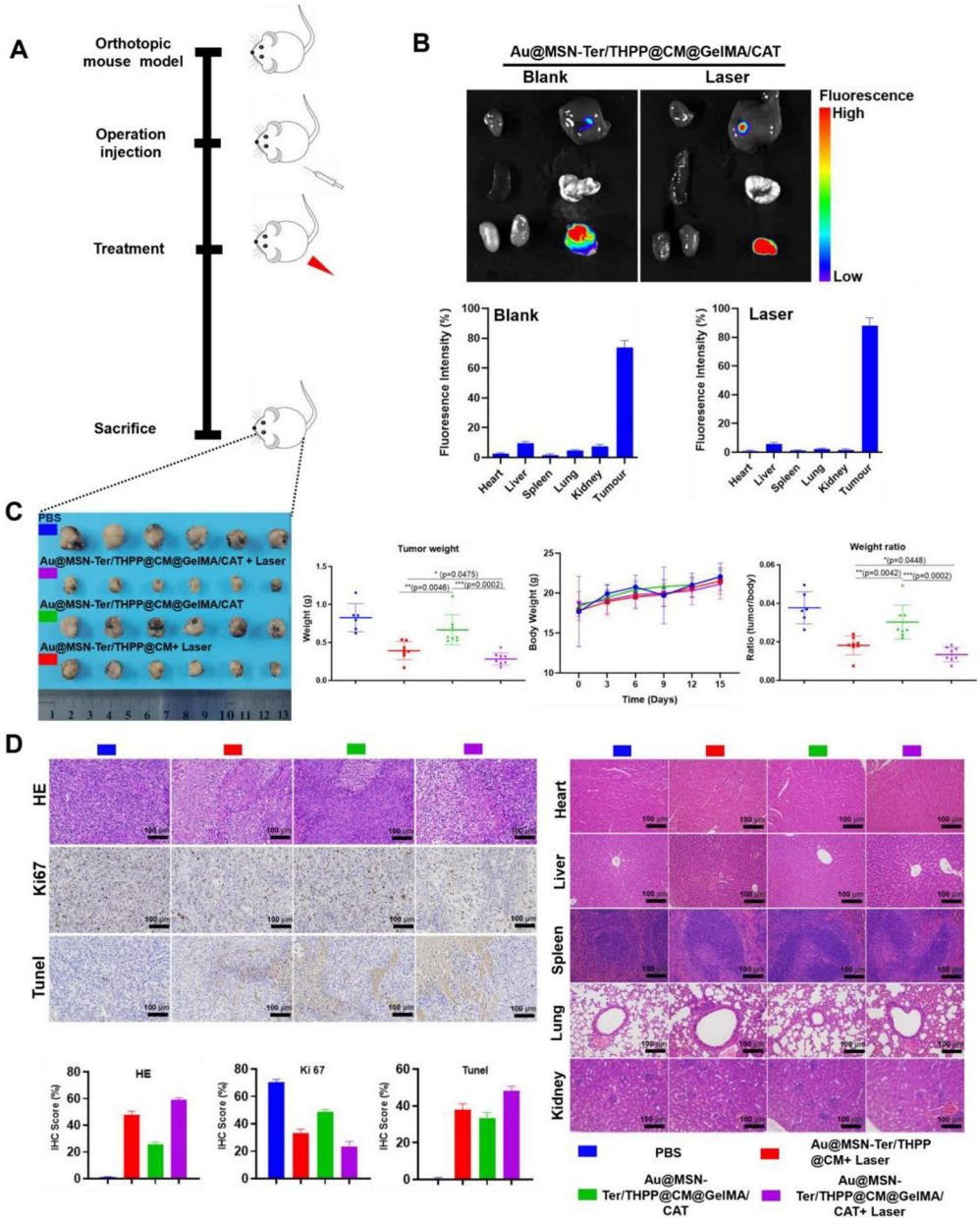

Figure 38. *Bio-imaging, tumors growth and histological analysis after different formulations of peritumoral administration. A. Illustration of animal experiment. B. Organ tissues THPP fluorescent signal captured by in vivo imaging system and quantifications (From left to right and up to down panels: Heart, liver, spleen, lung, kidney and tumor). C. Data of tumor images, tumor weight, mice body weight and weight ratio (tumor/body) (n ≥ 6). D. HE, Ki67 and Tunel staining images and quantifications of tumor, and HE staining images of different organs (n ≥ 6, 20 ×, scale bar: 100 μm).*

6. Conclusions and future remarks

6.1. Summary of the thesis results

The traditional chemotherapy drug delivery method and the inherent drawbacks of small molecule drugs make the effect of therapy unsatisfactory and even lead to increased drug toxicity. The delivery of antitumor nano prodrug system constructed by self-assembly or co-assembly of prodrug molecules can not only realize targeted delivery and controlled release of two or more drugs, improve pharmacokinetic properties of different drugs, enhance synergistic effect of the drugs and improve antitumor effect, but also reduce or avoid potential toxic and side effects of excessive use of nano carrier materials. In addition, through rational design and application of the prodrug technology to inorganic carriers, a targeted multifunctional nanodrug delivery system can be constructed.

In the first part of this thesis, a series of reduction-sensitive prodrugs were synthesized using PTX, DOX, CPT and THPP as reactants. These prodrug molecules can be self-assembled into spherical prodrug nanoparticles using microfluidics. Prodrug nanoparticles have a very high drug loading degree and can gradually release two active drugs within 24 hours in a reducing environment within tumor cells. The therapeutic strategy of dual prodrugs show significant synergistic inhibition on the proliferation of various tumor cells, which is conducive to overcoming the drug resistance of cancer cells.

In order to enrich the functions of the drug delivery system, an easily modified MSN-based system was used, and the prodrug technology and cancer cell membrane camouflage technology were applied to the system to construct a co-assembled nano prodrug. The Au@MSN carrier has a very good photothermal effect, so photothermal treatment can be performed. At the same time, DOX loaded in the pores and PTX prodrug on the surface of the carrier can synergistically treat breast cancer cells. The *in vitro* release experiments of the nanoparticles demonstrated that the drug delivery system had good reduction sensitivity and photothermal response. Drug toxicity experiments showed that the combination therapy with targeting function had good efficacy *in vivo* and *in vitro*.

In addition, Au@MSN-Ter with targeted endoplasmic reticulum function and catalase were co-encapsulated into GelMa microspheres to construct a low-dose minimally invasive sustained-release drug delivery system. It has been found that the microspheres can sustain the release of THPP for up to 20 days, and have the characteristics of temperature control. Targeted nanoparticles to the endoplasmic reticulum can effectively increase ER stress and enable more precise photodynamic therapy, thereby enhancing the effect of immunogenic cell death. Meanwhile, catalase can improve the hypoxia in tumor tissues. Based on these advantages, the sustained-release drug delivery system of GelMa microspheres has achieved very good antitumor effect in the in situ model of ovarian cancer. Therefore, the combination of organelle targeting strategy and prodrug technology has great potential for cancer treatment.

6.2. Future remarks

6.2.1. Precise treatment of prodrug

Although prodrug self-assembled nanoparticles have achieved good therapeutic effects, finer prodrugs that can target organelles have been investigated. In this study, we demonstrated that the self-assembled nanoparticles of prodrugs have extremely high drug loading capacity, controllable particle size, and environmental responsiveness. However, this study is limited to the combination therapeutic properties of the two prodrugs. Therefore, there is a need to further diversify the functions of prodrug molecules, expand the concept of prodrug, and design prodrug nanomaterials that can target organelles for accurate drug delivery.

6.2.2. Combination of metal catalysis and prodrug technology

In addition, the diverse modifications and high drug-loading capacity of mesoporous silica nanoparticles provide a broad platform for improving tumor delivery efficiency. With these advantages, we can design MSNs doped with disulfide bonds, which can degrade in the reductive intracellular environment of tumors. By encapsulating different metal nanoparticles and modifying the surface with prodrugs, multifunctional nanocarriers can be generated. Therefore, the combination of prodrug technology, metal catalysis, and MSNs holds great potential in the treatment of cancer or other diseases.

7. Acknowledgements

The long doctoral career is coming to the end. Looking back on the days when I was studying in Åbo Akademi University, I experienced the confusion and fear of scientific research, the pain and anxiety of experimental failure, and the joy after solving difficult problems. These will be valuable wealth for me to improve my personal ability and inject courage and strength into starting a new journey in the future.

First of all, I would like to sincerely thank my tutor Professor Hongbo Zhang. Thank you for your great help at the key point of my study, so that I can have the opportunity to continue my study. I can't grow up without your teaching and support. Your active scientific research and innovative ideas, meticulous logical thinking, broad research horizons and rigorous scholarship set an example for me, and your teaching and encouragement will also inspire me to continue on the road of scientific research. Your principles of putting others before yourself, dedication, optimism and open-mindedness and simple life style have deeply infected me, and will also guide and urge me in my future work and life.

Secondly, I would like to express my heartfelt gratitude to my co-supervisor, Professor Jessica M. Rosenholm, for selecting me as a doctoral student in the PSL group, which has provided me with a wonderful research experience in Finland. I am truly appreciative of your continuous guidance, selfless assistance, and encouragement throughout my studies. Thank you for taking the time to revise the grammar and content of my papers, as well as for providing me with invaluable guidance during my graduation process. Your unwavering support and encouragement have been instrumental in my personal and academic growth.

I would also like to thank Yuezhou Zhang, Junnian Zhou and Yong Guo for their guidance in the experiment. The successful completion of the thesis can not be separated from the selfless help and support of the members of the research group. Their companionship has made my scientific research smoother and my doctoral career more colorful. My thesis is permeated with their hard work and wisdom. I would like to express my deep gratitude to Chang, Xiaoyu, Wenhui, Ezgi, Jiaqi, Yonghui, Meixin, Wali, Oliver, Rawand, Fanny, Chengcheng, Shengyi, WuYang for their efforts!

Thank all the teachers, colleagues and friends who have cared, supported and helped me! Thank my family for their encouragement and support! This wonderful time will accompany me all the way forward!

Turku, 2023

Xiaodong Ma

8. References

Li S, Shan X, Wang Y, et al. Dimeric prodrug-based nanomedicines for cancer therapy[J]. Journal of Controlled Release, 2020, 326: 510-522.

Xie, Angel, et al. "Stimuli-responsive prodrug-based cancer nanomedicine." EBioMedicine 56 (2020): 102821.

Ding C, Chen C, Zeng X, et al. Emerging Strategies in Stimuli-Responsive Prodrug Nanosystems for Cancer Therapy[J]. ACS nano, 2022, 16(9): 13513-13553.

Dong X, Brahma R K, Fang C, et al. Stimulus-responsive self-assembled prodrugs in cancer therapy[J]. Chemical Science, 2022, 13(15): 4239-4269.

Sargazi S, Laraib U, Barani M, et al. Recent trends in the mesoporous silica nanoparticles with rode-like morphology for cancer theranostics: a review[J]. Journal of Molecular Structure, 2022: 132922.

2013. Image-based analysis of lipid nanoparticle-mediated siRNA delivery, intracellular trafficking and endosomal escape %J Nature biotechnology.

Adeel, M., Duzagac F., Canzonieri V., Rizzolio F. J. A. A. N. M., 2020. Self-therapeutic nanomaterials for cancer therapy: A review. 3, 4962-4971.

Al-Khedhairy, A. A., Wahab R. J. A. S., 2022. Size-dependent cytotoxic and molecular study of the use of gold nanoparticles against liver cancer cells. 12, 901.

Alavi, M., Hamidi M. J. D. m., therapy p., 2019. Passive and active targeting in cancer therapy by liposomes and lipid nanoparticles. 34,

Alberts, S. R. J. A. o. O., 2003. Gemcitabine and oxaliplatin for metastatic pancreatic adenocarcinoma: a North Central Cancer Treatment Group phase II study. 14, 580-585.

Aldahhan, R., Almohazey D., Khan F. A., in Seminars in Cancer Biology. (Elsevier, 2022), vol. 86, pp. 1056-1065.

AlQahtani, A. D., O'Connor D., Domling A., Goda S. K. J. B., Pharmacotherapy, 2019. Strategies for the production of long-acting therapeutics and efficient drug delivery for cancer treatment. 113, 108750.

Ashrafizadeh, M., Delfi M., Zarrabi A., Bigham A., Sharifi E., Rabiee N., Paiva-Santos A. C., Kumar A. P., Tan S. C., Hushmandi K. J. J. o. C. R., 2022. Stimuli-responsive liposomal nanoformulations in cancer therapy: Pre-clinical & clinical approaches. 351, 50-80.

Asiabi, H., Yamini Y., Alipour M., Shamsayei M., Hosseinkhani S. J. M. S., Engineering, 2019. Synthesis and characterization of a novel biocompatible pseudo-hexagonal NaCa-layered double metal hydroxides for smart pH-responsive drug release of dacarbazine and enhanced anticancer activity in malignant melanoma. 97, 96-102.

Attia, M. F., Anton N., Wallyn J., Omran Z., Vandamme T. F. J. J. o. P., Pharmacology, 2019. An overview of active and passive targeting strategies to improve the nanocarriers efficiency to tumour sites. 71, 1185-1198.

Azevedo, S., Costa-Almeida R., Santos S. G., Magalhães F. D., Pinto A. M. J. A. M. T., 2022. Advances in carbon nanomaterials for immunotherapy. 27, 101397.

Bai, S., Ma X., Shi X., Shao J., Zhang T., Wang Y., Cheng Y., Xue P., Kang Y., Xu Z. J. A. a. m., interfaces, 2019. Smart unimolecular micelle-based polyprodrug with dual-redox stimuli response for tumor microenvironment: enhanced in vivo delivery efficiency and tumor penetration. 11, 36130-36140.

Bayer, I. S. J. M., 2020. Hyaluronic acid and controlled release: A review. 25, 2649.

Bazak, R., Houri M., El Achy S., Hussein W., Refaat T. J. M., oncology c., 2014. Passive targeting of nanoparticles to cancer: A comprehensive review of the literature. 2, 904-908.

Bazak, R., Houri M., El Achy S., Kamel S., Refaat T. J. J. o. c. r., oncology c., 2015. Cancer active targeting by nanoparticles: a comprehensive review of literature. 141, 769-784.

Bertrand, N., Wu J., Xu X., Kamaly N., Farokhzad O. C. J. A. d. d. r., 2014. Cancer nanotechnology: the impact of passive and active targeting in the era of modern cancer biology. 66, 2-25.

Bian, W., Wang Y., Pan Z., Chen N., Li X., Wong W.-L., Liu X., He Y., Zhang K., Lu Y.-J. J. A. A. N. M., 2021. Review of functionalized nanomaterials for photothermal therapy of cancers. 4, 11353-11385.

Bing-Shuai, Z., Shi-Han X., Song-Tao H., Li-Heng S., Jie-Kai L., Rui S., Wei L., Xue B., Lin X., Lin W. J. C. J. o. A. C., 2022. Recent progress of upconversion nanoparticles in the treatment and detection of various diseases. 50, 19-32.

Cai, H., Tan P., Chen X., Kopytynski M., Pan D., Zheng X., Gu L., Gong Q., Tian X., Gu Z. J. A. M., 2022. Stimuli-Sensitive Linear–Dendritic Block Copolymer–Drug Prodrug as a Nanoplatform for Tumor Combination Therapy. 34, 2108049.

Cao, J., Zhang Y., Shi W., Du L., Cui Z., Liu S., Zhao R., Wang S., Zhang Q., Kong X. J. A. A. N. M., 2022. Mitochondria-Targeted Photodynamic Cancer Therapy of Nanoscale Liposome-Encapsulating Boron Dipyrromethene Photosensitizers Conjugated with Pyridine Cations. 5, 5459-5469.

Chan, H. K., Kwok P. C. L. J. A. d. d. r., 2011. Production Methods for Nanodrug Particles Using the Bottom-up Approach. 63, 406-416.

Chen, W., Sun Z., Lu L. J. A. C. I. E., 2021. Targeted Engineering of medicinal chemistry for cancer therapy: Recent advances and perspectives. 60, 5626-5643.

Chen, W. H., Luo G. F., Zhang X. Z. J. A. M., 2019. Recent advances in subcellular targeted cancer therapy based on functional materials. 31, 1802725.

Cheng, X., Li H., Ge X., Chen L., Liu Y., Mao W., Zhao B., Yuan W.-E. J. F. i. M. B., 2020. Tumor-microenvironment-responsive size-shrinkable drug-delivery nanosystems for deepened penetration into tumors. 7, 576420.

Cheng, Y., Ji Y. J. J. o. c. r., 2020. Mitochondria-targeting nanomedicine self-assembled from GSH-responsive paclitaxel-ss-berberine conjugate for synergetic cancer treatment with enhanced cytotoxicity. 318, 38-49.

Cheng, Y., Morshed R. A., Auffinger B., Tobias A. L., Lesniak M. S. J. A. D. D. R., 2014. Multifunctional nanoparticles for brain tumor imaging and therapy. 66, 42-57.

Chhabra, R., Sharma J., Liu Y., Rinker S., Yan H. J. A. d. d. r., 2010. DNA self-assembly for nanomedicine. 62, 617-625.

Chintamaneni, P. K., Nagasen D., Babu K. C., Mourya A., Madan J., Srinivasarao D. A., Ramachandra R., Santhoshi P. M., Pindiprolu S. K. S. J. J. o. C. R., 2022. Engineered upconversion nanocarriers for synergistic breast cancer imaging and therapy: Current state of art. 352, 652-672.

Chow, J. C. J. N., 2022. Application of Nanomaterials in Biomedical Imaging and Cancer Therapy. 12, 726.

Chu, B., Qu Y., He X., Hao Y., Yang C., Yang Y., Hu D., Wang F., Qian Z. J. A. F. M., 2020. ROS-responsive camptothecin prodrug nanoparticles for on-demand drug release and combination of chemotherapy and photodynamic therapy. 30, 2005918.

Chuang, Y.-C., Lee H.-L., Chiou J.-F., Lo L.-W. J. J. o. N., 2022. Recent advances in gold nanomaterials for photothermal therapy. 3, 117-131.

Curcio, A., Perez J. E., Prévéral S., Fromain A., Genevois C., Michel A., Van de Walle A., Lalatonne Y., Faivre D., Ménager C. J. S. R., 2023. The role of tumor model in magnetic targeting of magnetosomes and ultramagnetic liposomes. 13, 2278.

Da, A., in 2020 9th International Conference on Bioinformatics and Biomedical Science. (2020), pp. 1-7.

Deng, H., Zhou Z., Yang W., Lin L.-s., Wang S., Niu G., Song J., Chen X. J. N. L., 2020. Endoplasmic reticulum targeting to amplify immunogenic cell death for cancer immunotherapy. 20, 1928-1933.

Ding, J., Jin Y., Zhu F., Zhu C., Peng J., Su T., Cai J. J. J. o. H. E., 2022. Facile synthesis of NaYF4: Yb up-conversion nanoparticles modified with photosensitizer and targeting antibody for in vitro photodynamic therapy of hepatocellular carcinoma. 2022,

Ding, J., Xiao C., Li Y., Cheng Y., Wang N., He C., Zhuang X., Zhu X., Chen X. J. J. o. C. R., 2013. Efficacious hepatoma-targeted nanomedicine self-assembled from galactopeptide and doxorubicin driven by two-stage physical interactions. 169, 193-203.

Ding, X., Yu W., Wan Y., Yang M., Hua C., Peng N., Liu Y. J. C. p., 2020. A pH/ROS-responsive, tumor-targeted drug

delivery system based on carboxymethyl chitin gated hollow mesoporous silica nanoparticles for anti-tumor chemotherapy. 245, 116493.
Ding, Z., He Y., Rao H., Zhang L., Nguyen W., Wang J., Wu Y., Han C., Xing C., Yan C. J. N., 2022. Novel Fluorescent Probe Based on Rare-Earth Doped Upconversion Nanomaterials and Its Applications in Early Cancer Detection. 12, 1787.
Diwakar, B. S., Sekhar D. C., Reddy V., Bhavani P., Koduri R., Srinivasarao S., in Emerging Applications of Low Dimensional Magnets. (CRC Press, 2023), pp. 137-146.
Doghish, A. S., Hashem A. H., Shehabeldine A. M., Sallam A.-A. M., El-Sayyad G. S., Salem S. S. J. J. o. D. D. S., Technology, 2022. Nanocomposite based on gold nanoparticles and carboxymethyl cellulose: synthesis, characterization, antimicrobial, and anticancer activities. 77, 103874.
Doughty, A. C., Hoover A. R., Layton E., Murray C. K., Howard E. W., Chen W. R. J. M., 2019. Nanomaterial applications in photothermal therapy for cancer. 12, 779.
Durr, N. J., Larson T., Smith D. K., Korgel B. A., Sokolov K., Ben-Yakar A. J. N. l., 2007. Two-photon luminescence imaging of cancer cells using molecularly targeted gold nanorods. 7, 941-945.
Edis, Z., Wang J., Waqas M. K., Ijaz M., Ijaz M. J. I. J. o. N., 2021. Nanocarriers-Mediated Drug Delivery Systems for Anticancer Agents: An Overview and Perspectives. Volume 16, 1313-1330.
Eslami, P., Albino M., Scavone F., Chiellini F., Morelli A., Baldi G., Cappiello L., Doumett S., Lorenzi G., Ravagli C. J. N., 2022. Smart magnetic nanocarriers for multi-stimuli on-demand drug delivery. 12, 303.
Fahmy, H. M., Abu Serea E. S., Salah-Eldin R. E., Al-Hafiry S. A., Ali M. K., Shalan A. E., Lanceros-Méndez S. J. A. B. S., Engineering, 2022. Recent progress in graphene-and related carbon-nanomaterial-based electrochemical biosensors for early disease detection. 8, 964-1000.
Fan, J., He N., He Q., Liu Y., Ma Y., Fu X., Liu Y., Huang P., Chen X. J. N., 2015. A novel self-assembled sandwich nanomedicine for NIR-responsive release of NO. 7, 20055-20062.
Feng, X., Dixon H., Glen-Ravenhill H., Karaosmanoglu S., Li Q., Yan L., Chen X. J. A. T., 2019. Smart nanotechnologies to target tumor with deep penetration depth for efficient cancer treatment and imaging. 2, 1900093.
Fidler, I., Kripke M. J. S., 1977. Metastasis results from preexisting variant cells within a malignant tumor. 197, 893-895.
Filipów, S., Łaczmański Ł. J. F. i. g., 2019. Blood circulating miRNAs as cancer biomarkers for diagnosis and surgical treatment response. 10, 169.
Gailani, S. J. C., 2015. Comparison of treatment of metastatic gastrointestinal cancer with 5-fluorouracil (5-FU) to a combination of 5-FU with cytosine arabinoside. 29, 1308-1313.
Gannimani, R., Walvekar P., Naidu V. R., Aminabhavi T. M., Govender T. J. J. o. c. r., 2020. Acetal containing polymers as pH-responsive nano-drug delivery systems. 328, 736-761.
Gao, P., Pan W., Li N., Tang B. J. A. a. m., interfaces, 2019. Boosting cancer therapy with organelle-targeted nanomaterials. 11, 26529-26558.
Gao, P., Pan W., Li N., Tang B. J. C. s., 2019. Fluorescent probes for organelle-targeted bioactive species imaging. 10, 6035-6071.
Gao, P., Wang H., Cheng Y. J. C. C. L., 2022. Strategies for efficient photothermal therapy at mild temperatures: Progresses and challenges. 33, 575-586.
Gerelkhuu, Z., Lee Y.-I., Yoon T. H. J. N., 2022. Upconversion Nanomaterials in Bioimaging and Biosensor Applications and Their Biological Response. 12, 3470.
Ghimire, C., Wang H., Li H., Vieweger M., Xu C., Guo P. J. A. n., 2020. RNA nanoparticles as rubber for compelling vessel extravasation to enhance tumor targeting and for fast renal excretion to reduce toxicity. 14, 13180-13191.
Gratton, S., Ropp P., Pohlhaus P., Luft J., Madden V., Napier M., Desimone J. J. P. o. t. N. A. o. S. o. t. U. S. o. A., 2008. The effect of particle design on cellular internalization pathways. 105, 11613-11618.
Guo, K., Liu Y., Tang L., Shubhra Q. T. J. C. E. J., 2022. Homotypic biomimetic coating synergizes chemo-photothermal combination therapy to treat breast

cancer overcoming drug resistance. 428, 131120.
Guo, X., Wei X., Chen Z., Zhang X., Yang G., Zhou S. J. P. i. M. S., 2020. Multifunctional nanoplatforms for subcellular delivery of drugs in cancer therapy. 107, 100599.
Gupta, C., Prakash D., Gupta S. J. F. B., 2017. Cancer treatment with nano-diamonds. 9, 62-70.
Han, H. S., Choi K. Y. J. B., 2021. Advances in nanomaterial-mediated photothermal cancer therapies: toward clinical applications. 9, 305.
Hao, Y., Chen Y., He X., Yu Y., Han R., Li Y., Yang C., Hu D., Qian Z. J. A. S., 2020. Polymeric nanoparticles with ROS-responsive prodrug and platinum nanozyme for enhanced chemophotodynamic therapy of colon cancer. 7, 2001853.
He, M., Qin Z., Liang X., He X., Zhu B., Lu Z., Wei Q., Zheng L. J. R. B., 2021. A pH-responsive mesoporous silica nanoparticles-based drug delivery system with controlled release of andrographolide for OA treatment. 8, rbab020.
He, Q., Chen J., Yan J., Cai S., Xiong H., Liu Y., Peng D., Mo M., Liu Z. J. A. J. o. P. S., 2020. Tumor microenvironment responsive drug delivery systems. 15, 416-448.
He, W., Ma G., Shen Q., Tang Z. J. N., 2022. Engineering gold nanostructures for cancer treatment: spherical nanoparticles, nanorods, and atomically precise nanoclusters. 12, 1738.
He, Y., Guo S., Wu L., Chen P., Wang L., Liu Y., Ju H. J. B., 2019. Near-infrared boosted ROS responsive siRNA delivery and cancer therapy with sequentially peeled upconversion nano-onions. 225, 119501.
He, Y., Hu C., Li Z., Wu C., Zeng Y., Peng C. J. M. T. B., 2022. Multifunctional carbon nanomaterials for diagnostic applications in infectious diseases and tumors. 100231.
Heeke, S., Mograbi B., Alix-Panabières C., Hofman P. J. C., 2019. Never travel alone: the crosstalk of circulating tumor cells and the blood microenvironment. 8, 714.
Henderson, I. C. J. J. o. C. O. O. J. o. t. A. S. o. C. O., 2003. Improved outcomes from adding sequential Paclitaxel but not from escalating Doxorubicin dose in an adjuvant chemotherapy regimen for patients with node-positive primary breast cancer. 21, 976.
Hoare, T., Pelton R. J. M., 2004. Highly pH and temperature responsive microgels functionalized with vinylacetic acid. 37, 2544-2550.
Hou, S., Gao Y.-E., Ma X., Lu Y., Li X., Cheng J., Wu Y., Xue P., Kang Y., Guo M. J. C. E. J., 2021. Tumor microenvironment responsive biomimetic copper peroxide nanoreactors for drug delivery and enhanced chemodynamic therapy. 416, 129037.
Hsiang, Y. H., Hertzberg R. P., Hecht S. M., Liu L. F. J. J. o. B. C., 1985. Camptothecin induces protein-linked DNA breaks via mammalian DNA topoisomerase I. 260, 14873-14878.
Hu, X., Ha E., Ai F., Huang X., Yan L., He S., Ruan S., Hu J. J. C. C. R., 2022. Stimulus-responsive inorganic semiconductor nanomaterials for tumor-specific theranostics. 473, 214821.
Hua, S., He J., Zhang F., Yu J., Zhang W., Gao L., Li Y., Zhou M. J. B., 2021. Multistage-responsive clustered nanosystem to improve tumor accumulation and penetration for photothermal/enhanced radiation synergistic therapy. 268, 120590.
Huang, G., Qiu Y., Yang F., Xie J., Chen X., Wang L., Yang H. J. N. l., 2021. Magnetothermally triggered free-radical generation for deep-seated tumor treatment. 21, 2926-2931.
Huang, R., Zhou X., Chen G., Su L., Liu Z., Zhou P., Weng J., Min Y. J. W. I. R. N., Nanobiotechnology, 2022. Advances of functional nanomaterials for magnetic resonance imaging and biomedical engineering applications. 14, e1800.
Huang, T., Li S., Fang J., Li F., Tu S. J. B. M., 2021. Antibody-activated trans-endothelial delivery of mesoporous organosilica nanomedicine augments tumor extravasation and anti-cancer immunotherapy. 6, 2158-2172.
Huang, X., Jain P. K., El-Sayed I. H., El-Sayed M. A. J. L. i. m. s., 2008. Plasmonic photothermal therapy (PPTT) using gold nanoparticles. 23, 217-228.
Hussein, H. A., Abdullah M. A. J. A. N., 2022. Novel drug delivery systems based on silver nanoparticles, hyaluronic acid, lipid nanoparticles and liposomes for cancer treatment. 12, 3071-3096.

Jafari, S., Derakhshankhah H., Alaei L., Fattahi A., Varnamkhasti B. S., Saboury A. A. J. B., Pharmacotherapy, 2019. Mesoporous silica nanoparticles for therapeutic/diagnostic applications. 109, 1100-1111.

Jahangiri-Manesh, A., Mousazadeh M., Taji S., Bahmani A., Zarepour A., Zarrabi A., Sharifi E., Azimzadeh M. J. P., 2022. Gold nanorods for drug and gene Delivery: An overview of recent advancements. 14, 664.

Jiang, M., Han X., Guo W., Li W., Chen J., Ren G., Sun B., Wang Y., He Z. J. R. A., 2016. Star-shape paclitaxel prodrug self-assembled nanomedicine: combining high drug loading and enhanced cytotoxicity. 6, 109076-109082.

Jin, H., Zhu T., Huang X., Sun M., Li H., Zhu X., Liu M., Xie Y., Huang W., Yan D. J. B., 2019. ROS-responsive nanoparticles based on amphiphilic hyperbranched polyphosphoester for drug delivery: Light-triggered size-reducing and enhanced tumor penetration. 211, 68-80.

Kalashgrani, M. Y., Javanmardi N. J. A. i. A. N.-T., 2022. Multifunctional Gold nanoparticle: As novel agents for cancer treatment. 1-6.

Kang, M. S., Lee H., Jeong S. J., Eom T. J., Kim J., Han D.-W. J. B., 2022. State of the art in carbon nanomaterials for photoacoustic imaging. 10, 1374.

Kang, Y. S., Risbud S., Rabolt J. F., Stroeve P. J. C. o. M., 1996. Synthesis and characterization of nanometer-size Fe3O4 and γ-Fe2O3 particles. 8, 2209-2211.

Kankala, R. K., Han Y. H., Na J., Lee C. H., Sun Z., Wang S. B., Kimura T., Ok Y. S., Yamauchi Y., Chen A. Z. J. A. m., 2020. Nanoarchitectured structure and surface biofunctionality of mesoporous silica nanoparticles. 32, 1907035.

Karaman, D. Ş., Pamukçu A., Karakaplan M. B., Kocaoglu O., Rosenholm J. M. J. I. J. o. N., 2021. Recent advances in the use of mesoporous silica nanoparticles for the diagnosis of bacterial infections. 16, 6575.

Kaur, H., Thakur V. K., Siwal S. S. J. M. T. P., 2022. Recent advancements in graphdiyne-based nano-materials for biomedical applications. 56, 112-120.

Kearns, O., Camisasca A., Giordani S. J. M., 2022. Hyaluronic acid-conjugated carbon nanomaterials for enhanced tumour targeting ability. 27, 48.

Kievit, F. M., Zhang M. J. A. o. c. r., 2011. Surface engineering of iron oxide nanoparticles for targeted cancer therapy. 44, 853-862.

Klochkov, S. G., Neganova M. E., Nikolenko V. N., Chen K., Somasundaram S. G., Kirkland C. E., Aliev G., in Seminars in cancer biology. (Elsevier, 2021), vol. 69, pp. 190-199.

Knežević, N. Ž., Durand J.-O. J. N., 2015. Large pore mesoporous silica nanomaterials for application in delivery of biomolecules. 7, 2199-2209.

Konecny, G. E., Christoph T., Joachim L. c. H., Michael U., Wang H. J., Walter K., Holger E., Du B. A., Sigrid O., Dieter S. J. J. N. C. I., 2004. HER-2/neu Gene Amplification and Response to Paclitaxel in Patients With Metastatic Breast Cancer. 1141-1151.

Kostarelos, K. J. N., 2022. Mild hyperthermia accelerates doxorubicin clearance from tumour-extravasated temperature-sensitive liposomes. 6, 230.

Kumar, A., Sood A., Han S. S. J. B., Horizon P., 2022. Potential of magnetic nano cellulose in biomedical applications: Recent Advances. 1, 32-47.

Kumar, B., Priyadarshi R., Deeba F., Kulshreshtha A., Kumar A., Agrawal G., Gopinath P., Negi Y. S. J. M. S., C E., 2020. Redox responsive xylan-SS-curcumin prodrug nanoparticles for dual drug delivery in cancer therapy. 107, 110356.

L Arias, J. J. M. r. i. m. c., 2011. Drug targeting strategies in cancer treatment: an overview. 11, 1-17.

Lai, C., Li L., Luo B., Shen J., Shao J. J. C. M. C., 2023. Current Advances and Prospects in Carbon Nanomaterials-based Drug Deliver Systems for Cancer Therapy.

Li, D., Zhang C., Tai X., Xu D., Xu J., Sun P., Fan Q., Cheng Z., Zhang Y. J. C. E. J., 2022. 1064 nm activatable semiconducting polymer-based nanoplatform for NIR-II fluorescence/NIR-II photoacoustic imaging guided photothermal therapy of orthotopic osteosarcoma. 445, 136836.

Li, J., Luo Y., Zeng Z., Cui D., Huang J., Xu C., Li L., Pu K., Zhang R. J. N. C., 2022. Precision cancer sono-immunotherapy using deep-tissue activatable semiconducting polymer immunomodulatory nanoparticles. 13, 4032.

Li, K., Zhang Y., Hussain A., Weng Y., Huang Y. J. A. B. S., Engineering, 2021. Progress of Photodynamic and RNAi Combination Therapy in Cancer Treatment.

Li, Q., Huang Y. J. J. o. P. I., 2020. Mitochondrial targeted strategies and their application for cancer and other diseases treatment. 50, 271-293.

Li, R., Peng F., Cai J., Yang D., Zhang P. J. A. j. o. p. s., 2020. Redox dual-stimuli responsive drug delivery systems for improving tumor-targeting ability and reducing adverse side effects. 15, 311-325.

Li, S., Chen Y., Wu Y., Yao S., Yuan H., Tan Y., Qi F., He W., Guo Z. J. C. A. E. J., 2022. An Endoplasmic Reticulum Targeting Type I Photosensitizer for Effective Photodynamic Therapy against Hypoxic Tumor Cells. e202202680.

Li, W., Yang J., Luo L., Jiang M., Qin B., Yin H., Zhu C., Yuan X., Zhang J., Luo Z. J. N. c., 2019. Targeting photodynamic and photothermal therapy to the endoplasmic reticulum enhances immunogenic cancer cell death. 10, 3349.

Li, X., Zhang Y., Liu G., Zhou L., Xue Y., Liu M. J. R. a., 2022. Recent progress in the applications of gold-based nanoparticles towards tumor-targeted imaging and therapy. 12, 7635-7651.

Li, Y., Hong W., Zhang H., Zhang T. T., Chen Z., Yuan S., Peng P., Xiao M., Xu L. J. J. o. C. R., 2020. Photothermally triggered cytosolic drug delivery of glucose functionalized polydopamine nanoparticles in response to tumor microenvironment for the GLUT1-targeting chemo-phototherapy. 317, 232-245.

Li, Z., Barnes J. C., Bosoy A., Stoddart J. F., Zink J. I. J. C. S. R., 2012. Mesoporous silica nanoparticles in biomedical applications. 41, 2590-2605.

Liang, J., Huang Q., Hua C., Hu J., Chen B., Wan J., Hu Z., Wang B. J. C., 2019. pH-responsive nanoparticles loaded with graphene quantum dots and doxorubicin for intracellular imaging, drug delivery and efficient cancer therapy. 4, 6004-6012.

Liang, W., Dong Y., Shao R., Zhang S., Wu X., Huang X., Sun B., Zeng B., Zhao J. J. J. o. D. T., 2022. Application of nanoparticles in drug delivery for the treatment of osteosarcoma: focussing on the liposomes. 30, 463-475.

Liew, S. S., Qin X., Zhou J., Li L., Huang W., Yao S. Q. J. A. C. I. E., 2021. Smart Design of Nanomaterials for Mitochondria-Targeted Nanotherapeutics. 60, 2232-2256.

Lima, R., C. M. J. J. o. C. O. O. J. o. t. A. S. o. C. O., 2004. Irinotecan plus gemcitabine results in no survival advantage compared with gemcitabine monotherapy in patients with locally advanced or metastatic pancreatic cancer despite increased tumor response rate. 22, 3776.

Lin, C., Yang X., Li H., Zou Y., Mohammad I. S., Rong H., Rao Y., Song J., Leung S. S., Hu H. J. N., 2021. Self-assembled nanomedicine combining a berberine derivative and doxorubicin for enhanced antitumor and antimetastatic efficacy via mitochondrial pathways. 13, 6605-6623.

Lin, H., Yin L., Chen B., Ji Y. J. C., Biointerfaces S. B., 2022. Design of functionalized magnetic silica multi-core composite nanoparticles for synergistic magnetic hyperthermia/radiotherapy in cancer cells. 219, 112814.

Lin, L.-S., Cong Z.-X., Cao J.-B., Ke K.-M., Peng Q.-L., Gao J., Yang H.-H., Liu G., Chen X. J. A. n., 2014. Multifunctional Fe3O4@ polydopamine core–shell nanocomposites for intracellular mRNA detection and imaging-guided photothermal therapy. 8, 3876-3883.

Lin, X., Li L., Li S., Li Q., Xie D., Zhou M., Huang Y. J. A. S., 2021. Targeting the opening of mitochondrial permeability transition pores potentiates nanoparticle drug delivery and mitigates cancer metastasis. 8, 2002834.

Lin, X., Zhu R., Hong Z., Zhang X., Chen S., Song J., Yang H. J. A. F. M., 2021. GSH-Responsive Radiosensitizers with Deep Penetration Ability for Multimodal Imaging-Guided Synergistic Radio-Chemodynamic Cancer Therapy. 31, 2101278.

Link, S., El-Sayed M. A. J. T. J. o. P. C. B., 1999. Size and temperature dependence of the plasmon absorption of colloidal gold nanoparticles. 103, 4212-4217.

Liu, J., Chang B., Li Q., Xu L., Liu X., Wang G., Wang Z., Wang L. J. A. S., 2019. Redox-responsive dual drug delivery nanosystem suppresses cancer

repopulation by abrogating doxorubicin-promoted cancer stemness, metastasis, and drug resistance. 6, 1801987.
Liu, M., Zhu Y., Wu T., Cheng J., Liu Y. J. C. A. E. J., 2020. Nanobody-ferritin conjugate for targeted photodynamic therapy. 26, 7442-7450.
Liu, S., Pan X., Liu H. J. A. C., 2020. Two-dimensional nanomaterials for photothermal therapy. 132, 5943-5953.
Liu, Y., Ran Y., Ge Y., Raza F., Li S., Zafar H., Wu Y., Paiva-Santos A. C., Yu C., Sun M. J. P., 2022. pH-sensitive peptide hydrogels as a combination drug delivery system for cancer treatment. 14, 652.
Lo, P.-C., Rodríguez-Morgade M. S., Pandey R. K., Ng D. K., Torres T., Dumoulin F. J. C. S. R., 2020. The unique features and promises of phthalocyanines as advanced photosensitisers for photodynamic therapy of cancer. 49, 1041-1056.
Lu, B., Lv X., Le Y. J. P., 2019. Chitosan-modified PLGA nanoparticles for control-released drug delivery. 11, 304.
Luby, B. M., Walsh C. D., Zheng G. J. A. C. I. E., 2019. Advanced photosensitizer activation strategies for smarter photodynamic therapy beacons. 58, 2558-2569.
Lungu, I. I., Grumezescu A. M., Volceanov A., Andronescu E. J. M., 2019. Nanobiomaterials used in cancer therapy: An up-to-date overview. 24, 3547.
Luo, Y., Yin X., Yin X., Chen A., Zhao L., Zhang G., Liao W., Huang X., Li J., Zhang C. Y. J. P., 2019. Dual pH/redox-responsive mixed polymeric micelles for anticancer drug delivery and controlled release. 11, 176.
Ma, H., Yu G., Cheng J., Song L., Zhou Z., Zhao Y., Zhao Q., Liu L., Wei X., Yang M. J. B., 2023. Design of an Injectable Magnetic Hydrogel Based on the Tumor Microenvironment for Multimodal Synergistic Cancer Therapy.
Mahmoudi, Morteza, Lynch, Iseult, Ejtehadi, Mohammad, Reza, Monopoli, Marco, P., Protein—Nanoparticle Interactions: Opportunities and Challenges. (2011), pp. 5610-5637.
Mai, W. X., Meng H. J. I. B., 2013. Mesoporous silica nanoparticles: a multifunctional nano therapeutic system. 5, 19-28.
Mamuti, M., Zheng R., An H.-W., Wang H. J. N. T., 2021. In vivo self-assembled nanomedicine. 36, 101036.
Manzoor, A. A., Lindner L. H., Landon C. D., Park J. Y., Dewhirst M. W. J. C. R., 2012. Overcoming limitations in nanoparticle drug delivery: triggered, intravascular release to improve drug penetration into tumors. 72, 5566-5575.
Massadeh, S., Al-Aamery M., Bawazeer S., AlAhmad O., AlSubai R., Barker S., Craig D. J. J. B. B., 2016. Nano-materials for gene therapy: an efficient way in overcoming challenges of gene delivery. 7, 1-12.
Masserini, M. J. I. S. R. N., 2013. Nanoparticles for brain drug delivery. 2013,
Matsumoto, Y., Nichols J. W., Toh K., Nomoto T., Cabral H., Miura Y., Christie R. J., Yamada N., Ogura T., Kano M. R. J. N. N., 2016. Vascular bursts enhance permeability of tumour blood vessels and improve nanoparticle delivery.
Mayer, L. D., Tardi P., Louie A. C. J. I. j. o. n., 2019. CPX-351: a nanoscale liposomal co-formulation of daunorubicin and cytarabine with unique biodistribution and tumor cell uptake properties. 3819-3830.
Mazraedoost, S., Behbudi G. J. A. i. A. N.-T., 2021. Nano materials-based devices by photodynamic therapy for treating cancer applications. 2, 9-21.
Mazzaglia, A., Piperno A. J. N. (MDPI, 2022), vol. 12, pp. 1597.
Minchin, R. F., Martin D. J. J. E., 2010. Nanoparticles for molecular imaging--an overview. 474.
Mirhadi, E., Mashreghi M., Maleki M. F., Alavizadeh S. H., Arabi L., Badiee A., Jaafari M. R. J. I. j. o. p., 2020. Redox-sensitive nanoscale drug delivery systems for cancer treatment. 589, 119882.
Mohammad, Zaki, Ahmad, Saad, Ahmed, Alkahtani, Sohail, Akhter, Farhan, Targeting J. J. J. o. D., 2015. Progress in nanotechnology-based drug carrier in designing of curcumin nanomedicines for cancer therapy: current state-of-the-art.
Mohsin, A., Hussain M. H., Mohsin M. Z., Zaman W. Q., Aslam M. S., Shan A., Dai Y., Khan I. M., Niazi S., Zhuang Y. J. A. A. N. M., 2022. Recent Advances of Magnetic Nanomaterials for Bioimaging, Drug

Delivery, and Cell Therapy. 5, 10118-10136.
Mrówczyński, R. J. A. a. m., interfaces, 2017. Polydopamine-based multifunctional (nano) materials for cancer therapy. 10, 7541-7561.
Mu, Y., Gong L., Peng T., Yao J., Lin Z. J. O., 2021. Advances in pH-responsive drug delivery systems. 5, 100031.
Mukherjee, A., Bisht B., Dutta S., Paul M. K. J. A. P. S., 2022. Current advances in the use of exosomes, liposomes, and bioengineered hybrid nanovesicles in cancer detection and therapy. 1-18.
Müller, R., Schmidt S., Buttle I., Akkar A., Schmitt J., Pharmaceutics S. B. J. I. J. o., 2004. olEmuls®—novel technology for the formulation of i.v. emulsions with poorly soluble drug.
Mustafa, R. A., Ran M., Wang Y., Yan J., Zhang Y., Rosenholm J. M., Zhang H. J. S. M. i. M., 2023. A pH/temperature responsive nanocomposite for chemo-photothermal synergistic cancer therapy. 4, 199-211.
Na, Y., Lee J. S., Woo J., Ahn S., Lee E., Choi W. I., Sung D. J. J. o. M. C. B., 2020. Reactive oxygen species (ROS)-responsive ferrocene-polymer-based nanoparticles for controlled release of drugs. 8, 1906-1913.
Naher, H. S., Al-Turaihi B. A. H., Mohammed S. H., Naser S. M., Albark M. A., Madlool H. A., Al-Marzoog H. A. M., Jalil A. T. J. J. o. D. D. S., Technology, 2023. Upconversion nanoparticles (UCNPs): Synthesis methods, imaging and cancer therapy. 104175.
Nakayama, M., Okano T. J. R., Polymers F., 2011. Multi-targeting cancer chemotherapy using temperature-responsive drug carrier systems. 71, 235-244.
Net, A. E., Maedler L., Velegol D., Tian X., Hoek E., Somasundaran P., Klaessig F., Castranova V., Thompson M. J. N. M., 2009. Understanding biophysicochemical interactions at the nano-bio interface.
Niculescu, V.-C. J. F. i. M., 2020. Mesoporous silica nanoparticles for bio-applications. 7, 36.
Nikolova, M. P., Kumar E. M., Chavali M. S. J. P., 2022. Updates on Responsive Drug Delivery Based on Liposome Vehicles for Cancer Treatment. 14, 2195.
Noor, U., Ahmed T., Khalid S., Khalid M., Sharif A., Noor I., Waheed W., Jamil I., Zafar Z. S., Kulsum U. J. I. J. o. P., Sciences I. H., 2023. NANO-DRUG DESIGNING STRATEGIES AND TARGETED APPLICATIONS FOR CANCER TREATMENT. 4,
Olaussen, K. A., Dunant A., Fouret P., Brambilla E., André F., Haddad V., Taranchon E., Filipits M., Pirker R., Popper H. H. J. T. J. o. E.-B. M., 2010. DNA repair by ERCC1 in non-small-cell lung cancer and cisplatin-based adjuvant chemotherapy. 355, 983.
Pandey, A., Chauhan P., in Functionalized Carbon Nanomaterials for Theranostic Applications. (Elsevier, 2023), pp. 3-18.
Pandey, S., Mewada A., Thakur M., Pillai S., Dharmatti R., Phadke C., Sharon M. J. R. A., 2014. Synthesis of mesoporous silica oxide/C-dot complex (meso-SiO 2/C-dots) using pyrolysed rice husk and its application in bioimaging. 4, 1174-1179.
Pearce, A. K., O'Reilly R. K. J. B. c., 2019. Insights into active targeting of nanoparticles in drug delivery: Advances in clinical studies and design considerations for cancer nanomedicine. 30, 2300-2311.
Peng, J., Chen F., Liu Y., Zhang F., Cao L., You Q., Yang D., Chang Z., Ge M., Li L. J. T., 2022. A light-driven dual-nanotransformer with deep tumor penetration for efficient chemo-immunotherapy. 12, 1756.
Peng, S., Xiao F., Chen M., Gao H. J. A. S., 2022. Tumor-microenvironment-responsive nanomedicine for enhanced cancer immunotherapy. 9, 2103836.
Peng, X., Chen K., Liu W., Cao X., Wang M., Tao J., Tian Y., Bao L., Lu G., Teng Z. J. N.-M. L., 2020. Soft mesoporous organosilica nanoplatforms improve blood circulation, tumor accumulation/penetration, and photodynamic efficacy. 12, 1-19.
Perrault, S. D., Chan W. C. J. P. o. t. N. A. o. S., 2010. In vivo assembly of nanoparticle components to improve targeted cancer imaging. 107, 11194-11199.
Plouffe, B. D., Nagesha D. K., DiPietro R. S., Sridhar S., Heiman D., Murthy S. K., Lewis L. H. J. J. o. m., materials m., 2011. Thermomagnetic determination of Fe3O4 magnetic nanoparticle diameters

for biomedical applications. 323, 2310-2317.
Qi, J., Jia S., Kang X., Wu X., Hong Y., Shan K., Kong X., Wang Z., Ding D. J. A. M., 2022. Semiconducting Polymer Nanoparticles with Surface-Mimicking Protein Secondary Structure as Lysosome-Targeting Chimaeras for Self-Synergistic Cancer Immunotherapy. 34, 2203309.
Qu, Y., Chu B., Wei X., Lei M., Hu D., Zha R., Zhong L., Wang M., Wang F., Qian Z. J. J. o. c. r., 2019. Redox/pH dual-stimuli responsive camptothecin prodrug nanogels for "on-demand" drug delivery. 296, 93-106.
Ren, G., Jiang M., Xue P., Wang J., Wang Y., Chen B., He Z. J. N. N., Biology, Medicine, 2016. A unique highly hydrophobic anticancer prodrug self-assembled nanomedicine for cancer therapy. 12, 2273-2282.
Robert, M., Rifkin, Stephanie, A., Gregory, Ann, Mohrbacher, Mohamad, Cancer A. J., 2006. Pegylated liposomal doxorubicin, vincristine, and dexamethasone provide significant reduction in toxicity compared with doxorubicin, vincristine, and dexamethasone in patients with newly diagnosed multiple myeloma : A Phase III multicenter randomized trial. 106, 848-858.
Rosemary, Kanasty, Joseph, Robert, Dorkin, Arturo, Materials V. J. N., 2013. Delivery materials for siRNA therapeutics.
Sai, D. L., Lee J., Nguyen D. L., Kim Y.-P. J. E., Medicine M., 2021. Tailoring photosensitive ROS for advanced photodynamic therapy. 53, 495-504.
Salve, R., Gajbhiye K. R., Babu R. J., Gajbhiye V., in Stimuli-Responsive Nanocarriers. (Elsevier, 2022), pp. 367-392.
Sekar, R., Basavegowda N., Jena S., Jayakodi S., Elumalai P., Chaitanyakumar A., Somu P., Baek K.-H. J. P., 2022. Recent Developments in Heteroatom/Metal-Doped Carbon Dot-Based Image-Guided Photodynamic Therapy for Cancer. 14, 1869.
Shen, J., Sun C., Liu Q., Kai G., Qian J. J. C., 2022. Nano Drug Delivery Systems: Effective Therapy Strategies to Overcome Multidrug Resistance in Tumor Cells. 7, e202104321.
Shen, S., Lin S., Chen Y., Zhang Y., He Y., Xu X., Feng Y., Lu Y., Mo R. J. N. l., 2022. Combating cancer stem-like cell-derived resistance to anticancer protein by liposome-mediated acclimatization strategy. 22, 2419-2428.
Shi, Y., Wang S., Wu J., Jin X., You J. J. J. o. C. R., 2021. Pharmaceutical strategies for endoplasmic reticulum-targeting and their prospects of application. 329, 337-352.
Shi, Z., Li Q., Mei L. J. C. C. L., 2020. pH-Sensitive nanoscale materials as robust drug delivery systems for cancer therapy. 31, 1345-1356.
Singh, O. P., Nehru R. J. A. J. E. S., 2008. Nanotechnology and cancer treatment. 22, 6.
Slowing, I. I., Vivero-Escoto J. L., Trewyn B. G., Lin V. S.-Y. J. J. o. M. C., 2010. Mesoporous silica nanoparticles: structural design and applications. 20, 7924-7937.
Stine, Z. E., Schug Z. T., Salvino J. M., Dang C. V. J. N. R. D. D., 2022. Targeting cancer metabolism in the era of precision oncology. 21, 141-162.
Sun, Q., Bi H., Wang Z., Li C., Wang X., Xu J., Zhu H., Zhao R., He F., Gai S. J. B., 2019. Hyaluronic acid-targeted and pH-responsive drug delivery system based on metal-organic frameworks for efficient antitumor therapy. 223, 119473.
Sun, Z., Song C., Wang C., Hu Y., Wu J. J. M. p., 2019. Hydrogel-based controlled drug delivery for cancer treatment: a review. 17, 373-391.
Sushnitha, M., Evangelopoulos M., Tasciotti E., Taraballi F. J. F. i. b., biotechnology, 2020. Cell membrane-based biomimetic nanoparticles and the immune system: immunomodulatory interactions to therapeutic applications. 8, 627.
Tan, S., Chen C., Chen X., Zhou W. J. C. (Multidisciplinary Digital Publishing Institute, 2021), vol. 11, pp. 1361.
Tang, L., Li J., Pan T., Yin Y., Mei Y., Xiao Q., Wang R., Yan Z., Wang W. J. T., 2022. Versatile carbon nanoplatforms for cancer treatment and diagnosis: strategies, applications and future perspectives. 12, 2290.
Tian, B., Liu Y., Liu J. J. C. p., 2021. Smart stimuli-responsive drug delivery systems based on cyclodextrin: A review. 251, 116871.
Toro-Córdova, A., Llaguno-Munive M., Jurado R., Garcia-Lopez P. J. P., 2022. The Therapeutic Potential of Chemo/Thermotherapy with

Magnetoliposomes for Cancer Treatment. 14, 2443.
Vikash, P., Chauhan, Rakesh, K., Materials J. J. N., 2013. Strategies for advancing cancer nanomedicine.
Vu, M. N., Rajasekhar P., Poole D. P., Khor S. Y., Truong N. P., Nowell C. J., Quinn J. F., Whittaker M., Veldhuis N. A., Davis T. P. J. A. A. N. M., 2019. Rapid assessment of nanoparticle extravasation in a microfluidic tumor model. 2, 1844-1856.
Wan, M. M., Chen H., Da Wang Z., Liu Z. Y., Yu Y. Q., Li L., Miao Z. Y., Wang X. W., Wang Q., Mao C. J. A. S., 2021. Nitric oxide-driven nanomotor for deep tissue penetration and multidrug resistance reversal in cancer therapy. 8, 2002525.
Wang, L., Xiao L., Zhao Z., Zhong K., Zhu W., Liu H., Li X. J. N. R., 2023. Hybrid transcytosis nanopomegranates for sensitizing breast cancer radiotherapy in deep tumor tissue. 1-9.
Wang, R., Yang H., Khan A. R., Yang X., Xu J., Ji J., Zhai G. J. J. o. C., Science I., 2021. Redox-responsive hyaluronic acid-based nanoparticles for targeted photodynamic therapy/chemotherapy against breast cancer. 598, 213-228.
Wang, W., Zhang X., Ni X., Zhou W., Xie C., Huang W., Fan Q. J. B. S., 2022. Semiconducting polymer nanoparticles for NIR-II fluorescence imaging-guided photothermal/thermodynamic combination therapy. 10, 846-853.
Wang, X., Qi Y., Hu Z., Jiang L., Pan F., Xiang Z., Xiong Z., Jia W., Hu J., Lu W. J. A. C., Materials H., 2022. Fe3O4@ PVP@ DOX magnetic vortex hybrid nanostructures with magnetic-responsive heating and controlled drug delivery functions for precise medicine of cancers. 5, 1786-1798.
Wang, X., Qiu Y., Wang M., Zhang C., Zhang T., Zhou H., Zhao W., Zhao W., Xia G., Shao R. J. I. j. o. n., 2020. Endocytosis and organelle targeting of nanomedicines in cancer therapy. 9447-9467.
Wang, X., Zhu L., Gu Z., Dai L. J. N., 2022. Carbon nanomaterials for phototherapy. 11, 4955-4976.
Wang, Y., Xie Y., Kilchrist K. V., Li J., Duvall C. L., Oupický D. J. A. a. m., interfaces, 2020. Endosomolytic and tumor-penetrating mesoporous silica nanoparticles for siRNA/miRNA combination cancer therapy. 12, 4308-4322.
Wang, Y., Zhao K., Xie L., Li K., Zhang W., Xi Z., Wang X., Xia M., Xu L. J. C., Biointerfaces S. B., 2022. Construction of calcium carbonate-liposome dual-film coated mesoporous silica as a delayed drug release system for antitumor therapy. 212, 112357.
Wang, Y., Zhou K., Huang G., Hensley C., Huang X., Ma X., Tian Z., Sumer B. D., Deberardinis R. J., Gao J. J. N. M., 2014. A nanoparticle-based strategy for the imaging of a broad range of tumours by nonlinear amplification of microenvironment signals. 13, 204.
Watermann, A., Brieger J. J. N., 2017. Mesoporous silica nanoparticles as drug delivery vehicles in cancer. 7, 189.
Wei, Q., Xu D., Li T., He X., Wang J., Zhao Y., Chen L. J. B., 2022. Recent Advances of NIR-II Emissive Semiconducting Polymer Dots for In Vivo Tumor Fluorescence Imaging and Theranostics. 12, 1126.
Wei, Y., Wang Z., Yang J., Xu R., Deng H., Ma S., Fang T., Zhang J., Shen Q. J. J. o. C., Science I., 2022. Reactive oxygen species/photothermal therapy dual-triggered biomimetic gold nanocages nanoplatform for combination cancer therapy via ferroptosis and tumor-associated macrophage repolarization mechanism. 606, 1950-1965.
Winocur, G., Vardy J., Binns M. A., Kerr L., Tannock I. J. P. B., Behavior, 2006. The effects of the anti-cancer drugs, methotrexate and 5-fluorouracil, on cognitive function in mice. 85, 66-75.
Włodarczyk, A., Gorgoń S., Radoń A., Bajdak-Rusinek K. J. N., 2022. Magnetite Nanoparticles in Magnetic Hyperthermia and Cancer Therapies: Challenges and Perspectives. 12, 1807.
Wong, C., Stylianopoulos T., Cui J., Martin J., Chauhan V. P., Jiang W., Popovic Z., Jain R. K., Bawendi M. G., Fukumura D. J. P. o. t. N. A. o. S. o. t. U. S. o. A., 2011. Correction for Wong et al., Multistage nanoparticle delivery system for deep penetration into tumor tissue. 108, 6336.
Wu, K. C.-W., Yamauchi Y. J. J. o. M. C., 2012. Controlling physical features of mesoporous silica nanoparticles (MSNs) for emerging applications. 22, 1251-1256.
Xia, X., Yang X., Huang P., Yan D. J. A. a. m., interfaces, 2020. ROS-Responsive

Nanoparticles Formed from RGD–Epothilone B Conjugate for Targeted Cancer Therapy. 12, 18301-18308.
Xiong, X., Xu Z., Huang H., Wang Y., Zhao J., Guo X., Zhou S. J. B., 2020. A NIR light triggered disintegratable nanoplatform for enhanced penetration and chemotherapy in deep tumor tissues. 245, 119840.
Xu, Z., Huang H., Xiong X., Wei X., Guo X., Zhao J., Zhou S. J. B., 2021. A near-infrared light-responsive extracellular vesicle as a "Trojan horse" for tumor deep penetration and imaging-guided therapy. 269, 120647.
Yang, K., Zhang S., Zhang G., Sun X., Lee S.-T., Liu Z. J. N. l., 2010. Graphene in mice: ultrahigh in vivo tumor uptake and efficient photothermal therapy. 10, 3318-3323.
Yang, K., Zhao S., Li B., Wang B., Lan M., Song X. J. C. C. R., 2022. Low temperature photothermal therapy: Advances and perspectives. 454, 214330.
Yang, L., Patel K. D., Rathnam C., Thangam R., Hou Y., Kang H., Lee K. B. J. S., 2022. Harnessing the therapeutic potential of extracellular vesicles for biomedical applications using multifunctional magnetic nanomaterials. 18, 2104783.
Yang, L., Shi P., Zhao G., Xu J., Peng W., Zhang J., Zhang G., Wang X., Dong Z., Chen F. J. S. t., therapy t., 2020. Targeting cancer stem cell pathways for cancer therapy. 5, 8.
Yang, N., Cao C., Li H., Hong Y., Dong X. J. S. S., 2021. Polymer-based Therapeutic Nanoagents for Photothermal ⸗nhanced Combination Cancer Therapy.
Yang, X., Shi X., Zhang Y., Xu J., Ji J., Ye L., Yi F., Zhai G. J. J. o. C. R., 2020. Photo-triggered self-destructive ROS-responsive nanoparticles of high paclitaxel/chlorin e6 co-loading capacity for synergetic chemo-photodynamic therapy. 323, 333-349.
Yang, Y., Zheng X., Chen L., Gong X., Yang H., Duan X., Zhu Y. J. I. j. o. n., 2022. Multifunctional gold nanoparticles in cancer diagnosis and treatment. 2041-2067.
Yang, Z., Wang D., Zhang C., Liu H., Hao M., Kan S., Liu D., Liu W. J. F. i. O., 2022. The applications of gold nanoparticles in the diagnosis and treatment of gastrointestinal cancer. 11, 5855.
Yasuoka, H., Naganuma A., Kurihara E., Kobatake T., Ijima M., Tamura Y., Suzuki Y., Hoshino T., Ishida F., Hosaka H. J. O., 2022. Efficacy and safety of the combination of Nano-liposomal irinotecan and 5-fluorouracil/L-leucovorin in unresectable advanced pancreatic cancer: A real-world study. 100, 449-459.
Yin, C., Tai X., Li X., Tan J., Lee C.-S., Sun P., Fan Q., Huang W. J. C. E. J., 2022. Side chain engineering of semiconducting polymers for improved NIR-II fluorescence imaging and photothermal therapy. 428, 132098.
Yu, J., He X., Wang Z., Liu S., Huang Y. J. J. o. M. C. B., 2021. Combination of Starvation Therapy and Pt-NPs based Chemotherapy for Synergistic Cancer Treatment.
Yuan, B., Liu J., Guan R., Jin C., Ji L., Chao H. J. D. T., 2019. Endoplasmic reticulum targeted cyclometalated iridium (iii) complexes as efficient photodynamic therapy photosensitizers. 48, 6408-6415.
Yuan, X., Cen J., Chen X., Jia Z., Zhu X., Huang Y., Yuan G., Liu J. J. J. o. C., Science I., 2022. Iridium oxide nanoparticles mediated enhanced photodynamic therapy combined with photothermal therapy in the treatment of breast cancer. 605, 851-862.
Yujuan, Z., Xuelin Z., Juan X., Shanshan P., Wei H., Rakesh J., Ying C., Yanling L., Rong L., Keng Y. J. S. R., 2018. Temperature-dependent cell death patterns induced by functionalized gold nanoparticle photothermal therapy in melanoma cells. 8, 8720.
Zare-Zardini, H., Ferdowsian F., Soltaninejad H., Ghorani Azam A., Soleymani S., Zare-Shehneh M., Mofidi M., Rafati R., Ebrahimi L., in Journal of Nano Research. (Trans Tech Publ, 2016), vol. 35, pp. 55-66.
Zeng, F., Tang L., Zhang Q., Shi C., Huang Z., Nijiati S., Chen X., Zhou Z. J. A. C., 2022. Coordinating the mechanisms of action of ferroptosis and the photothermal effect for cancer theranostics. 134, e202112925.
Zhan, J., Wang Y., Ma S., Qin Q., Wang L., Cai Y., Yang Z. J. B. M., 2022. Organelle-inspired supramolecular nanomedicine

to precisely abolish liver tumor growth and metastasis. 9, 120-133.
Zhang, H., Zhang H. J. L. S., Applications, 2022. Rare earth luminescent materials. 11, 260.
Zhang, L., Ji Z., Zhang J., Yang S. J. P., therapy p., 2019. Photodynamic therapy enhances skin cancer chemotherapy effects through autophagy regulation. 28, 159-165.
Zhang, Q., O'Brien S., Grimm J. J. N., 2022. Biomedical applications of lanthanide nanomaterials, for imaging, sensing and therapy. 6, 184.
Zhang, W., Lu Y., Zang Y., Han J., Xiong Q., Xiong J. J. I. J. o. M. S., 2022. Photodynamic Therapy and Multi-Modality Imaging of Up-Conversion Nanomaterial Doped with AuNPs. 23, 1227.
Zhang, W., Zang Y., Lu Y., Han J., Xiong Q., Xiong J. J. I. J. o. M. S., 2022. Photodynamic therapy of up-conversion nanomaterial doped with gold nanoparticles. 23, 4279.
Zhang, X., Zhao M., Cao N., Qin W., Zhao M., Wu J., Lin D. J. B. s., 2020. Construction of a tumor microenvironment pH-responsive cleavable PEGylated hyaluronic acid nano-drug delivery system for colorectal cancer treatment. 8, 1885-1896.
Zhang, X., Zhao S., Gao Z., Zhou J., Xia Y., Tian J., Shi C., Wang Z. J. N. R., 2021. Liposome trade-off strategy in mitochondria-targeted NIR-cyanine: balancing blood circulation and cell retention for enhanced anti-tumor phototherapy in vivo. 14, 2432-2440.
Zhang, Y., Zhang S., Zhang Z., Ji L., Zhang J., Wang Q., Guo T., Ni S., Cai R., Mu X. J. F. i. C., 2021. Recent progress on NIR-II photothermal therapy. 9, 728066.
Zhang, Y., Zhang Y. J. T. A.-I. A., Nanocrystals T. f. L., 2022. RGD-RE-1 Bifunctional Short Peptide Enhances the Interaction Between Rare Earth Nanomaterials and Cancer Cells and the Effect of Cell Autophagy. 143-152.
Zhang, Z., Li W., Liu Y., Fang X., Wu C. J. A. O. M., 2022. Semiconducting Polymer Nanoparticles in the Second Near-Infrared Region for Biomedical Imaging and Therapy. 2202052.
Zhang, Z., WeiXie, LisiLi, WenxiLi, BeiLi, JieTian, HaoYuan, ZhenZhao, QiDai, Yunlu %J Angewandte Chemie, 2021. Polyphenol-Based Nanomedicine Evokes Immune Activation for Combination Cancer Treatment. 60,
Zhao, T., Liang C., Zhao Y., Xue X., Ma Z., Qi J., Shen H., Yang S., Zhang J., Jia Q. J. J. o. N., 2022. Multistage pH-responsive codelivery liposomal platform for synergistic cancer therapy. 20, 177.
Zhao, W., Zhao Y., Wang Q., Liu T., Sun J., Zhang R. J. S., 2019. Remote light-responsive nanocarriers for controlled drug delivery: Advances and perspectives. 15, 1903060.
Zhao, X., Wu D., Ma X., Wang J., Hou W., Zhang W. J. B., Pharmacotherapy, 2020. Exosomes as drug carriers for cancer therapy and challenges regarding exosome uptake. 128, 110237.
Zhao, Z., Ukidve A., Kim J., Mitragotri S. J. C., 2020. Targeting strategies for tissue-specific drug delivery. 181, 151-167.
Zheng, P., Ding B., Shi R., Jiang Z., Xu W., Li G., Ding J., Chen X. J. A. M., 2021. A multichannel Ca2+ nanomodulator for multilevel mitochondrial destruction-mediated cancer therapy. 33, 2007426.
Zhi, D., Yang T., O'hagan J., Zhang S., Donnelly R. F. J. J. o. C. R., 2020. Photothermal therapy. 325, 52-71.
Zhong, L., Xu L., Liu Y., Li Q., Zhao D., Li Z., Zhang H., Zhang H., Kan Q., Wang Y. J. A. P. S. B., 2019. Transformative hyaluronic acid-based active targeting supramolecular nanoplatform improves long circulation and enhances cellular uptake in cancer therapy. 9, 397-409.
Zhou, J., Yang X.-J., Yu Q., Li X.-L., Chen H.-Y., Xu J.-J. J. A. A. N. M., 2022. Near-Infrared-Driven Plasmon-Enhanced Au@ PtAg Cascade Nanozymes for Cancer Therapy. 5, 7009-7018.
Zhou, L., Wei F., Xiang J., Li H., Li C., Zhang P., Liu C., Gong P., Cai L., Wong K. M.-C. J. C. S., 2020. Enhancing the ROS generation ability of a rhodamine-decorated iridium (III) complex by ligand regulation for endoplasmic reticulum-targeted photodynamic therapy. 11, 12212-12220.
Zhou, Q., Dong C., Fan W., Jiang H., Xiang J., Qiu N., Piao Y., Xie T., Luo Y., Li Z. J. B., 2020. Tumor extravasation and infiltration as barriers of nanomedicine for high efficacy: The current status and transcytosis strategy. 240, 119902.
Zhou, Q., Li J., Xiang J., Shao S., Zhou Z., Tang J., Shen Y. J. A. D. D. R., 2022.

Transcytosis-enabled active extravasation of tumor nanomedicine. 114480.

Zhu, L., Yan T., Alimu G., Zhang L., Ma R., Alifu N., Zhang X., Wang D. J. J. o. B. N., 2022. Liposome-Loaded Targeted Theranostic Fluorescent Nano-Probes for Diagnosis and Treatment of Cervix Carcinoma. 18, 1289-1301.

Zhu, L., Zhang W., Song P., Li W., Chen X., Ge F., Gui L., Yang K., Tao Y., Du G., 2022. Redox-responsive mesoporous silica nanoparticles for chemo- photodynamic combination cancer therapy.

Rao L, Yu G T, Meng Q F, et al. Cancer cell membrane - coated nanoparticles for personalized therapy in patient - derived xenograft models[J]. Advanced Functional Materials, 2019, 29(51): 1905671.

Zhu, Y., Yao Z., Liu Y., Zhang W., Geng L., Ni T. J. I. J. o. N., 2020. Incorporation of ROS-responsive substance P-loaded zeolite imidazolate framework-8 nanoparticles into a Ca2+-cross-linked alginate/pectin hydrogel for wound dressing applications. 333-346.

Zhang Z, Wang L, Wang J, et al. Mesoporous silica - coated gold nanorods as a light - mediated multifunctional theranostic platform for cancer treatment[J]. Advanced materials, 2012, 24(11): 1418-1423.

ISBN 978-952-12-4334-9